NAS 8-2696-QPR-006

RESEARCH AND DEVELOPMENT
ON
FUEL CELL SYSTEMS

Sixth Quarterly Progress Report
Since Modification Number 6, Contract NAS 8-2696
For the Period Ending December 31, 1965

Prepared for

NATIONAL AERONAUTICS AND SPACE ADMINISTRATION
George C. Marshall Space Flight Center
Huntsville, Alabama

Research Division, Department 3341
Allis-Chalmers Manufacturing Company
Milwaukee, Wisconsin

Approved: J. L. Platner

J. L. Platner, Program Manager

TABLE OF CONTENTS

FOREWORD

This is the sixth quarterly report submitted after Modification Number 6 to Contract Number NAS 8-2696. The report covers the technical progress of "Research and Development on Fuel Cell Systems" for the period of October 1, 1965 through December 31, 1965.

Work under this contract is being performed by the Research Division of Allis-Chalmers, Milwaukee, Wisconsin. Mr. R. M. Casper, a Vice-President of the Company, is the Director of Research. The Program Manager, Mr. J. L. Platner, reports directly to the Director of Research.

A project-type organization has been formed to carry out the program specified in the contract. The Program Manager has direct responsibility for the management and technical aspects of the program. Program management includes: D. P. Ghere, Assistant Program Manager; Dr. J. R. Hurley, Manager, Systems Research and Development; P. D. Hess, Manager, Engineering; R. E. Lochen, Manager, Fabrication and Testing; C. R. Martin, Manager, Quality Assurance; and Gunnar Johnson, Manager, Business Administration.

ABSTRACT

During this reporting period, work was continued in the three major task areas defined in this contract.

Under Part I Tasks (Research and Technology) cell testing has continued in the following areas:

Reactant Impurity Tests - A test cell was operated with 0.5% argon in the reactant oxygen to establish performance and characteristics following purge and to investigate performance effects of operating with insufficient purge. No permanent performance effects resulting from "strangulation" under load were observed.

Anode Catalyst Density - From the results of testing cells using anodes with various catalyst densities, it has been determined that catalyst densities less than 30/30 mg/in^2 of Pt and Pd are not sufficient to provide satisfactory life performance.

Environmental Storage - Testing to determine the effects of high temperature storage (121°C) and low temperature cycling -174°C to +88°C is continuing. Results to date indicate that the electrical performance has not been significantly changed during the test.

Water Transport Matrix Evaluation - The reliability of a thicker water transport matrix has been demonstrated in a test cell which was operated for 2526.5 hours.

Cell Matrix Analysis - Analysis of a number of test cells using 30 mil and 20 mil cell matrices has indicated that better performance was obtained with the 20 mil matrix.

In addition, the dynamic gas flow characteristics in the cell were duplicated by a flow model to determine the effectiveness of the manifolding design of the fuel cell plates. Results of these tests indicate that the present design is adequate.

Under Part II Tasks (Breadboard Fuel Cell Systems) cell sections removed from the MSC 1.8 KW Fuel Cell breadboard were flushed with KOH to determine if rejuvenation of spent cells is possible. Test results have shown that the rejuvenated cells have been restored to their initial performance in the breadboard stack.

Systems fabrication and testing is continuing under Part III Tasks. The purpose of the testing of these 2.0 KW fuel cell power systems is primarily for engineering evaluation of the design and the capability of self-sustained automatic operation as an integrated system. The following is a brief summary of the status of these systems.

System No. 5 - This open loop system (no water recovery) was the first unit in this series to be operated as an integrated system. The system was successful in attaining the primary objective of evaluating the automatic operation of the integrated subsystems. Testing of this unit was terminated after 250 hours of operation due to leakage. The stack for this system was constructed with 30 mil water removal matrices. Subsequent testing has shown that increasing the thickness of this matrix to 50 mils will greatly improve the performance life of the system. As a result, the centerline design was changed to incorporate the 50 mil matrices.

System No. 2 - This first closed loop system (with water recovery) was successful in accomplishing the operation of all subsystems as a complete integrated system. This system was operated for 873 hours, exceeding its performance goal of 720 hours.

System No. 3 - This open loop system successfully passed all its system acceptance tests and was shipped to NASA-MSFC in August, 1965.

System No. 4 - This was the first system constructed with the thicker water removal matrix. As an open loop system, its performance was satisfactory, but it was determined during closed loop operation that the KOH loading of the water removal matrix was not compatible with a Water Recovery Subsystem. It was determined that the vapor pressure in the water removal cavity was too low for effective and efficient condensation of the vapor in the WRS. Special test sections were constructed with modified KOH loading in the water removal matrices and an optimum KOH loading for the matrix was determined which resolved this problem.

As a result of these tests, the centerline specification has been changed to adjust the KOH loading. System No. 4 is still on test having exceeded 800 hours of operation under load.

System No. 8 - This open loop system successfully passed all its system acceptance tests and was shipped to NASA-MSFC in December, 1965.

System No. 6 - This closed loop system using the thicker water removal matrices and the optimum KOH loading has successfully completed its subsystem acceptance tests, and is being assembled into a complete system. The unit is scheduled for delivery to NASA-MSC in February, 1966.

System No. 1 - This is an equivalent system which will be used for qualification type testing and is not scheduled for operation as a complete system. The stack for this system has successfully completed its acceptance test.

System No. 7 - This system is in the process of being fabricated, and is scheduled for final assembly in January, 1966. It will be used for in-house evaluation testing at Allis-Chalmers.

A Program Analysis is included at the back of this report which assesses the work performed during this period and interprets the results obtained in relation to the program objectives.

INTRODUCTION

This report covers the technical progress accomplished under Modification Number 6 and 9 to Contract Number NAS 8-2696 during the period of October 1, 1965 through December 31, 1965.

The report is divided into the following three main sections corresponding to Part I, II, and III Tasks defined in the modified contract.

Part I Tasks - Research and Technology
Part II Tasks - Breadboard and Experimental Items
Part III Tasks - System Test Models

For a detailed definition and explanation of these tasks, see the First Quarterly Report, NAS 8-2696-QPR-001, revised January 20, 1965.

PART I TASKS

RESEARCH AND TECHNOLOGY

FUEL CELL WARMUP THROUGH SELF-EXCITATION

Introduction

In an isolated fuel cell system, i.e., a system without any auxiliary energy source, it is desired to bring the cell module up to operating temperature using its own energy source.

A simple closed form function relates the absolute temperature to time. This function determines the warmup time of a cell module from initial temperature, T_o, to operating temperature, T. In the derivation of this function, it is assumed that:

(1) All energy developed by the cell module is returned to the module as heat energy,

(2) The resistive impedance of the cell heaters remains substantially constant,

(3) Heat loss is due principally to Newtonian cooling; the Stefan-Boltzman radiant cooling is negligible.

Neglecting heat losses, this function is:

$$t = \frac{1}{AK} \ln \frac{aT - b}{aT_o - b}$$

where

t = time in seconds

T_o = initial module temperature and environment temperature (°K)

T = final module temperature (°K)

a and b = constants, characteristics of the energy-temperature relationship for electrodes

K = constant, a physical characteristic of the system relating system mass, specific heat, and the mechanical equivalent of heat

A = total electrode area of module (cm^2)

Warmup Time

Calculation of the warmup time required to raise the cell module temperature from -18 to 88° C (0 to 190° F) results in:

t = 1.59 hours assuming a system specific heat of 20 Btu/°F

t = 1.98 hours assuming a system specific heat of 25 Btu/°F

These results agree quite well with measured or other calculated values.

Additional assumptions are that the maximum heat input to the system is 1,600 watts, thereby, limiting the maximum current density to 150 ma/cm^2 at 0.9 volt with 12,280 cm^2 of active electrode surface in the module.

Effects of Module Size

Warmup time is the same for any size system if heat loss is neglected and the ratio of support components (canister, fans, etc.) to cell mass is the same. However, a larger system generally has a more favorable surface-to-volume ratio, and a smaller support component-to-cell mass ratio. Thus, it is apparent that the larger system will have a faster warmup time.

Critical Heat Loss and System Decay

Under certain conditions, the rate of heat loss could exceed the rate of input, and the energy output would decay to zero. This condition could result from an unusual design configuration or an extreme temperature differential.

Considering cooling, the equation for final module temperature, T, is

$$T = T_o e^{(Ka - G)\,t} - \frac{Kb - GT_o}{Ka - G} e^{(Ka - G)t} + \frac{Kb - GT_o}{Ka - G}$$

where G is the Newtonian cooling coefficient.

Decay would result when the Newtonian cooling coefficient exceeds the value of Ka, thus causing the exponent to be negative.

Derivations

By the conservation of energy

$$\frac{dQ}{dt} = \frac{MC}{A} \frac{dT}{dt} = q \qquad (1)$$

where

$\frac{dQ}{dt}$ = rate of heat flow (cal/sec cm^2)

M = mass (gm)

C = specific heat (cal/gm °C)

A = total electrode area of module (cm^2)

Rearranging the above equation

$$dT = \frac{A}{MC} qdt$$

But $q = W/J$; therefore

$$dT = \frac{A}{MCJ} \, Wdt \tag{3}$$

the rate of temperature change due to internal heat generation only.

J is the mechanical equivalent heat (4.18 watts/cal), and W is the power generation rate in watts/sec cm^2.

Let K be a system constant defined as $K = \frac{A}{MCJ}$

Therefore

$$dT = KWdt \tag{4}$$

Due to Newtonian cooling only,

$$dT = -(T - T_o)Gdt \tag{5}$$

and

$$W = aT - b \quad \text{(refer to Equation 12)}$$

Then the rate of temperature change due to both heat generation and cooling can be obtained by adding Equations 3 and 5.

$$dT = \left[K(aT - b) - (T - T_o)\, G\right]dt \tag{6}$$

Integrating this equation

$$\int_{T_o}^{T} \frac{dT}{T(Ka - G) - (Kb - T_o G)} = \int_{o}^{t} dt \tag{7}$$

This has as a solution

$$\frac{1}{(Ka - G)} \ln \left[\frac{T(Ka - G) - (Kb - T_o G)}{T_o(Ka - G) - (Kb - T_o G)} \right] = t \tag{8}$$

Solving for T

$$T = T_o e^{(Ka - G)t} - \frac{Kb}{(Ka - G)} e^{(Ka - G)t} + \frac{GT_o}{(Ka - G)} e^{(Ka - G)t} - \frac{Kb - GT_o}{Ka - G} \tag{9}$$

Considering the heat loss as negligible, Equation (8) reduces to

$$\frac{1}{Ka} \ln \left[\frac{aT - b}{aT_o - b} \right] = t \tag{10}$$

and

$$T = T_o e^{aKt} - \frac{b}{a} e^{aKt} + \frac{b}{a} \tag{11}$$

Determination of Constants

An empirical equation approximating data for operation of a fuel cell at various temperatures and corrected for a constant external impedance is of the type

$$W = aT - b \tag{12}$$

where

T = temperature (°K)
W = watts/cm^2 of electrode area

From the data given below which was determined from single section tests:

$W = 0.001162T - 0.281$

$a = 0.001162$

$b = 0.281$

Reference	Cell Temperature °K	Current Density amp/cm^2	Cell Voltage	Power Density watts/cm^2
NAS 8-2696 MPR-012	283	0.09	0.53	0.476
NAS 8-2696 MPR-012	288.6	0.1	0.59	0.059
NAS 8-2696 MPR-012	305	0.117	0.67	0.0785
NAS 8-2696 MPR-014	361	0.17	0.9	0.138

Assuming a typical heater load of 1600 watts at 80°C and V = 28 volts, then the current, i, will be 57.2 amperes.

The system specific heat, MC is 20 Btu/°F (9,080 cal/°C)

The total electrode area of the module, A, is calculated as

$$A = (929 \text{ cm}^2/\text{ft}^2)(0.4 \text{ ft}^2)(33) = 12,280 \text{ cm}^2/\text{module}$$

It is then possible to determine the value of the constant K

$$K = \frac{A}{MCJ} = \frac{12,280}{(9,080)(4.18)} = 0.325$$

MOMENT OF INERTIA STUDIES

Experimental Method

An accurate experimental method for determining the moment of inertia of an object with a complex configuration has been developed. Moment of inertia data for the fuel cell is necessary for space mechanics calculations.

The method employs the properties of a torsion pendulum. A circular platform of suitable size and mass (Figure 1) is suspended by three long steel wires equally spaced around the platform periphery. The object to be measured is placed on the platform with its center of gravity at the platform center and the desired axis vertical. The platform is gently rotated about its vertical axis so that it oscillates slightly. By timing the number of these oscillations, the average period of oscillation can be determined. Using the following equation, the moment of inertia of the object, I_o, can be calculated

$$t = 2\pi \frac{(I_p + I_o)\, l}{(m_p + m_o) g r^2}$$

where

I_p = moment of inertia of the platform about the axis of oscillation

I_o = moment of inertia of the object (fuel cell) about the axis of oscillation

l = length of support wires

r = radius from the support wires to the center of oscillation

m_p = mass of the supports

m_o = mass of object (fuel cell)

t = period of oscillation

A high degree of accuracy can be obtained with this method provided the angle of rotation is small (less than five degrees), the ratio of I_o/I_p is greater than five, and l is large compared to r. If the oscillations are too rapid, viscous damping will affect the accuracy of the measurements.

Estimation of the Moments of Inertia

An estimate of the moment of inertia of a 33 section fuel cell stack and canister weighing 125.5 pounds was made by numerical calculation involving the mass and radius of gyration of each component.

x-axis	along the length of a plate,
y-axis	along the width of a plate,
z-axis	along the length of the stack,

the corresponding moments of inertia about the center of mass are

$$I_x = 4.3 \text{ slug-ft}^2,$$

$$I_y = 4.6 \text{ slug-ft}^2,$$

$$I_z = 0.43 \text{ slug-ft}^2.$$

The estimated accuracy of the moment of inertia using this method is $\pm$ 15 percent. The center of mass is located approximately 3/16 inch below the geometrical center of the stack.

CELL MATRIX ANALYSIS

Introduction

All single section test cells, numbered 59 and above, have been investigated, however, only 11 of these cells were constructed and operated in a manner similar enough to warrant comparison. The performance of each cell was compared with respect to:

(1) Degradation

(a) microvolts/hour

(b) microvolts/ampere-hour

(2) Lifetime

(a) hours

(b) ampere-hours

(3) V-A data after 16,000 ampere-hours

(4) Probable cause of failure

Results

The degradation rate of the cells having 30 mil electrolyte matrices was 2-$\frac{1}{2}$ times higher than that of the 20 mil cells.

Life time was not a very good figure of merit for these cells, since it was not usually determined by the cell matrix. The lifetimes of the two classes of cells were approximately the same.

After 16,000 ampere-hours of operation, the voltage at 80 amperes of the 20 mil cells averaged 33 millivolts higher than that of the 30 mil cells.

The cells exhibited no failure pattern. One 30 mil cell (#78) was shut down due to a cross leak. Three of the 20 mil cells (Nos. 59, 60, and 62) failed due to both cavity and cross leaks. The order of occurance of the leaks could not be determined. To date, the longest lifetime, in terms of ampere-hours, is possessed by a 20 mil cell (#60).

The data obtained from this analysis is presented in Table I.

TABLE I CELL MATRIX ANALYSIS DATA

Cell Number	Cell/Water Removal Matrix Thickness, mils	Degradation (μv/hr)	Degradation (μv/amp-hr)	Lifetime (hours)	Lifetime (10^3 amp-hrs)	Voltage at 80 amps (mv)	Failure	Nominal Operating Current (amps)	Electrolyte Penetration
65	30/30	260	3.30	-----	---	819	Terminated at 240 hours	80	.561
76	30/30	155	1.93	352	25	835	Cavity	80	.599
77	30/50	112	1.87	2350	100	813	2350 hrs & running	60-30	.523
78	30/50	142	2.36	1044	60	850	Cross	60	.548
59	20/30	54	0.67	1153	90	875	Cavity & Cross	80	.705
Average for 30 mil cells		167	2.4	1260	62	829			.558
60	20/30	80	1.00	1429	120	892	Cavity & Cross	80	.775
62	20/30	71	0.89	982	80	875	Cavity & Cross	80	.699
68	20/30	26	0.65	744	30	826	Cavity	40	.756
71	20/30	94	1.18	755	60	877	Cavity	80	.737
88	20/30	63	1.57			861	450 hrs & running	40	.625
93	20/50	50	0.84			841	800 hrs & running	60	.644
Average for 20 mil cells		63	0.97	1010	76	862			.706

Comments

The results of this analysis are limited somewhat in accuracy for the following reasons:

(1) The cell population was small,

(2) Operating conditions (from cell to cell, and within one cell) varied widely,

(3) Failures were not sufficiently documented,

(4) Some tests have not yet been terminated.

Each cell exhibited a degradation band, i.e, any value of degradation within the band may be achieved by a judicious choice of time interval. The degradation band, along with the value of degradation for the longest time interval for each cell has been plotted against the extent to which the electrolyte penetrated the electrodes during operation. This is shown in Figure 2. It can be seen that the 20 mil cells were operated under wetter conditions than the 30 mil cells.

Conclusions

Based on this cell analysis, a 20 mil cell matrix is recommended for future cells.

The wetter operation of the 20 mil cells may be a contribution to their lower and more stable degradation rates.

Cavity pressure settings should be based on electrolyte penetration in addition to voltage.

SMALL CELL TESTS

Single section (two parallel 0.2 ft^2 cells) testing was performed in five areas:

(1) Evaluation of reactant gas impurities on cell performance,

(2) Testing of modified electrodes,

(3) Environmental testing,

(4) Evaluation of KOH flushing on electrical performance, and

(5) Design development testing.

Reactant Impurity Testing

One section was tested to determine the effect of 0.5 ± 0.002% argon in the reactant oxygen on fuel cell performance and operating life. The test was conducted in three segments. The first and third segments (0 to 100 hours and 283 to 1137 hours, respectively) were run using standard reactant gases. The second segment was run using the special oxygen-argon mixture.

Voltage versus time data from the first and third segments was fitted with a linear function by the least squares method. The results of that fit are given below.

	First Segment 0 to 100 hours	Third Segment 283 to 1137 hours
Current Density (ma/cm^2)	107.7	107.7
Zero Time Potential from Least Squares Curve (mv)	953	934.2
Degradation Rate (mv/hour)	170.9	66.7
Standard Deviation (mv)	1.94	6.2

During the second segment, a series of runs was made to establish performance and characteristics following purge and to investigate the transient and permanent effects of operating with insufficient purge.

Voltage degradation as a function of purge cycle length and load is shown in Figure 3. The difference in voltage reduction for the various loads are thought to be the result of differences in distribution of inerts in the oxygen plate manifold resulting from diffusion.

The average voltage decay versus time for operation without purge and at constant load current densities of 215 and 150 ma/cm^2 is shown in Figure 4. Figure 5 presents the same function for constant load impedances of 10, 16, 24, and 58 milliohms. No permanent effects resulting from "strangulation" under load were observed.

Electrode Evaluation Tests

Anode Catalyst Density - The effect of anode catalyst density on fuel cell electrical performance has been investigated. Modules with densities of 10, 15, 20, and 30 mg/in^2 of platinum and palladium were tested. The resulting degradation rates are presented below.

Plating	Average Degradation Rate
10/10	4500 microvolts/hour
15/15	1500 microvolts/hour
20/20	500 microvolts/hour
30/30	60 microvolts/hour

Four-cell units were used for the 10/10, 15/15, and 20/20 density tests, while the 30/30 density tests were made with double-cell units. The results indicate that a catalyst density less than 30/30 mg/in^2 is not sufficient to provide satisfactory life performance.

Modified HYSAC # 8 Electrodes - Two double-cell units have been tested to evaluate the performance of HYSAC # 8 electrodes from Lot 4-6-8. One unit was fabricated with an AC-464 nickel anode plaque, and the other with a Clevite anode plaque. The plating density was 30/30 mg/in^2 for all anodes. The results indicate a performance comparable to the standard HYSAC # 8 electrode.

Modified Clevite Nickel Electrodes - One double-cell unit has been tested to determine the performance of a special Clevite nickel anode. The unit has been operated for approximately 640 hours at a constant load of 80 amperes.

Degradation over this period has been approximately 100 microvolts/hour from an initial value of 0.865 volts. This performance compares favorably with the conventional Clevite electrode in a similar cell configuration.

Cyanamid AB-40 Electrodes - A cell unit using the Cyanamid AB-40 electrode as the anode and the standard HYSAC # 8 electrode as the cathode has been operated for approximately 900 hours at a constant load of 80 amperes. The degradation rate over this interval was 26 microvolts/hour.

AC-464 Nickel Electrode - The performance of the AC-464 nickel anode with a standard HYSAC # 8 cathode has been evaluated on two double-cell units. In both units, the voltage degradation rate exceeded the rate for standard Clevite electrodes.

Environmental Storage

High Temperature Storage - Testing of one of the units in the current series was terminated after 140 hours of pre-storage operation due to poor performance. This particular unit was constructed with gold-plated plates and was operated initially at 210°F. A second unit, using conventional plates, has logged over 200 hours of storage time at 250°F.

Low Temperature Storage - A total of 1,050 hours of operation has been accumulated on a module undergoing low temperature environmental testing. The module was first stored at -35°C for 150 hours and then subjected to the temperature cycles presented in Table II. All cavities were filled with helium at atmospheric pressure. Voltage degradation data for the first 800 hours of operation is presented in Table III. The results indicate that electrical performance has not been significantly changed by low temperature cycling.

TABLE II

Temperature Cycles for Low Temperature Storage Test

Segment	Description	Total Operation Time (hours)	Temperature (°C)
1	150-hour Storage	200	-35°C
2	Temperature Cycle	306	-174 to + 88
3	Temperature Cycle	578	-107 to + 88
4	Temperature Cycle	738	-165 to + 88
5	Temperature Cycle	761	- 33 to + 88
6	Temperature Cycle	790	- 72 to + 88
7	Temperature Cycle	817	- 66 to + 88
8	Temperature Cycle	860	- 70 to + 88

NOTE: All operating time between segments was at the following conditions:

Reactant Pressure:	2.5 atm
Cavity Pressure:	225 mm of Hg
Temperature:	88°C
Current Density:	107.7 ma/cm^2

TABLE III

Voltage Degradation for First 800 Hours

of Low Temperature Storage Test

	Single Segment Fit 0 to 800 Hours	Double Segment Fit	
		4 to 200 Hours	200 to 800 Hours
Current Density (ma/cm^2)	107.7	107.7	107.7
Initial Potential (mv)	957.24	966.4	948.7
Degradation Rate ($\mu v/hr$)	59.63	118.7	44.6
Standard Deviation	5.29	3.51	4.34

Evaluation of KOH Flushing on Electrical Performance

In order to evaluate the effects of KOH flushing on the performance of fuel cells that have been operated for an extended period, a number of double-cell sections were removed intact during the MSC 1.8 KW fuel cell breadboard disassembly and placed between end plates for individual testing. One of the sections was operated, without special treatment, at a current density of 53.9 ma/cm^2 for 10.3 hours. Its electrical output was essentially the same as during its operation in the breadboard. A second module was flushed with KOH and operated at 107.7 ma/cm^2 for 450 hours. A comparison of the voltage-current characteristics of this section before and after KOH treatment is shown in Figure 6. It is apparent that the KOH treatment raised the section's output above its initial performance in the breadboard.

Design Development Tests

Water Transport Matrix Evaluation - Life testing of Cell # 77 was terminated after 2526.5 hours of operation under load. Although the cell was still operable, performance was quite low. However, the design goal of 2,500 hours of operation from the standpoint of water matrix integrity has been achieved.

System # 6 Design Verification - Two four-cell units have been built according to the specifications given in Table IV and operated for 792 and 768 hours, respectively. The performance, operating stability, and voltage degradation of the cells employing the 160 mesh screen supported water removal matrix appeared to be superior to the other types tested.

2 KW Fuel Cell Breadboard # 4 Design Verification - Two double-cell modules have been tested for Breadboard # 4 verification. The testing of one module included a period of 18 hours on standby at operating temperature. The effects of standby shutdown on performance were not significantly different than those arising for normal shutdown. This unit was operated for 1,362 hours before testing was terminated. A second unit was operated for 960 hours prior to test termination. The performance of both test units was good.

TABLE IV

Material Specifications for Test Cells

	Section # 112		Section # 113	
	Cell 1	Cell 2	Cell 1	Cell 2
H_2 side support plaque	Sintered nickel fibre support 10 mil thick	160 mesh screen 5 mil thick	Sintered nickel fibre support 10 mil	20 mesh screen 14 mil
Cavity side support plaque	23 mil sintered nickel	28 mil sintered nickel	23 sintered nickel	28 mil sintered nickel
Water Removal Matrix	50 mil	50 mil	50 mil	50 mil

DATA ACQUISITION SYSTEM

Specifications for a Data Acquisition System have been formalized and the system has been ordered.

The system will include the following three modes of operation.

(1) Continuous logging at set time intervals with a variable home position. Between scans, the system will read, but not record a preselected channel.

(2) Manual initiation of each scan. Time interval initiation is switched out automatically.

(3) Manual logging of any preselected channel. Selection is by a 3-decade thumb-wheel switch.

The mode of recording is selected independently of the mode of operation. Under any mode of operation, either or both means of recording (paper and magnetic tape) may be used. The only exception is in the operation of the comparators, in which case recording is only on paper tape.

Time will be recorded at the beginning of each scan and each time a comparator commands a print.

The paper tape format will be as follows:

Column	12	11	10	9	8	7	6	5	4	3	2	1
	Channel Number			Readings commanded by either comparator all other readings - Blank			Data Value with Decimal automatically placed. Time in hours, minutes and seconds. Zeros in Column 6 suppressed.					

Function	Symbol
DC Positive	Blank
DC Negative	
AC	A
Frequency	F
Time	P

Range	Symbol
AC	Blank
DC	1 or 2
Frequency	1, 2, or 3

Magnetic tape format will be as follows:

Each scan will constitute one record. The first word of each record will be the time. The time will be expressed in a six digit word and the channel data will be presented in an eleven digit word.

Time Format: Recording is from Column 1 to Column 6

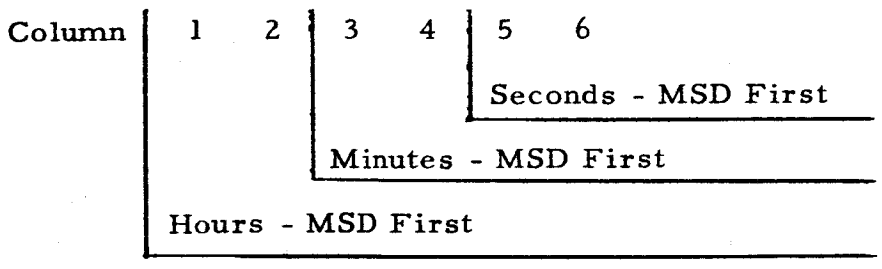

Data Format: Recording is from Column 1 to Column 11

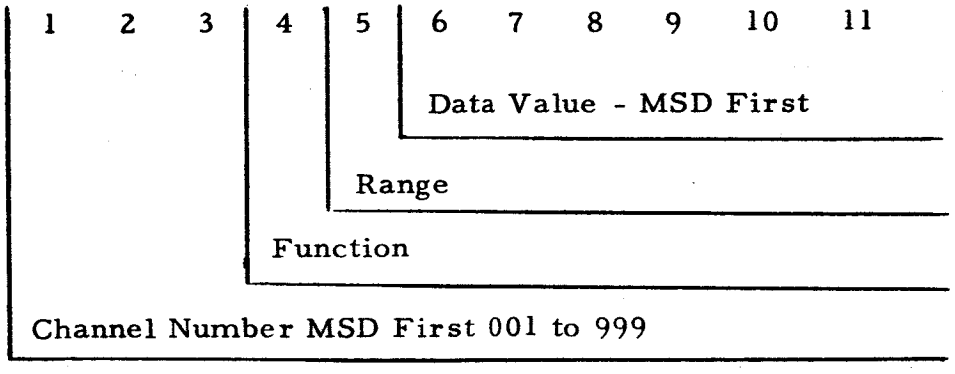

Each record is followed by a longitudinal parity and a 3/4 inch gap. Vertical parity may be selected plus or minus as desired. Recording density may be either 200 or 556 bits/inch. Change over requires replacement of two cards, which are supplied.

CELL GAS FLOW CHARACTERISTICS

Introduction

A flow model that duplicates the reactant gas flow characteristics has been operated to determine the effectiveness of the manifolding design of the fuel cell plates. Water and silicon fluids were used to simulate the oxygen and hydrogen flow, respectively. These liquids were chosen because, at convenient experimental flow rates and pressure heads, they have Reynold's numbers corresponding to the gas flow in a fuel cell plate, thus assuring the dynamical equivalence of the model. Four plate designs were tested; a standard and a specially modified oxygen plate (Figure 7) and a standard and specially modified hydrogen plate (Figure 8). Color photographs, taken through a plexiglass window in the model, provided a graphical description of the flow patterns.

Description of Test

The fuel cell plate was sandwiched between a sheet of clear plexiglass and a filter system. The plexiglass allowed for observing and photographing the flow patterns. The liquid was fed into the plate through an EDM port, and the filter, composed of alternate layers of asbestos and fine mesh screen, was adjusted to produce a liquid flow rate that would correspond to the stoichiometric consumption of reactant gas. A valve at the second EDM port allowed for the inclusion of a purge mode simulation. Two five gallon tanks mounted above the test fixture, supplied the liquids at the proper pressure head. Each tank was filled with the same liquid; one clear, the other dyed.

The test fixture was mounted on a ring stand and leveled. Clear liquid from one of the supply tanks was then fed into the test plate. By compressing the filter system, the proper flow rate was established. If the simulation was to be of a purge mode, the height of the orifice of the flexible tubing leading from the purge valve was adjusted until the purge flow was 1.5 times the consumption flow. The flow rates were continually measured and adjusted until all transients had died out. Switching the supply liquid from clear to colored permitted the observation of the flow pattern within the test plate.

Determination of Model Parameters

In order to simulate fuel cell operation, the liquid flow model must operate under conditions equivalent to fuel cell operating conditions.

If a fuel cell is producing a current of 80 amperes, the flow of oxygen into a single plate is

$$Q = \frac{I}{nF} = 2.65 \text{ cm}^3/\text{sec} \text{ (corrected to 190°F and 22 psig)}$$

where

nF = Faraday's constant for oxygen

I = fuel cell current (amperes)

The area of the inlet EDM port, A, is 0.0645 cm^2. Therefore, the velocity of oxygen gas through the port is

$$V = \frac{Q}{A} = 41.1 \text{ cm/sec}$$

The Reynold's number for the oxygen flow through the EDM port is defined as

$$N_{Re} = \frac{V D}{v}$$

where

v = kinematic viscosity of oxygen at operating conditions (9.29×10^{-2} cm^2/sec)

D = a characteristic linear dimension of the flow which is arbitrarily taken as 1 cm.

then

$$N_{Re} = 443$$

To attain dynamic equivalence, the Reynold's number of the liquid flow in the EDM port of the model must also equal 443. Water was chosen as the simulating liquid for oxygen. For water at room temperature, $v = 1.0 \times 10^{-2}$ cm^2/sec. Since an actual fuel cell plate was used in the model, the characteristic dimension, D, is also 1 cm. Solving for V and Q, respectively, gives 4.43 cm/sec and 0.286 cm^3/sec. Therefore, a water flow rate of 0.286 cm^3/sec through the flow model will produce the same flow pattern as oxygen would in a fuel cell operating at 80 amperes.

Similar calculations have been made for the silicon fluid used to simulate the hydrogen flow.

Results

Sketches of the flow patterns were made from the original color photographs and are included in this report. The curves drawn in the sketches represent the approximate position of the boundary separating the incoming dyed fluid from the clear fluid initially present in the plate.

Oxygen Plates - Figure 9 shows the oxygen gas flow in a standard plate. Curve 5 indicates that the flow resistance along the webbing area is less than that across the slot and groove area. An explanation of this effect was afforded by an unforeseen error. During the initial test run, one of the plates used was unplated. The simulating liquid, water, reacted with the raw magnesium to form magnesium oxide and free hydrogen gas. When the almost imperceptible hydrogen bubbles formed in the webbing area, they were swept along the webbing at a uniform velocity. However, those formed in the slot and groove area were accelerated across the groove, and then lost momentum as they entered the relatively larger volume of the next slot. Hence, the continual variation in available volume required a continual variation in momentum, which was responsible for the increased flow resistance.

The U-shaped modified oxygen plate was designed in an attempt to make the flow boundary sweep across the plate with greater uniformity. The gas flow in this plate is depicted in Figure 10. As can be seen, the flow boundary

maintains a uniform sweep for Curves 2, 3, and 4. Unfortunately, the neck of the U was made too large, and the pattern is disrupted as the fluid enters the left side of the U.

Figure 11 shows the flow during purge of a standard oxygen plate. The non-distinct boundaries indicate that a substantial amount of mixing and diffusion occurs even during purge. Curve 3 shows that even though the purge is only half completed, some of the fresh incoming gas has already traveled down the webbing, across the last slot, and out the purge port. The remaining three seconds of purge is, therefore, inefficient. At the end of a six-second purge, a section of the plate (approximated by Curve 4) had not been thoroughly swept out.

The purge of the modified oxygen plate, Figure 12, shows less mixing and diffusion in the first three seconds, since the boundary itself is smaller. After three seconds of purge, the over-sized neck of the U has again disrupted the intent of the design.

Hydrogen Plates - The flow characteristics of the standard hydrogen plate, shown in Figure 13, seem to be quite satisfactory.

The modified plate (Figure 14), having a set of four extra-deep grooves in line with each EDM port, exhibited an inferior flow pattern. The variation of groove depth across the plate prevented a uniform flow pattern from developing.

The purge flow pattern of a standard hydrogen plate is shown in Figure 15. After a six second purge (at 31 amperes) only a very small section of the plate (approximated by Curve 6) has not been completely swept out.

The purge characteristic of the modified hydrogen plate is very poor. Figure 16 shows that the flow is dominated by the two deep groove sections. Approximately one-quarter of the plate has not been influenced at all by the six-second purge.

Conclusions

In general, Figures 13 and 15 for the standard hydrogen plate indicate that the present design is adequate. Multiple or expanded inlet ports, which in general may tend to decrease water removal matrix dehydration, have not been tested.

It is evident from Figures 14 and 16 that the slot and groove design of any one plate should be as uniform as possible. The slight change in depth of some of the grooves had a very substantial and detrimental effect on the flow pattern. If the internal grid is uniform, the flow pattern is primarily determined by the position of the ports and the shape of the boundaries.

It is possible to redesign the present oxygen plate to obtain a more uniform flow pattern and a more efficient purge sweep. Figures 10 and 12 indicate that this may be accomplished by a longer, and perhaps narrower, central obstruction with both inlet and purge ports on the same edge of the plate. If the ports are to be located on opposite ends of the plate, the disparity of flow resistance between the webbing area and the slot and groove area should be reduced. This can probably be done by including webbing in the slots adjacent to the EDM ports. Further testing would be the only way to verify the effectiveness of this arrangement.

PART II TASKS

BREADBOARD AND EXPERIMENTAL ITEMS

MSC 1.8 KW FUEL CELL BREADBOARD

The unit has been disassembled and a detailed visual inspection of all components has been completed. All observations have been documented. Upon the completion of the various post-disassembly tests and chemical analysis, an analytical and explanatory report will be made.

Included in the post-disassembly tests are a series of tests to establish the feasibility of using a KOH flush procedure to improve the electrical performance of fuel cells which have been operated for an extended period. Four double cell, common cathode sections were removed intact from the stack and assembled between end plates to form small test modules. Three of these test modules were subjected to a KOH flushing procedure, and then operated. The fourth section was operated as a test module without pretreatment.

The KOH flush procedure consisted of the following:

(a) The hydrogen inlet and purge ports were capped.

(b) Four liters of a 20% KOH solution were fed into the cell through the oxygen inlet and purge ports at a pressure of 5 psig. The KOH was allowed to flow out through the water removal ports.

(c) Following the flushing, all three cavities were drained and then flushed with approximately 500 cubic centimeters of nitrogen at a flow rate of approximately 100 cubic centimeters per minute to remove the residual KOH.

The results of this test are reported under "Part I Tasks".

2 KW FUEL CELL BREADBOARD NO. 4 (THERMAL DESIGN MODEL)

Fabrication of this breadboard stack has been completed and preparations are being made to place the unit on test.

A thermal mockup of Breadboard # 4 is being fabricated to establish the performance of the advanced thermal control design of BB # 4. This mock-up will consist of the bottom plate, canister and heat exchanger, dome, fans, ducts and baffles of the BB # 4 design configuration. Electric heaters will be used to simulate the heat produced by the stack. This mockup will be used to investigate the cooling capability of the canister-type heat exchanger used in this design, to determine the flow resistance of the gas coolant through the ducts and the cooling fin system, and to demonstrate the performance of advanced design coolant control valves.

PART III TASKS

SYSTEM TEST MODELS

DESCRIPTION OF THE ALLIS-CHALMERS FUEL CELL POWER SYSTEM

The Allis-Chalmers Fuel Cell Power System consists of the following functionally interrelated subsystems:

(a) Fuel Cell Stack (FCS)
(b) Reactant Control and Conditioning Subsystem (RCCS)
(c) Thermal Control and Conditioning Subsystem (TCCS)
(d) Moisture Removal Subsystem (MRS)
(e) Water Recovery Subsystem (WRS)
(f) Electrical Monitoring and Control Subsystem (EMCS)

The fuel cell system, except for the WRS, is shown schematically in Figure 17.

Theory of Operation

Since the cells are the power producing elements of the system, an understanding of the cell itself is a prerequisite for understanding the operation of the system.

The basic elements of the cell are shown in Figure 18. The cell consists of two porous electrodes separated by an asbestos capillary matrix which contains the electrolyte, an aqueous solution of potassium hydroxide (KOH). The electrode support plates, adjacent to the electrodes, provide the mechanical support for the electrodes, provide passageways for distributing the reactant gases over the surface of the electrodes, serve as current collectors, and provide thermal control for the cells.

The simplified equations for the fuel cell reaction are as follows:

Anode

$$H_2 + 2\,OH^- \longrightarrow 2\,H_2O + 2e^-$$

Cathode

$$\tfrac{1}{2}O_2 + H_2O + 2e^- \longrightarrow 2\,OH^-$$

Overall Reaction

$$H_2 + \tfrac{1}{2}O_2 \longrightarrow H_2O + \text{electrical energy} + \text{heat}$$

Electrical energy is produced and reactants are consumed only when current flows in the system.

The unique feature of this cell construction is the asbestos capillary matrix. The matrix holds the electrolyte in proper contact with the electrodes regardless of the orientation of the cell, provides a uniform separation of the electrodes, isolates the reactant gases, and allows communication of water and hydroxyl ions between the electrodes. The possibility of non-consumable voids (bubbles) occurring between the electrodes is eliminated by the use of this construction. The matrix is compressed between the electrodes, which are supported by the support plates. Thus, a compact cell is formed that is highly resistant to shock and vibration. Repeated thermal cycling does not materially affect the matrix or the electrodes. The corrosion resistance of the asbestos material to the electrolyte is excellent.

During the assembly of the cell, the asbestos capillary matrix is filled with a predetermined amount of electrolyte. When the cell is compressed, some of the electrolyte is forced into the electrodes, forming the necessary interface between the electrolyte, catalyst, and reactants. The difference in capillary potentials between the asbestos matrix and the porous electrode establishes an electrolyte front. By choosing the proper amount of electrolyte, this front is maintained in the electrode and the unfilled pore volume of the electrode provides a reservoir for storage of water and electrolyte. The reservoir is an important feature of this type of cell because it allows the cell to operate through a broad range of electrolyte concentration without

any appreciable effect on performance. Thus, a measure of safety is provided to compensate for unforeseen variations in operating conditions.

If the water produced by the reaction is allowed to remain in the cell, the electrolyte concentration is reduced. The effect of this reduction in concentration on the performance of a particular cell is shown in Figure 19. This curve shows that for the amount of KOH used in this particular cell, the best performance is obtained from 36 to 40 percent KOH concentration. However, good performance can be obtained throughout the entire range of 34 to 41 percent. Had the cell been constructed with a different amount of KOH, the curve would retain the same relative shape, but the curve would be shifted either right or left. Normally, the optimum operating concentration is adjusted by varying the volume of KOH solution during assembly.

The vapor pressure, temperature, and concentration characteristics of potassium hydroxide solutions is shown in Figure 20. This figure shows that for a given temperature the vapor pressure increases as the concentration decreases. These characteristics are used for removing the water from the cell.

Water removal is accomplished by positioning another asbestos matrix (water transport matrix in Figure 18) directly in contact with the hydrogen gas cavity. The water transport matrix is filled with a KOH solution whose concentration is slightly higher than that of the cell matrix. As water is produced, the KOH in the water transport matrix absorbs some of the water vapor from the hydrogen gas cavity, tending to equalize the KOH concentration in the two matrices. By maintaining a predetermined water cavity pressure, control of the KOH concentration in both matrices is accomplished. The driving force for the operation of the moisture removal system is provided by the difference in the vapor pressures and KOH concentrations existing in the cell. A typical condition is shown in Figure 21 where illustrative values have been assigned. Since the water is produced at the hydrogen electrode, the electrolyte in this vicinity has the lowest concentration. The magnitude of the concentration gradients depends upon the density and

thickness of the material holding the electrolyte, and upon the rate at which water is produced.

The water transport matrix also isolates the hydrogen reactant gas from the water removal cavity.

The system is completely static, the only moving parts being the valve which controls the water cavity pressure. The system will operate in zero gravity since fluid transfer occurs only in the gaseous state and there are no free liquid surfaces, or components dependent upon gravity.

Subsystem Description

Fuel Cell Stack (FCS) - The stack shown in Figure 22 consists of 33 two-cell sections. The cells in a section are connected in parallel and the sections are connected in series to provide a nominal 29 volts, d.c. at the output terminals. Each cell has an effective electrochemical reaction area of 0.2 square foot.

Reactant Control and Conditioning Subsystem (RCCS) - The Reactant Control and Conditioning Subsystem provides the stack with the reactant gases at a controlled pressure, and provides the means of purging the cells of accumulated inert gas contaminants which build up during operation. The RCCS, shown mounted on the canister in Figure 23, consists of the following major items.

(a) Dual Inlet Valve - Isolates the stack from the reactant supply when the fuel cell system is not operating.

(b) Hydrogen and Oxygen Pressure Regulators - Maintain the reactant pressures to the stack at 37 psia.

(c) Hydrogen and Oxygen Purge Valves - Open the hydrogen and oxygen

reactant cavity purge ports to allow the cavities to be flushed of inert contaminants.

(d) Hydrogen and Oxygen Reactant Pressure Transducers - Monitor the reactant pressure in the stack.

(e) Hydrogen and Oxygen Overpressure Switches - Close inlet valve if an abnormal inlet pressure occurs.

Thermal Conditioning and Control Subsystem (TCCS) - The simplified reaction equations, previously discussed, show that the reaction of hydrogen and oxygen produces electrical energy, water, and heat. Approximately 35% of this heat is removed from the fuel cell stack with the water vapor as latent heat of vaporization. The remaining heat, over the small amount required to maintain the stack at operating temperature, is removed by the TCCS.

The heat produced at the electrodes is conducted by the support plates to the stack cooling fins, which are the edges of the support plates extending beyond the surface of the stack. Two motor-driven fans continuously circulate helium gas over the cooling fins and through a gas-to-liquid heat exchanger to remove the heat from the canister. Figure 24 shows the flow pattern of the helium gas, and Figure 25 shows the fans and heat exchanger mounted in the canister dome.

The stack temperature is maintained by controlling the flow of liquid coolant through the heat exchanger. A schematic diagram of the TCCS is shown in Figure 26. The temperature of the stack is sensed by a thermistor imbedded in the stack which provides a signal to the electronic control circuitry, which, in turn, operates the liquid coolant valve. During the periods when the liquid coolant valve is closed, the coolant bypasses the heat exchanger through the coolant bypass valve.

During startup the warmup heaters and the fan motors are energized, and

the liquid coolant valve is closed. Heat is transferred from the heaters to the stack via the circulating helium gas. The heaters are de-energized when the stack temperature reaches 185°F. A section of the heater is used to maintain the stack at operating temperature during low load or standby conditions.

Moisture Removal Subsystem (MRS) - The Moisture Removal Subsystem removes the water vapor from the cells by controlling the pressure in the water removal cavity.

Figure 27 shows the basic technique used for controlling the water cavity pressure. The temperature sensing circuit of the vacuum controller has an output characteristic which closely matches the vapor pressure temperature characteristic of KOH solutions. Thus, a reference voltage is provided which is equivalent to the proper vapor pressure for the sensed temperature, and the preset KOH concentration. A pressure transducer, ahead of the moisture removal solenoid valve, senses the actual pressure of the water removal cavity and provides a voltage signal equivalent to this pressure. The difference between these two voltage signals controls the operation of the moisture removal valve.

Water vapor from the fuel cell stack may be vented to space, to the Water Recovery Subsystem for mission use, or to a ground support vacuum venting system.

Water Recovery Subsystem (WRS) - The water vapor removed by the MRS is condensed, recovered, accumulated and transferred to a storage interface as potable water by the Water Recovery Subsystem. A schematic diagram of this subsystem is shown in Figure 28. Figure 29 shows a breadboard model of the subsystem. The WRS consists of a condenser assembly, a deionizer, and a diaphragm pump along with its associated valves, regulators and monitoring devices. Helium is supplied from an interface to operate the pump and to maintain the gas coolant pressure in the canister. Liquid coolant lines and bypass valve for the condenser are as shown in Figure 28.

Before entering the condenser, the water vapor passes through a 3-way valve, where it can bypass the condenser and be vented directly to space vacuum without any adverse effect on fuel cell performance. (In the breadboard model shown in Figure 29, two 2-way valves are used in place of the 3-way valve.)

A cell section of the condenser is shown exploded in Figure 30. The section consists of a steam plate and two water coolant plates, separated by asbestos matrices and porous support plaques. The condenser assembly consists of two such cell sections. The water enters the condenser cell at the steam plate. Liquid coolant is circulated on the outside surface of the water coolant plates, establishing, by conduction, a condensing surface at the innermost support plaque. The condensed vapor is forced through the asbestos matrix by the pressure differential established across the cell, and thus, operation under zero gravity conditions is achieved. The capillary action of the asbestos matrix will allow only water to pass, thus the liquid water is separated from any non-condensible gases and water vapor. Water is removed from the cell at the inside surface of the water coolant plates.

The condensed water passes through a deionizer where it is neutralized by removing any small amount of ionic impurities such as K^+ and OH^- which may be carried over. The resin capacity of the deionizer is adequate to remove all KOH carry over for the entire life of the fuel cell system, thus assuring reliable potable water production.

The diaphragm pump is used to accumulate the water and to maintain a lower pressure on the water side of the condenser to affect water transport through the condenser cells. During the fill cycle the pump is powered by space vacuum. During the pump cycle helium pressure is used to provide the driving force to transfer the water to the storage interface. The 3-way valve which operates the pump is controlled by magnetic reed switches incorporated into the pump assembly. These switches are actuated by the amount of water in the pump.

Electrical Monitoring and Control Subsystem (EMCS) - This subsystem provides the controls for operating the fuel cell. It consists of a Master Controller, Temperature Controller, Purge Controller, Water Cavity Controller, and Power Supply. The various circuits are constructed on a number of printed circuit boards, all mounted in a single package. Figure 31 shows a breadboard model of the EMCS.

The basic functions of the EMCS can be divided into the following:

(a) Start, stop, load on/off and interlock controls,
(b) Automatic operational controls,
(c) Safety and protective controls,
(d) Readout signals,
(e) Manual override controls.

A brief description of the controllers relating to the functions each performs follows.

Master Controller - The Master Controller contains the circuitry to perform the control functions associated with a, c, and e, above. It performs these functions by processing the input signals and commands in such a manner as to produce a coordinated output. The following is a listing of the primary items monitored by the Master Controller, and their effect.

(a) Senses the presence of proper control power voltage.

(b) Receives and executes the start, stop, load "on" and "off" signals provided the necessary operating conditions are present. For example, a load "on" command will not be executed unless normal reactant pressure signals are being received.

(c) Provides external interlock capability.

(d) Provides control power for valves and other devices in response to small power command signals.

(e) Provides selection of automatic protection such as dropping the load or shutting off the reactant inlet valve if the reactant cavity pressure becomes excessive or if the module temperature reaches an excessive predetermined temperature.

(f) Provides manual override for several of the primary module controls.

Temperature Controller - The Temperature Controller operates the warmup heaters during startup and maintains the proper stack temperature during operation.

During warmup the temperature controller provides a signal to energize the warmup heaters located in the gas coolant ducts. These heaters are de-energized when the stack temperature reaches 185°F.

Although the fuel cell will operate over a wide temperature range, the normal operating temperature is maintained within 195 $\pm$ 5°F. for optimum performance and efficiency. When load is applied to the cell, cooling is required to control the stack temperature within this range. This is accomplished by controlling the liquid coolant solenoid valve to regulate the flow of coolant through the fuel cell heat exchanger.

During periods of standby or low power output operation, the heat produced by the electro-chemical reaction in the stack may not be sufficient to maintain the system at its operating temperature. Under these conditions a portion of the warmup heater (standby heater) is energized by the EMCS to maintain the stack temperature between 180°F and 185°F.

Purge Controller - This controller provides an automatically timed command signal to the reactant purge valves on a predetermined ampere-hour basis. In addition, the purge controller provides for the initiation of a purge cycle whenever a "load on", or a manual purge signal is applied to the system.

Water Cavity Controller - This controller regulates the removal of by-product water vapor from the fuel cell stack to maintain a preset KOH concentration in the cell matrices. The operating temperature and actual water cavity pressure are sensed to control the operation of the moisture removal valve.

Power Supply - All supply voltages needed to operate the EMCS circuitry are supplied by a dc-dc inverter. The power supply is designed to supply the necessary regulated voltages while operating over an input voltage range of 18 to 35 volts dc, with an overall efficiency of over 75 percent.

Readout Signals - The present EMCS provides the excitation voltage for all transducer devices used in the fuel cell module. In addition, it provides a common point for the availability of all system readout devices and signals, except for thermocouples and single cell voltage monitoring.

STATUS OF SYSTEM TEST MODELS

The following is a report on the status of the eight 2 KW system test models which are being built and tested under this contract. These systems are described generally in the preceding section of this report starting on Page 30.

The testing being conducted on these system test models is for engineering evaluation. Its primary purpose is to assess the integration of the subsystems, and to gather essential data on the performance of the complete systems and subsystems, and on the electrical performance of the stack.

In the normal sequence of system testing, each subsystem (including the stack) first is acceptance tested to verify and assess its operation and performance. The subsystems then are assembled into a complete fuel cell system which is acceptance tested to verify its operation and performance as a complete system. A minimum of approximately 50 hours of operation under load is logged during the system acceptance test. Follow-on engineering evaluation testing is then conducted on the "in-house" units, and the deliverable units are shipped to their designated destinations for evaluation by NASA.

In general, system testing of the in-house units during this quarter varied from 250 to 900 hours, with some units continuing on test. The performance of several of the systems during the system acceptance tests is described in this report, and V/P curves are included which summarize the follow-on testing.

System No. 5

This open loop system (no water recovery) was the first unit in this series to be operated as an integrated system capable of self-sustained operation. Testing of this unit has been completed and the test results have been reported in the preceding Quarterly Report (NAS8-2696-QPR-005).

The system was successful in attaining the primary objective of evaluating

the automatic operation of the integrated subsystems for the first time. As part of the test program for this unit, control settings such as purge requirements, moisture removal set points, etc., were optimized; operating procedures were established; and trouble areas were noted.

The system was operated for 250 hours before a hydrogen leak into the moisture removal cavity developed and the test was terminated. (Including the stack subsystem acceptance test, the stack accumulated a total of 315 hours of operating time under load.) The experimental nature of the testing of this system was a contributing factor to the early occurance of the hydrogen leak. The stack for this unit was constructed with 30 mil thick water removal matrices, which in previous testing had indicated a minimum life expectancy in the range of 500-600 hours. In a test program conducted to improve the reliability of the water removal matrix, a 50 mil thick matrix has demonstrated a greatly improved life expectancy with a subsequent improvement in the reliability of the moisture removal subsystem. As a result of this evaluation, the fuel cell system centerline design has been modified to include the 50 mil water removal matrices.

The performance of the Reactant Control and Conditioning Subsystem (RCCS) was good, although some reactant pressure set-point drift was noted in the pressure regulators. The vendor's analysis of this problem indicates the cause to be improper annealing of the aneroid assembly. The aneroid assemblies of all regulators in stock have been annealed and rechecked for calibration. Those units displaying out-of-tolerance performance have been returned to the supplier for correction and recalibration.

Some difficulties also were encountered early in the test with the Moisture Removal Subsystem (MRS) due to a malfunctioning moisture removal valve. A failure analysis has been received from the vendor which indicates that a small area of plating in the solenoid cavity became loosened. This condition caused partial jamming of the solenoid plunger. The vendor is reworking and improving the design of this valve to provide a smoother solenoid cavity without sharp corners and recesses that cause plating voids and corner

buildup problems when electro-depositing plating inside of holes and cavities. It is expected that this corrective action will eliminate the difficulties encountered.

The moisture removal valve was replaced with an available valve of similar design, but with a smaller orifice. From then on, the cavity pressure control was very stable and the subsystem functioned satisfactorily.

The automatic purge controller in the Electrical Monitoring and Control Subsystem (EMCS) did not function properly, and purging was performed manually throughout the test. The automatic purge cycle based on an ampere-hour interval was erratic. Random actuation of the purge controller is believed to have been caused by circuit noise. The purge controller circuits have been subsequently redesigned to eliminate the random purge cycle problems.

The V-P performance characteristics of System No. 5 is shown in Figure 32.

A refurbishment plan for System No. 5 has been established. System No. 5 will be rebuilt with 50 mil water removal matrices and will be delivered to NASA-MSFC.

System No. 2

The primary objectives of testing of this first closed loop system (WRS included) was to accomplish the operation of all subsystems as a complete integrated system; to determine satisfactory normal operation and control settings for purge, moisture removal, etc.; to identify possible problem areas, or areas which may require additional investigation; and to establish necessary procedures for system operation.

Test Procedure - This system was operated on a load profile which was varied from 20 amperes to 75 amperes. The load profile is shown in the following table.

Elapsed Time (Hours)	Load (Amps)
0 - 2.3	20
2.3 - 26.2	40
26.2 - 29	60
29 - 37	30
37 - 45	60
45 - 47	75
47 - 48	30

The hydrogen, oxygen, helium, coolant and vacuum supplies, along with the associated valving, gages, flowmeters necessary for the test were supplied by a test bench. Figure 33 shows the system mounted on the test bench.

Results of the Acceptance Test - This test was conducted for 48 hours under the specified load profile after initial checkout. The average power generated by the system was 1162 watts and 55.7 kw-hrs of energy was produced. The system performed well during the entire acceptance test. The following list shows the maximum variation in voltage between cell sections at various current densities, and elapsed times. The voltage measurements were made after a purge cycle was completed.

Time (Hours)	Current Density (ma/cm^2)	Voltage Variation (Volts)
0.8	54	0.028
10.6	108	0.007
24.5	108	0.015
36.9	81	0.014
44.9	162	0.030

The following lists the purge data and the resultant voltage changes.

Elapsed Time (Hours)	Current (Amps)	Purge Interval (Amp-Hrs)	Stack Voltage Increase Volts	%	Cell No.	Cell Voltage Increase Volts	%
7.6	40	240	0.25	0.81	23	0.041	4.6
10.6	40	120	0.07	0.23	29	0.016	1.71
18.3	40	88	0.03	0.10	1	0.030	3.33
24.5	40	248	0.11	0.36	23	0.020	2.20
36.9	30	228	0.10	0.31	23	0.018	1.93
41.0	60	240	0.23	0.78	23	0.038	4.59
44.9	60	240	0.18	0.61	23	0.039	4.66

Purging was scheduled on a 240 amp-hr basis and was carried out effectively except at 10.6 and 18.3 hours when extra purging was accomplished to raise the voltage of Cells # 29 and # 1, respectively.

The chemical analysis of the product water is shown in Figure 34. The average pH value of the recovered water was 8.4.

Subsystem Performance During the Acceptance Test - The following is an evaluation of the performance of the subsystems during the system acceptance test.

(a) EMCS - The Master Controller satisfactorily performed its function of insuring the adequacy of the necessary inputs and safety controls during startup, operation and shutdown. No special evaluation tests were performed on this controller.

The Auxiliary Master Controller satisfactorily initiated all inter-related internal control functions for start and stop and supplied the amplified output signals for subsystem control. No special evaluation tests were performed on this controller.

The Moisture Removal Vacuum Controller performed satisfactorily while maintaining the KOH concentration in the fuel cell stack between 37.7% and 40.9%. As indicated by the following table, the optimum setting was 38 to 40%.

% KOH	% of Time at Setting*
37.7 - 37.99	1.1
38.0 - 40.0	83.8
40.0 - 40.9	15.1

* 1/2 hour sampled intervals

The Temperature Controller maintained the system temperature within a 10°F band for any given one hour interval. The average of the band, however, varied approximately 10°F as indicated by the plot of the temperature control band in Figure 35. The specified operating temperature of the fuel cell stack is 195 ± 5°F.

Figure 36 shows the short term thermal response to temperature adjustment. The plot of recorded mean water cavity pressure shows its direct relationship to cell temperature. The thermal response to load change for a short sampled time interval is shown in Figure 37.

The Purge Controller was not used during the test, and all purging was performed manually. The problems with the purge controller were the same as reported under System No. 5.

(b) MRS - The performance of this subsystem, including the operation of the valve, was satisfactory throughout the test.

(c) RCCS - This subsystem performed satisfactorily. Both the hydrogen and the oxygen pressures were maintained in a 0.4 psi band, within the 37 ± 1 psia required value.

(d) TCCS - Automatic warmup of the fuel cell stack was attempted, but the duct heaters would not function under automatic control.

After completion of the testing, the canister was opened, and it was discovered that the heaters had become detached from the heater duct and also from the over-temperature sensing thermostat. To correct

this problem on future systems, an improved heater installation with optimized heat transfer to the thermostat has been designed.

Temperature measurements within the fuel cell stack versus load current is shown in the following table. The maximum temperature spread was 2.5°F at the 30 ampere load.

Load Current (Amps)	30	40	60	75
Cell No.	Temperature (°F)			
1 and 2	194.5	198.5	201	197
1 and 2	194	198	200.5	196
11	194	198.5	201	196
1 and 2	196	198.5	200.5	196
11	196	198.5	200.5	197.5
11	194.5	198.5	200	196.5
11	195	198.5	201.5	197.7
11	195	198.5	201	197
18 and 19	195	199	199	194.7
21 and 22	195	198.5	200.4	197
32	194	197.5	199.7	195
32	195	198.5	201	197

Several changes in temperature were recorded as a function of the load.

Load Current		Temperature (°F) ($\frac{1}{2}$ Hr. Average)	
Before	After	Before	After
20	40	190	195
40	60	195	200
60	30	197	191
30	60	194	197
60	75	194	197
75	30	195	185

Figure 38 and Figure 39 describe the character of the monitored temperature as a function of the load current. Figure 40 shows the demand on the primary coolant valve as a function of the load. At an 80 ampere load current, the coolant valve was open only 34% of the time, indicating a considerable cooling capacity design margin and a minimized coolant valve cycling.

Follow-On Testing of System No. 2 - Following the acceptance test of this system, the system was used for special engineering evaluation tests, and for performance testing.

(a) Fuel Cell Transient Voltage and Current Response Test - A study was made of fuel cell voltage and current transient response due to step changes in load.

With the fuel cell operating under normal conditions, the voltage and current response was recorded for step changes in load for 0 to 40, 40 to 0, 40 to 80, and 80 to 40 amperes. In each case the data was recorded for a minimum of 20 seconds after the load change. Voltage response was recorded on an oscilloscope connected directly across the output terminals. Current response was recorded on an oscillograph connected across the load shunt. The time constant of the recording equipment was 0.2 milliseconds for voltage and 1.5 milliseconds for current.

A summary of the characteristics of the voltage transient response is shown below.

Voltage Transient Response Data

Load Change Amperes	Voltage Change Volts	Time in Seconds to Steady State 70%	80%	90%	100%
0 to 40	35.30 to 30.18			0.77	34
40 to 0	30.18 to 35.32			5.6	39
39 to 82	30.34 to 27.09	0.0193	0.175	0.65	24
82 to 39	26.99 to 30.35	0.0175	0.175	0.77	25

A summary of the characteristics of current response is shown in the following table:

Current Transient Response Data

Load Change (Amperes)	Time in Seconds to Steady State 94%	98%	100%
39 to 82	0.053	0.77	3.0
82 to 39		0.053	0.53

The time required to achieve 90% of the change in voltage after a step load change of 40 to 80 amperes, nominal, was on the order of 650 to 770 milliseconds.

The transient current response was considerably shorter since 94% of the current change was achieved in 53 milliseconds.

(b) Fuel Cell Impedance Test - The fuel cell impedance in the frequency range of 10 to 10,000 cps was determined in the following manner.

With the fuel cell operating under normal conditions at a load of 41 amperes, a sinusoidal voltage, variable from 10 to 10,000 cps, was superimposed across the fuel cell by means of an oscillator. The oscillator output was passed through a power amplifier to provide 5 amperes of current except at frequencies below 40 cps where 2 amperes was the maximum obtainable with the test equipment. The peak frequency was repeated at an 80 ampere dc load for comparison with the data obtained at 41 amperes. Results of this test are shown in Figure

41. Also shown on this figure is the phase angle of the impedance.

(c) Follow-on Performance Testing - The system accumulated 873 hours of system time under load before it was shut down due to hydrogen leakage into the water cavity. The stack of this system was constructed with 30 mil thick water removal matrices as was System No. 5. The system was operated in excess of 630 hours as a closed loop system using the breadboard model WRS. Performance of the system at various times during the test is shown in Figure 42.

The following subsystem problems were encountered during performance testing.

(1) EMCS - The operation of the automatic purge controller was erratic and all purging was conducted manually at approximately 120 amp-hour intervals. The purge controller problems were the same as encountered on System No. 5.

Several component failures were experienced in the temperature controller early in the test. This trouble was eliminated when higher quality components became available.

Other controllers in the EMCS (moisture control and temperature control) performed satisfactorily. A redesign program for the EMCS was accomplished to correct these control problems.

(2) RCCS - The performance of the RCCS was good, although some reactant pressure set-point shift was noted during the performance test. The reactant pressure regulator problems were the same as encountered on System No. 5.

(3) MRS - Problems with the Moisture Removal Valve were the same as encountered on System No. 5 and the same corrective action was taken. After substitution of the valve, the subsystem operated well, with no further problems.

System No. 3

This open-loop fuel cell system was acceptance tested and shipped to NASA-MSFC on August 15, 1965. This unit is for use by MSFC personnel for familiarization of operating techniques and for environmental testing at a later date. Personnel from Allis-Chalmers assisted in the initial installation of this unit at the MSFC Test Facility, and in the initial startup of the unit. A special test cabinet was also designed and constructed for the MSFC Test Facility. The system and the test cabinet are shown in Figure 43.

Acceptance Test of System No. 3 - The acceptance test of System No. 3 was conducted for 29 hours to the load profile shown below.

Elapsed Time (Hours)	Load (Amps)
0 - 2	20
2 - 12	40
12 - 14	50
14 - 18	60
18 - 18.5	70
18.5 - 23	60
23 - 25	70
25 - 27	40
27 - 28	80
28 - 29	30

The average power generated was 1450 watts and the system produced 42.12 KW-hrs of energy during the test. Figure 44 shows the system performance during its acceptance test.

The following is a listing of the variation in cell section voltages at various current densities and elapsed times during the test. The voltage measurements were made after the completion of a purge cycle.

Elapsed Time (Hours)	Current Density (ma/cm^2)	Cell Section Voltage Variation (Volts)
15.0	108	.025
18.0	162	.030
30.0	216	.035
31.5	108	.029
31.5	162	.037
31.5	216	.047

The fuel cell reaction to a purge after 400 ampere-hours of operation at a current density of 108 ma/cm^2 was as follows:

	Cell Voltage Variation	Total Voltage
Before Purge	.085	30.82
After Purge	.025	31.11

The product water record and chemical analysis is shown in Figure 45. The average pH reading for the test was 9.5.

Subsystem Performance During Test - The following is an evaluation of the performance of the subsystems during the system acceptance test.

(a) EMCS - The Master Controller performed well during the entire test.

During the test, the dual reactant inlet solenoid valve closed several times. With the fuel cell under load, this caused a rapid depletion of gases in the reactant cavities of the stack with an accompanying decrease in stack voltage and load current. Subsequent opening of the valve restored the fuel cell to normal operation with no detrimental effects on the system. This problem was caused by circuit noise in the Auxiliary Master Controller which controls this valve. The faulty circuit board was replaced, and no further problems were encountered.

Performance of the Temperature Compensated Vacuum Controller which operates the moisture removal valve to maintain the desired KOH concentration in the fuel cell stack was good at loads up to 60 amperes. No evaluation of the controller could be made at loads above 60 amperes because of the moisture removal restriction imposed by the moisture removal valve (see following Paragraph b).

The Temperature Controller maintained the temperature of the fuel cell stack within the range of 190 $\pm$ 5°F after initial adjustment.

The ampere-hour counter of the Purge Controller did not function properly in the early part of the test. After an error in the circuitry of the purge controller was corrected, the controller performed satisfactorily. Figure 46 shows the results of monitoring the ampere-hour counter of the purge controller for a period of five hours. It can be noted from this data that the ampere-hour counter performed quite well with a slight deviation at a load of 30 amperes. The recorded data indicates a slight tendency of a "slow count" at loads of 70 and 80 amperes, and a "fast count" at loads of 30 and 40 amperes.

(b) MRS - Because of the unavailability of the intended moisture removal valve, a substitute valve of the same type, but with a smaller orifice was used in the MRS. It became evident during the test that at high loads the orifice of this substitute valve was restricting the removal of water from the fuel cell. This resulted in dilution of the KOH electrolyte and necessitated limiting operation of the fuel cell at the 80 ampere load to periods of less than one hour.

(c) RCCS - No performance deviations occurred in the RCCS during the test. The reactant pressure regulators controlled their respective reactant pressures within a range of one psi. The hydrogen pressure varied from 36.9 to 37.8 psia and the oxygen pressure varied from 35.8 to 36.8 psia.

(d) TCCS - Warmup of the fuel cell stack to the operating temperature of 190° F was accomplished with the electric heating elements located in the helium coolant ducts. However, since this heater design was the same as for System No. 2, the heater switching was performed manually rather than automatically until the new heater assembly design became available.

The ducts, heating elements, and thermostats were removed from the stack and were replaced with the redesigned units. In the new design the heating elements are mechanically attached to the surface of the duct with a metal plate which also provides a better heat transfer and a heat sink for the thermostat. A subsequent successful warmup test verified the automatic operation of the warmup heaters.

Typical temperatures recorded in the fuel cell stack and the TCCS at various loads during the test are shown in Table V. The maximum spread in fuel cell stack temperatures was 5°F, which occurred at a load of 60 amperes.

The thermal response of the system to changes in load is shown in Figure 47. As the load current was changed from 40 to 80 amperes and then to 30 amperes, the average temperature changed approximately 3°F with each load change. Also shown are the water cavity pressure, stack temperature, and voltage.

General Conclusions on the Performance - The performance of System No. 3 was satisfactory except for operation at loads above 70 amperes where the substitute moisture removal valve limited moisture removal from the cell. This difficulty will be eliminated when the properly designed valve becomes available.

The test results have adequately demonstrated that the EMCS, as presently designed, is capable of performing its automatic control functions.

TABLE V

Fuel Cell Stack and TCCS Temperatures (°F) During Performance Test of System No. 3

Thermocouple Location	Load Current 20	30	40	50	60	70	80
Cell 1 & 2	191	192	191	191	192	191	192
Cell 1 & 2	191	192	189	189	189	189	192
Cell 1 & 2	190	191	191	191	193	191	191
Cell 11	191	192	192	192	194	192	192
Cell 11	191	192	190	190	194	192	192
Cell 11	191	192	191	191	191	191	192
Cell 11	191	192	192	191	193	191	192
Cell 11	191	192	192	191	193	191	191
Cell 18 & 19	191	192	193	192	194	192	192
Cell 21 & 22	191	192	192	191	193	191	191
Cell 32	191	192	193	193	194	192	192
Heater Surface	191	192	187	187	188	190	190
Heater Surface	191	192	186	186	191	190	190
Fan Exhaust # 1	191	192	187	187	191	188	191
Fan Exhaust # 2	191	192	189	189	188	188	192
Helium Return # 2	190	191	191	191	193	190	191
Helium Return # 1	191	192	191	191	191	191	192
Heat Exchanger Out	191	192	191	190	191	190	191

System No. 4

The stack of this closed-loop system was acceptance tested with satisfactory results. However, when the complete system was tested with the WRS, (closed-loop), excessive voltage drop was experienced at loads above 1200 watts. Performance curves for stack and system acceptance testing are shown in Figure 48. When operated as an open loop system (without the WRS) the system performance was good throughout its full power range. This condition had not been observed in previous Mod. 6 systems.

This system incorporated several design changes in the water removal portion of the stack, namely:

(a) the thickness of the water removal matrix was increased to 50 mils,

(b) modified water removal matrix support plaques were used, and,

(c) the amount of KOH used in the water removal matrix was increased.

Extensive testing on System No. 4 and on specially constructed test cells was conducted to determine the reasons for the poor performance. An analysis of the test results showed that the lower than normal performance was due to the following factors:

(a) Operation as a closed loop system at loads greater than 1200 watts caused the fuel cell stack to operate under dilute electrolyte conditions.

(b) The operating requirements of the WRS imposed operating conditions on the fuel cell stack such that the KOH loading of this system was not correct for closed loop operation.

As a result of this evaluation test, subsequent stacks were constructed with a modified KOH loading in the water removal matrices. This corrective action eliminated the incompatibility between the water recovery device and the fuel cell stack.

System No. 4 was originally scheduled for delivery as a closed loop system to NASA-MSC for engineering evaluation, but because of its performance, this system was retained at Allis-Chalmers for further evaluation testing. The performance of this system in the subsequent evaluation testing is also shown in Figure 48. The testing of this unit is continuing.

System No. 8

This open loop fuel cell system was performance tested for approximately 100 hours to ensure proper operation as a complete system before delivery to MSFC. During the first thirty hours of the test, all subsystems were evaluated and test instrumentation checkout was completed. The remainder of the test was conducted using the acceptance test load profile. The test was completely successful and was trouble free except for minor adjustments required during the initial checkout period.

High purity hydrogen and ultra high purity oxygen reactant gases were used on this test. Figure 49 shows the V/P curves for elapsed times of 45 and 100.5 hours. During this test the fuel cell operated at an average power of 1.29 KW and generated a total of 129.7 KW hours electrical energy. As shown in Figure 48, the system output voltage at 2.0 KW load, at the end of this test, was 29.1 volts. The pH measurements of the product water varied between 9.1 and 9.7 during the test.

The Electrical Monitoring and Control Subsystem (EMCS) provided complete control of the fuel cell temperature and KOH concentration. Throughout the test, the fuel cell stack temperature control performed satisfactorily at all load levels. With the exception of the initial KOH optimization testing, the KOH percent remained within a 2% band throughout the test. Purging of the reactant gas impurities was performed on a lapsed time basis with manual purges interjected when a decrease in the stack voltage was observed. Accelerometers were installed internally and externally on the fuel cell stack for vibration testing to be conducted at MSFC.

This system was shipped to NASA-MSFC on December 28, 1965.

System No. 1

The stack for System No. 1 has been assembled and acceptance tested. The performance of the stack during the acceptance test is shown in Figure 50. System No. 1 is an equivalent system and will not be tested as a complete system.

System No. 6

This closed-loop system is scheduled for delivery to NASA-MSC in February 1966. Several design improvements have been incorporated into this system as a result of evaluation tests performed on System No. 4. The improvements include: 50 mil water removal matrix, modified KOH loading, and an improved water removal matrix support plaque. This system is presently being fabricated.

System No. 7

Parts for this system are being fabricated and the system is scheduled for final assembly in January 1966.

PROGRAM ANALYSIS

The major objective of this research and development contract is to accomplish adequate research and development of materials and processes and to establish engineering criteria that will assure an operational fuel cell power system for space vehicle applications. To demonstrate the accomplishment of this objective, eight 2 KW, 29 volt nominal, H_2-O_2 fuel cell power systems are being built. These systems are being used for engineering evaluation of the Allis-Chalmers design and shall have as a design goal, 720 hours of reliable operation.

Two major milestones were achieved during this quarter in that automatic self-sustained operation of both an open loop and a closed loop integrated fuel cell system was demonstrated, and two systems have exceeded 720 hours of operational testing. Performance in excess of 2500 hours has been demonstrated by test cells.

As a result of system testing and technological studies, the following design concepts were established:

(a) A thicker water removal matrix and a more permeable matrix support plaque will greatly increase the reliability of the moisture removal subsystem and the endurance life of the fuel cell system.

(b) An optimum KOH loading for the water removal matrix was established to provide compatibility of the static moisture removal concept of the Allis-Chalmers fuel cell design to the water recovery subsystem.

Advanced technological studies in the area of high loading catalyst anodes has shown that fuel cell system voltage regulation goals of 29 $\pm$ 2 volts throughout a range of 800 to 2000 watts can be met and exceeded.

No limiting technological problems have been identified during this reporting period.

DIAGRAM OF SETUP FOR EXPERIMENTALLY DETERMINING MOMENT OF INERTIA

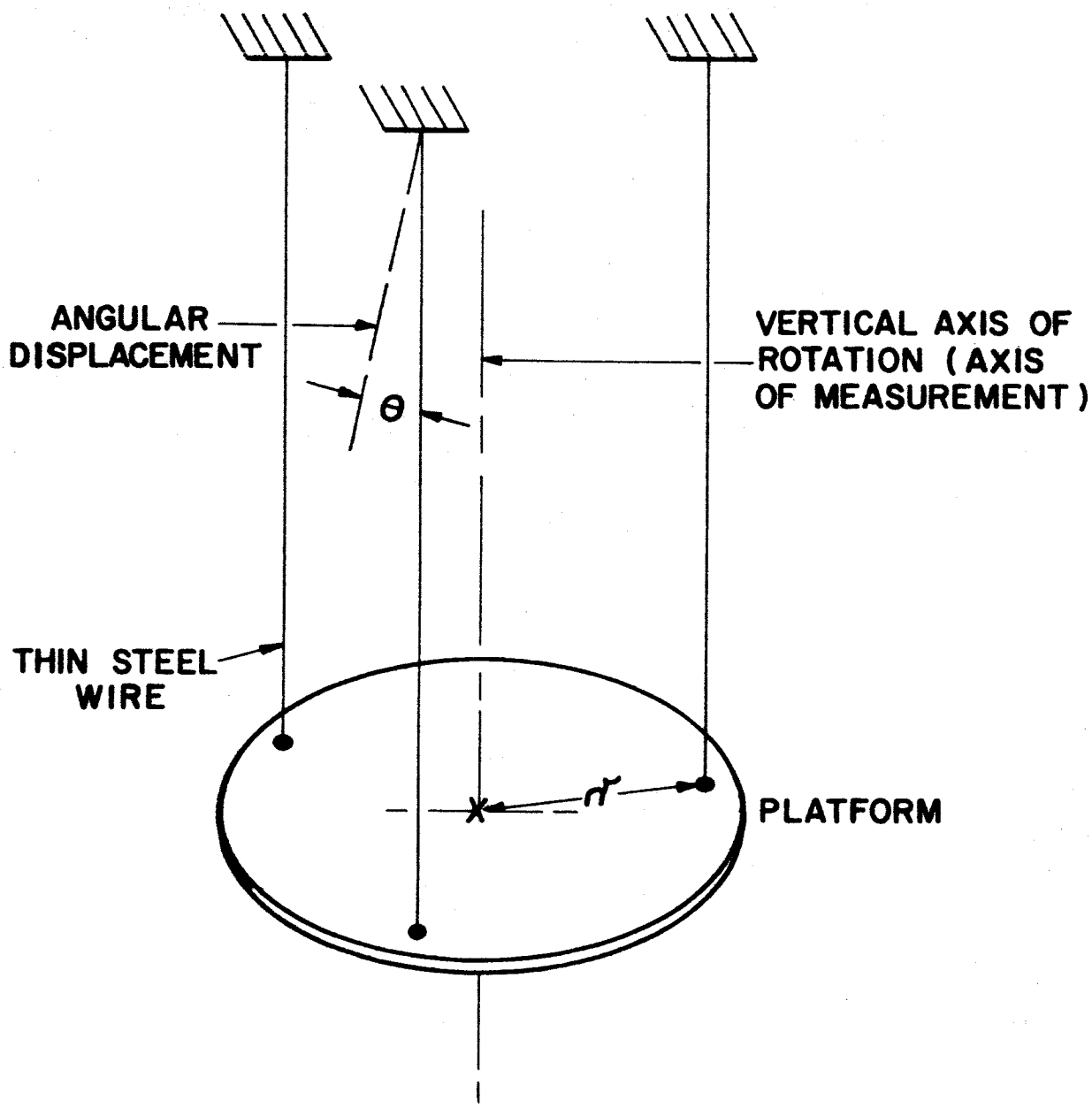

FIGURE 1

RELATIONSHIP BETWEEN DEGRADATION AND ELECTROLYTE PENETRATION FOR ELEVEN SINGLE - CELL TESTS

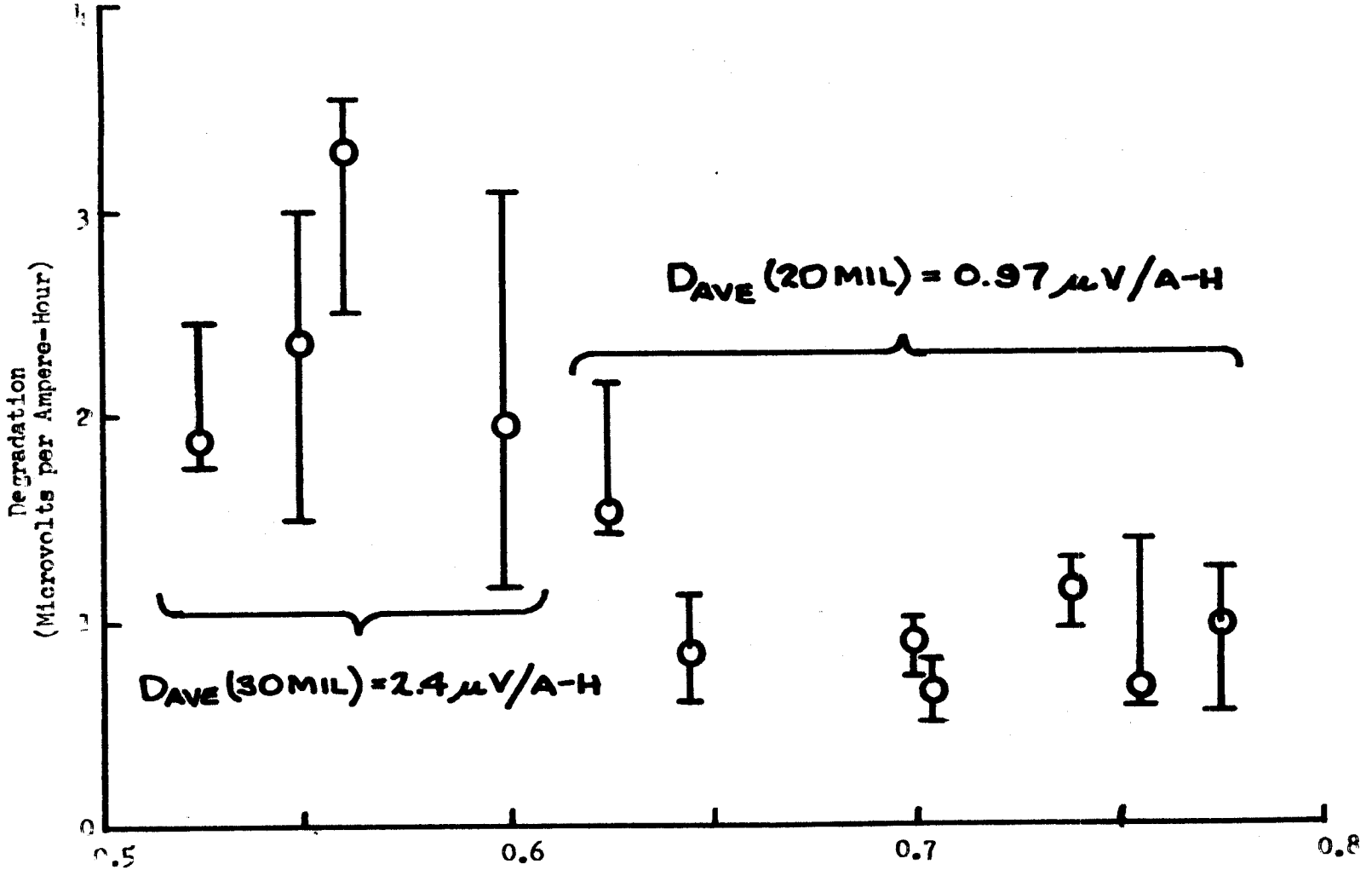

Electrolyte Penetration
(Percent of Electrode Pore Volume Filled With Electrolyte)

Figure 2

STACK # 74 VOLTAGE DECAY AS A FUNCTION OF PURGE CYCLE INTERVAL

REACTANT GASES:
OXYGEN CONTAINING 0.5% ARGON
HYDROGEN - ULTRA PURE

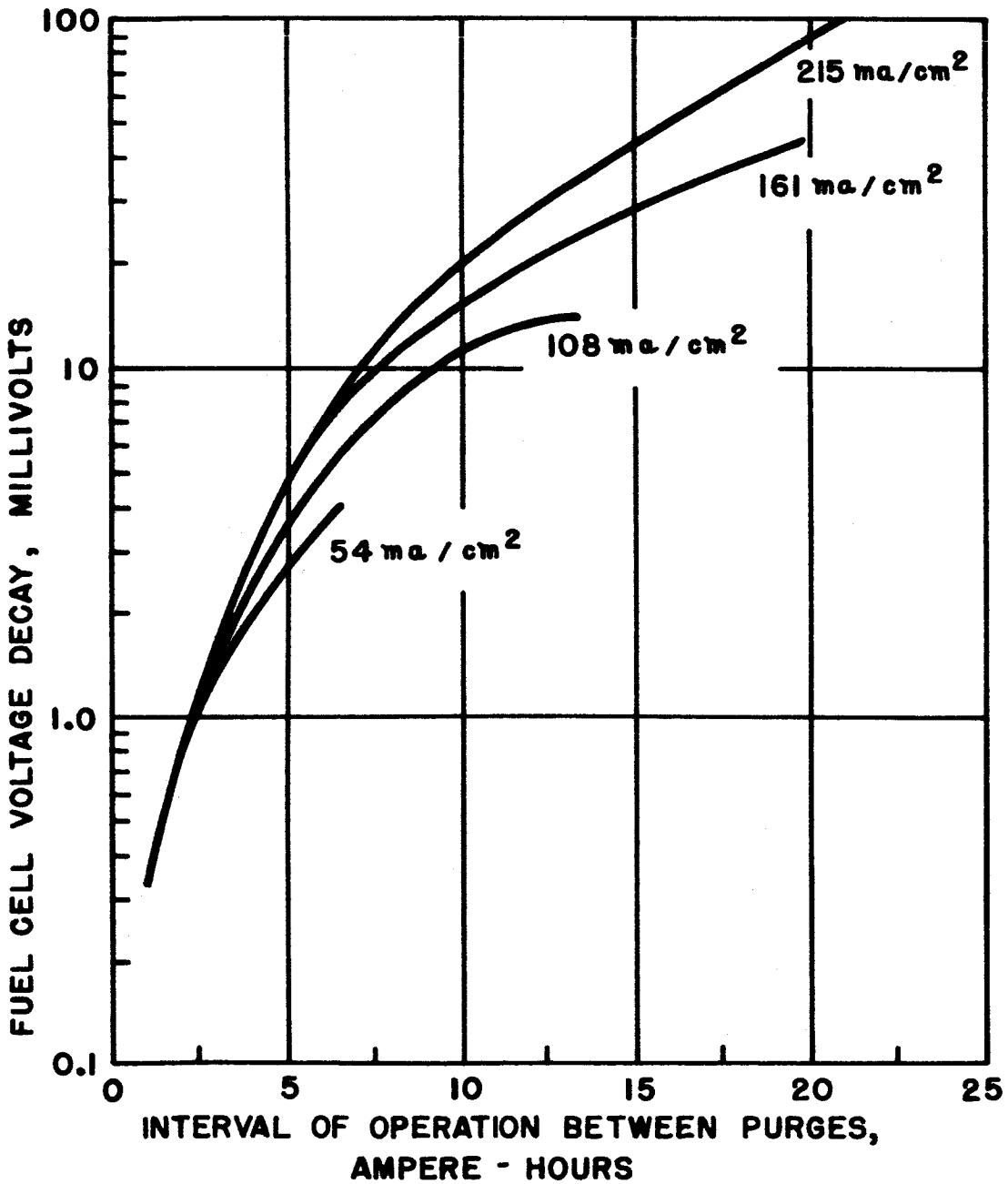

FIGURE 3

STACK #74 VOLTAGE DECAY AS A FUNCTION OF INERTS BUILD-UP TIME-CONSTANT LOAD CURRENT

REACTANT GASES:
OXYGEN CONTAINING 0.5% ARGON
HYDROGEN - ULTRA PURE

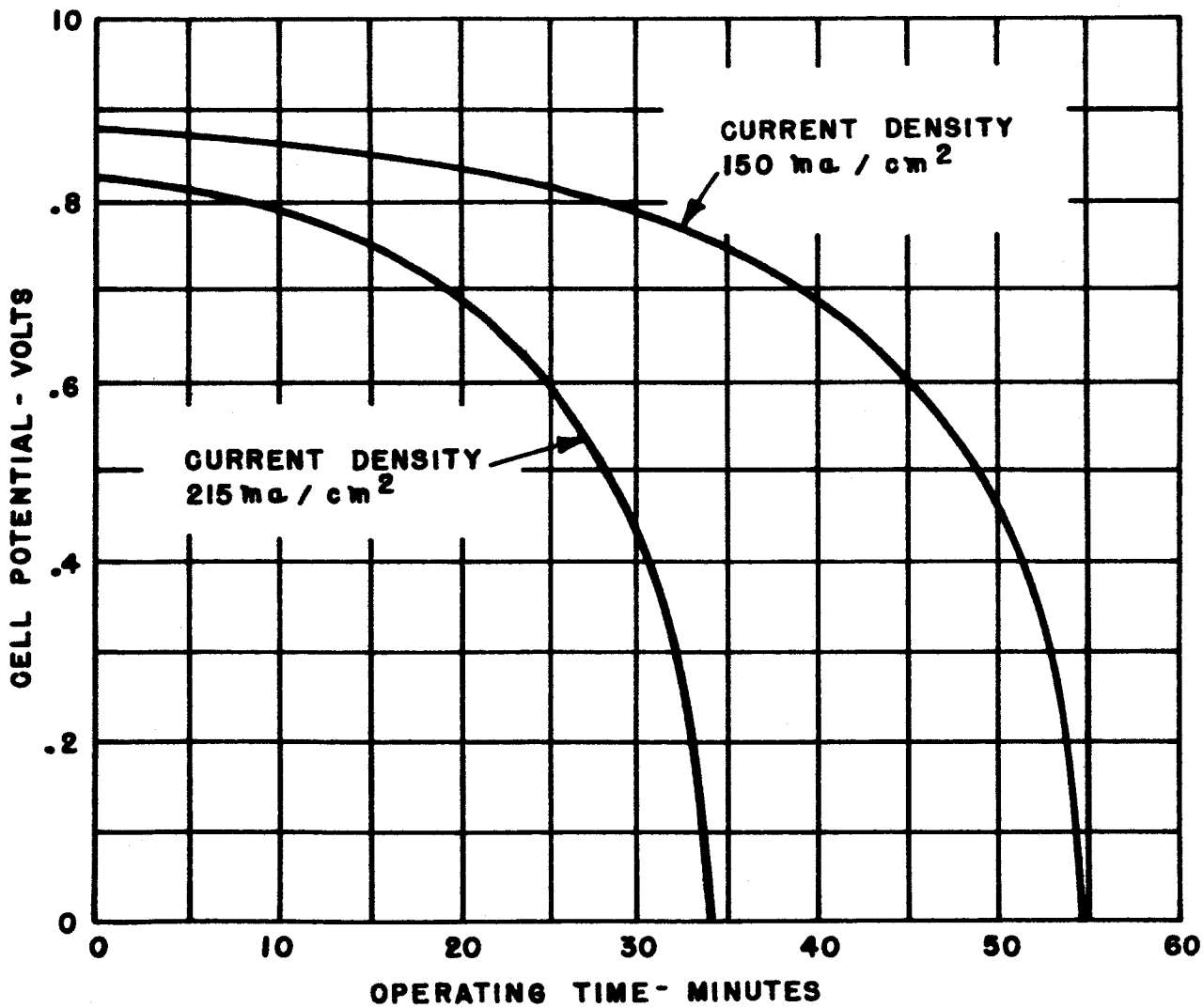

FIGURE 4

MODULE #74 VOLTAGE DECAY AS A FUNCTION OF INERTS BUILD-UP TIME - CONSTANT LOAD IMPEDANCE

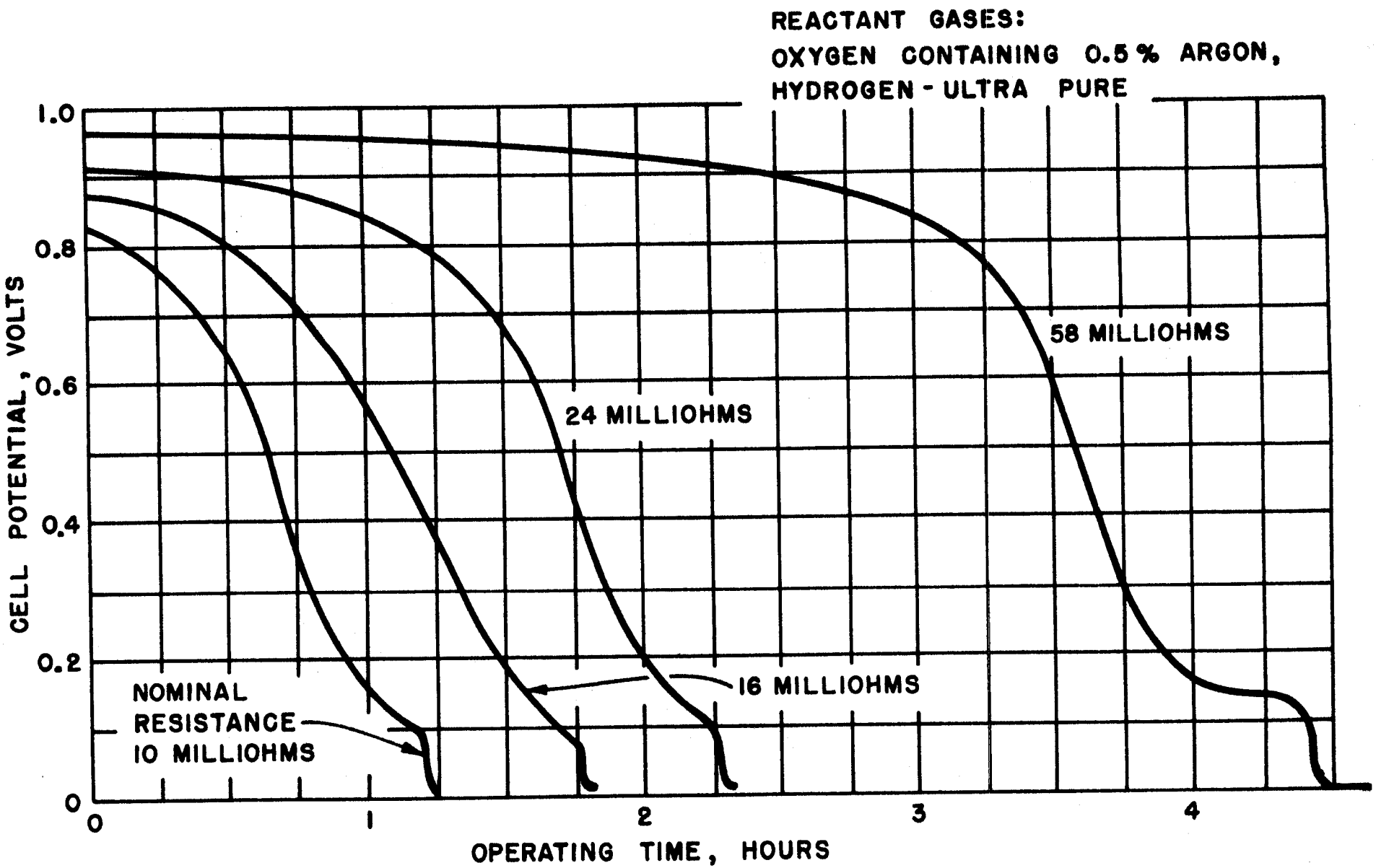

FIGURE 5

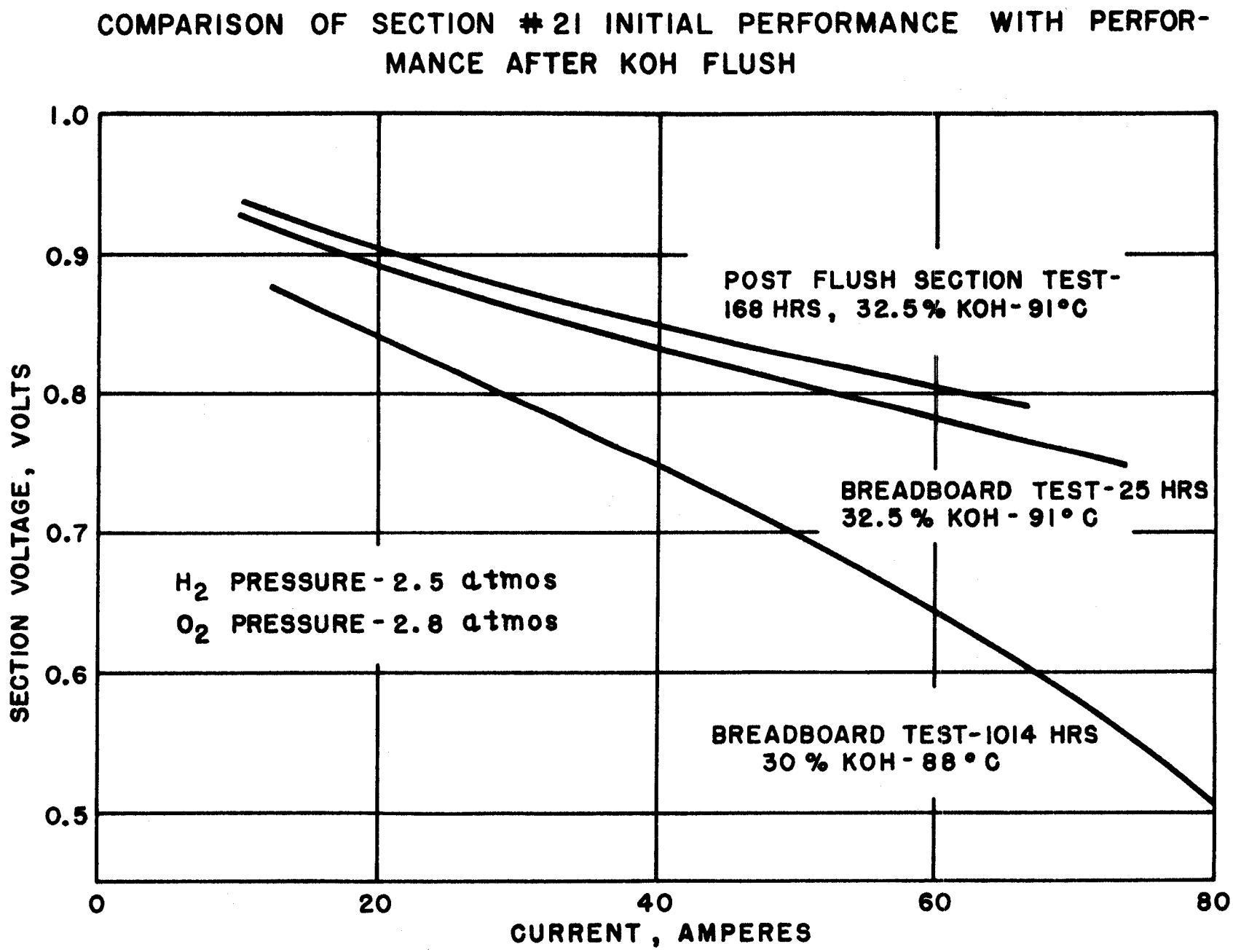
COMPARISON OF SECTION #21 INITIAL PERFORMANCE WITH PERFORMANCE AFTER KOH FLUSH
1.0
0.9
0.8
0.7
0.6
0.5
SECTION VOLTAGE, VOLTS
POST FLUSH SECTION TEST-
168 HRS, 32.5% KOH-91°C
BREADBOARD TEST-25 HRS
32.5 % KOH - 91° C
H_2 PRESSURE - 2.5 atmos
O_2 PRESSURE - 2.8 atmos
BREADBOARD TEST-1014 HRS
30 % KOH - 88 ° C
0
20
40
60
80
CURRENT, AMPERES

FIGURE 9

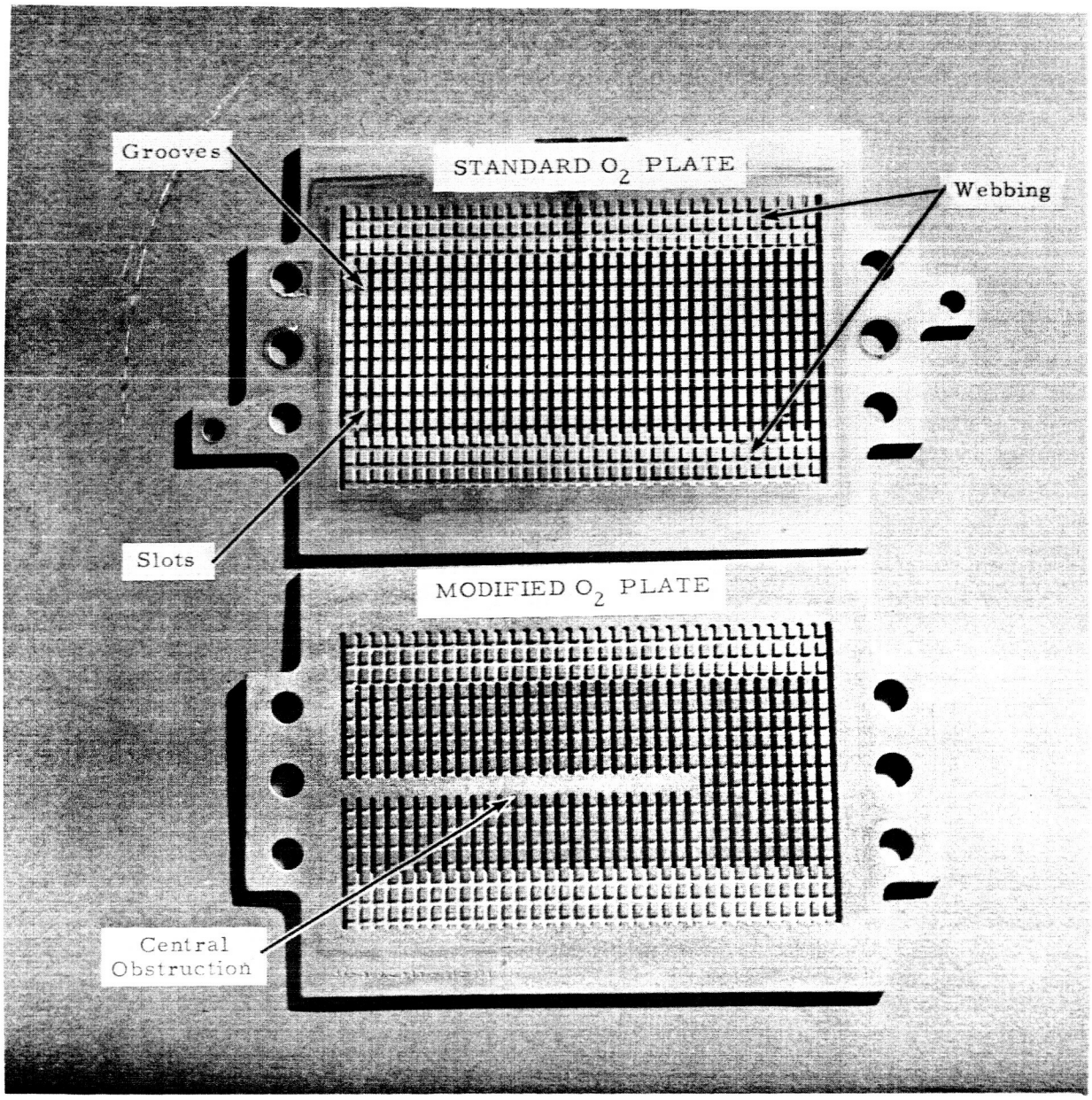

Figure 7 - Oxygen Plate Configuration

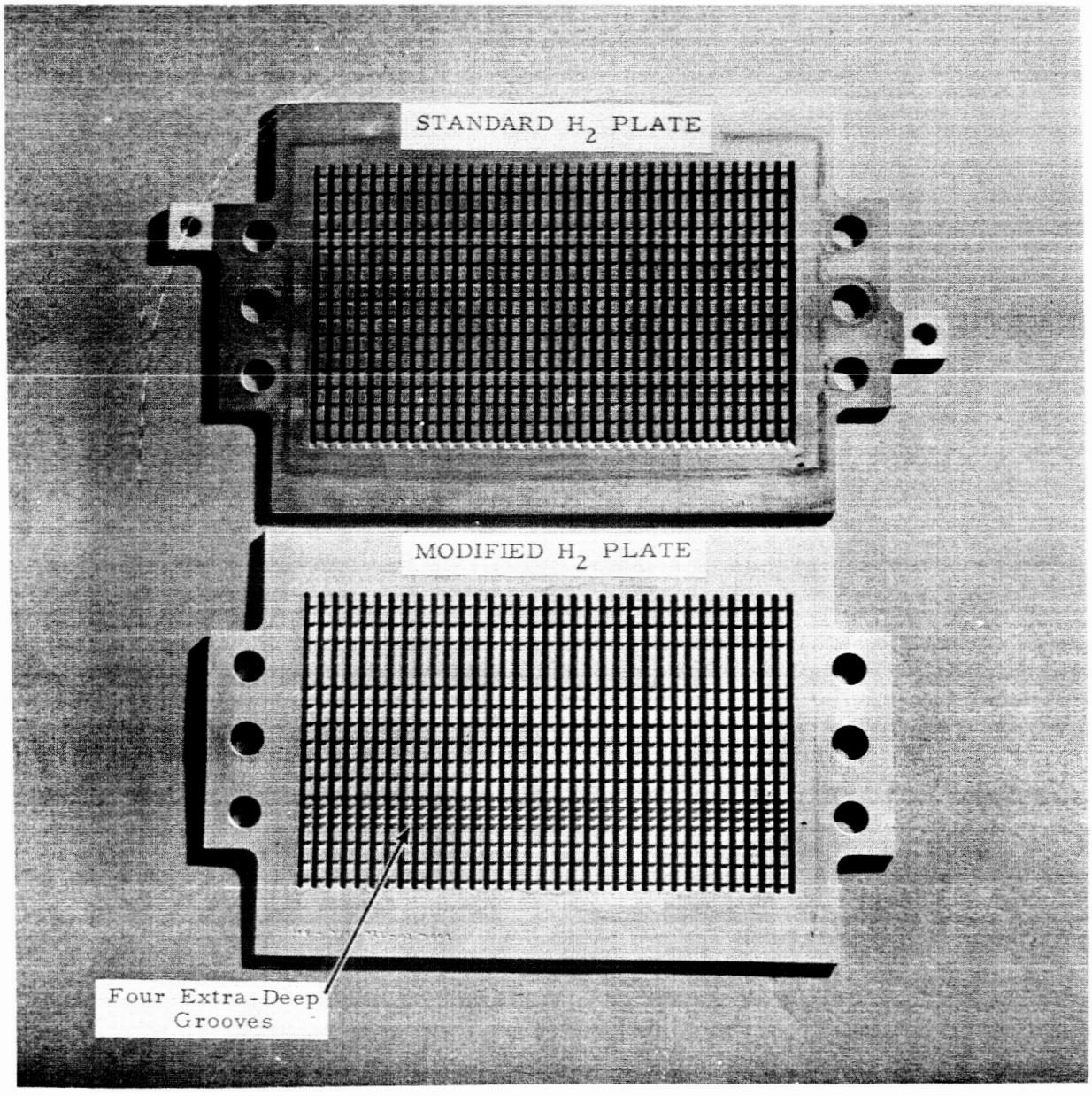

Figure 8 - Hydrogen Plate Configuration

STANDARD OXYGEN PLATE, NORMAL FLOW

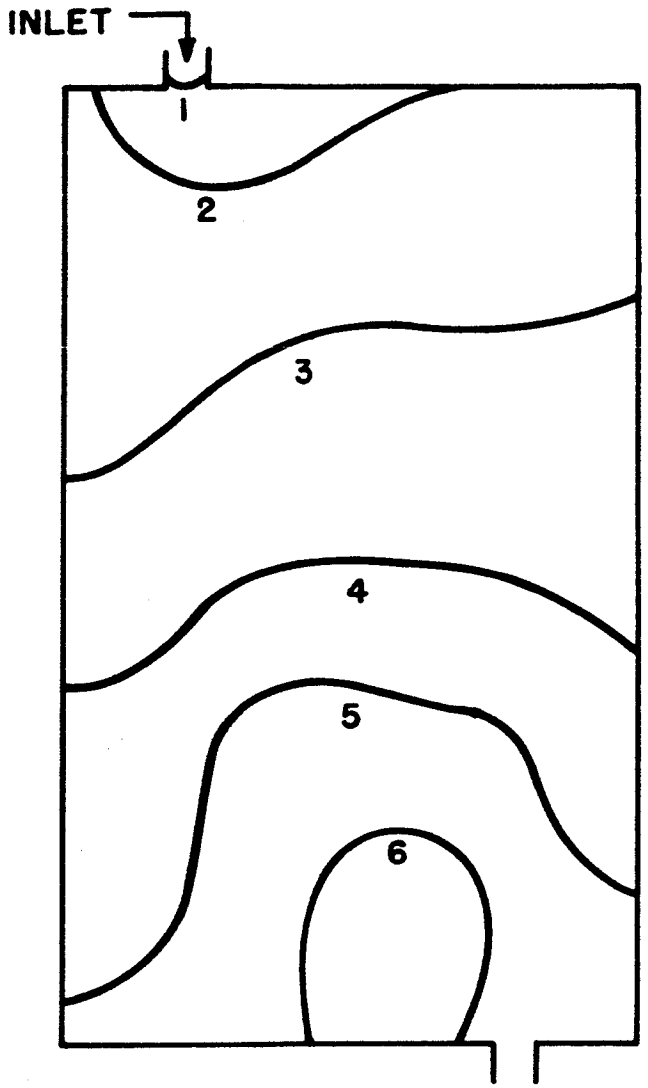

CURRENT = 50 AMPERES

PURGE = ZERO

CURVE	TIME
1	0.00 SEC.
2	0.63 SEC.
3	1.4 SEC.
4	3.7 SEC.
5	10.0 SEC.
6	26.3 SEC.

FIGURE 9

MODIFIED OXYGEN PLATE, NORMAL FLOW

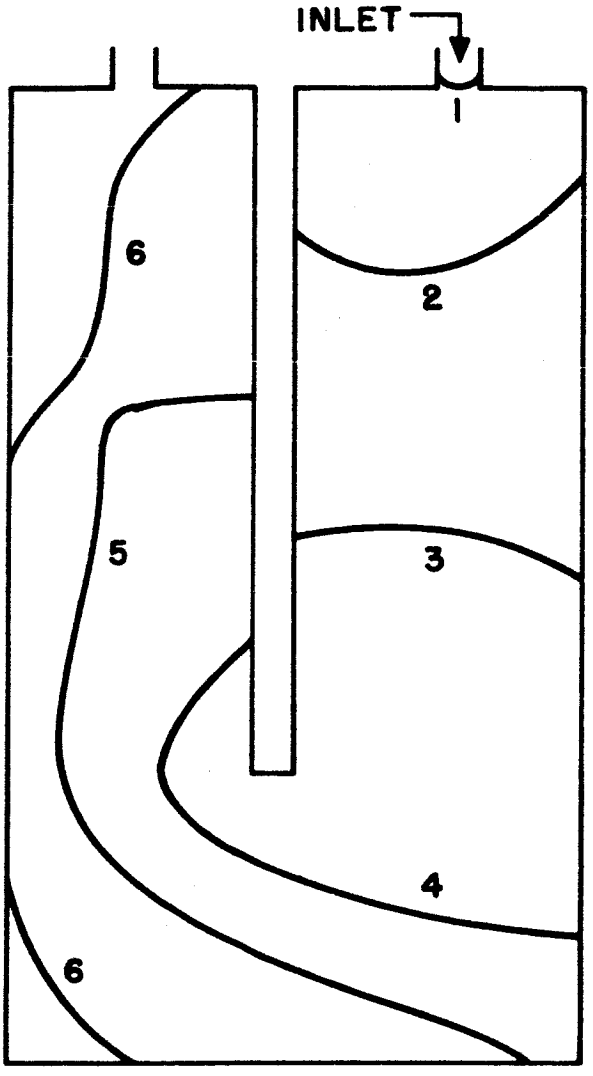

CURRENT = 51 AMPERES

PURGE = ZERO

CURVE	TIME
1	0.00 SEC.
2	0.63 SEC.
3	1.4 SEC.
4	3.7 SEC.
5	10.0 SEC.
6	26.3 SEC.

FIGURE 10

STANDARD OXYGEN PLATE, PURGE

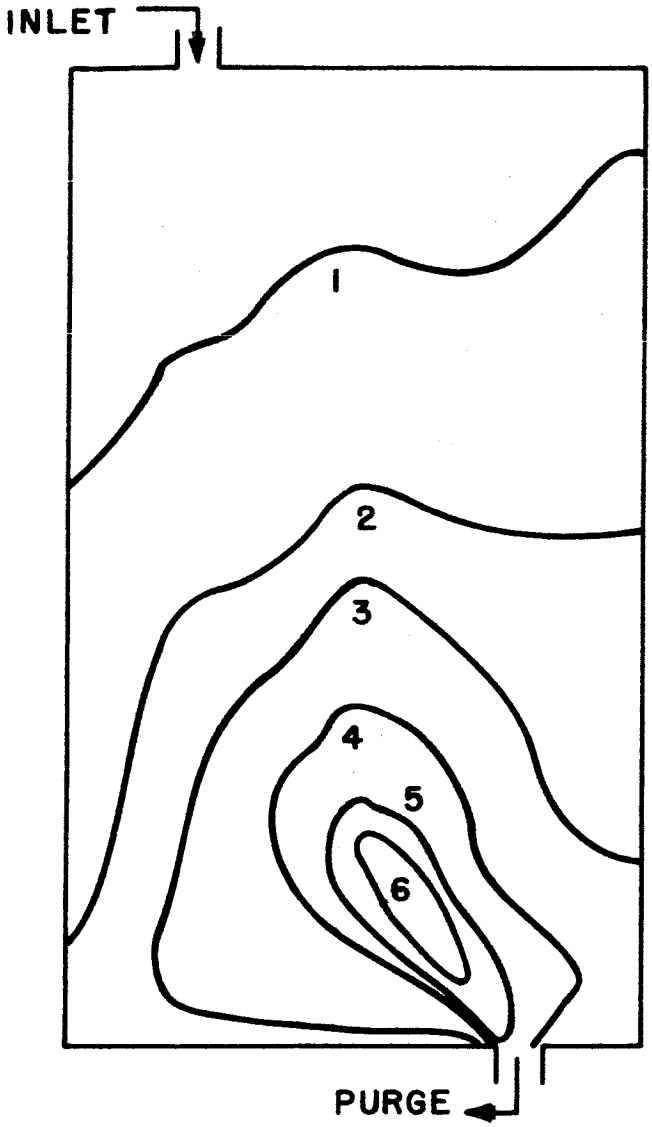

CURRENT = 35 AMPERES

PURGE = 1.5

CURVE	TIME
1	1.0 SEC.
2	2.0 SEC.
3	3.0 SEC.
4	4.0 SEC.
5	5.0 SEC.
6	6.0 SEC.

FIGURE 11

MODIFIED OXYGEN PLATE, PURGE

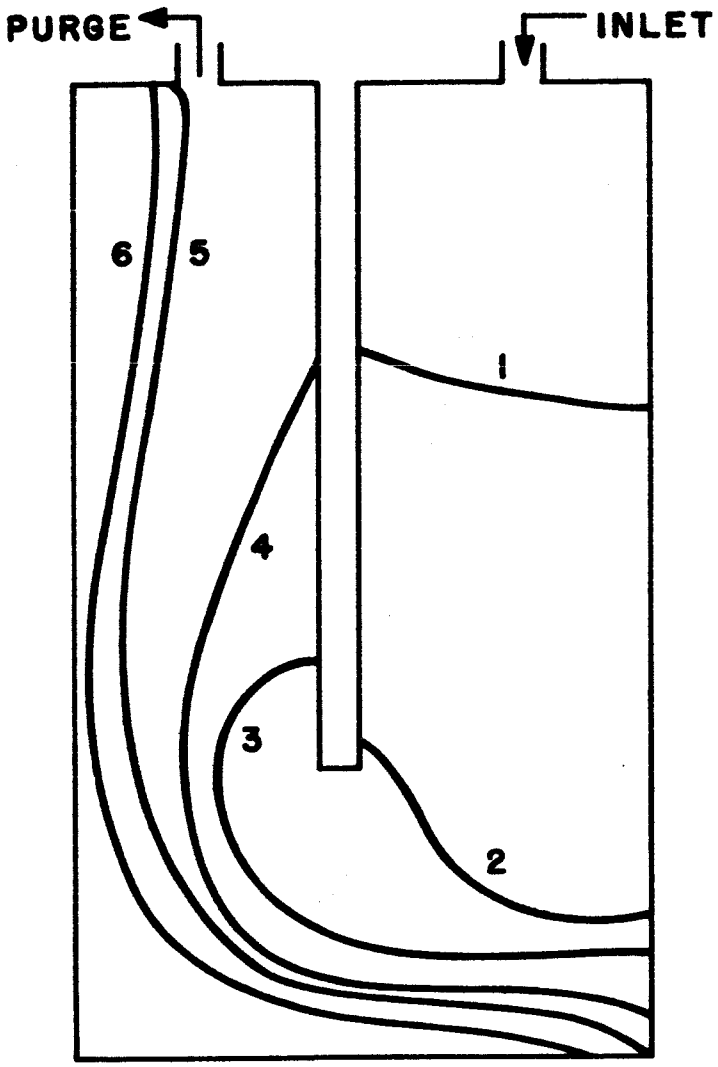

CURRENT = 35 AMPERES

PURGE = 1.6

CURVE	TIME
1	1.0 SEC.
2	2.0 SEC.
3	3.0 SEC.
4	4.0 SEC.
5	5.0 SEC.
6	6.0 SEC.

FIGURE 12

STANDARD HYDROGEN PLATE, NORMAL FLOW

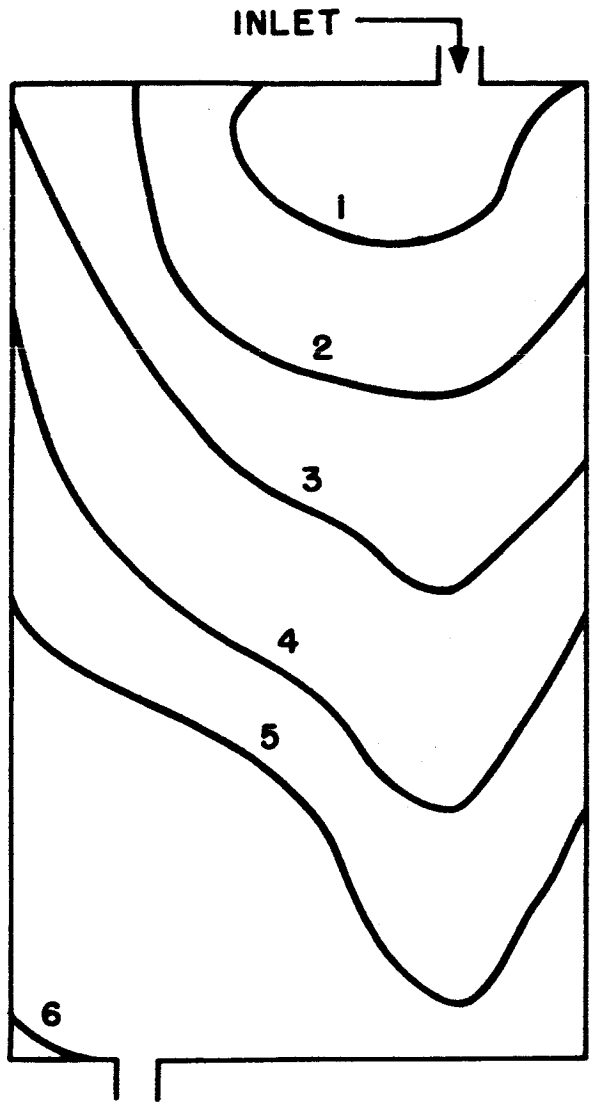

CURRENT = 51 AMPERES

PURGE = ZERO

CURVE	TIME
1	1.0 SEC.
2	3.0 SEC.
3	5.0 SEC.
4	7.5 SEC.
5	10.0 SEC.
6	22.0 SEC.

FIGURE 13

MODIFIED HYDROGEN PLATE, NORMAL FLOW

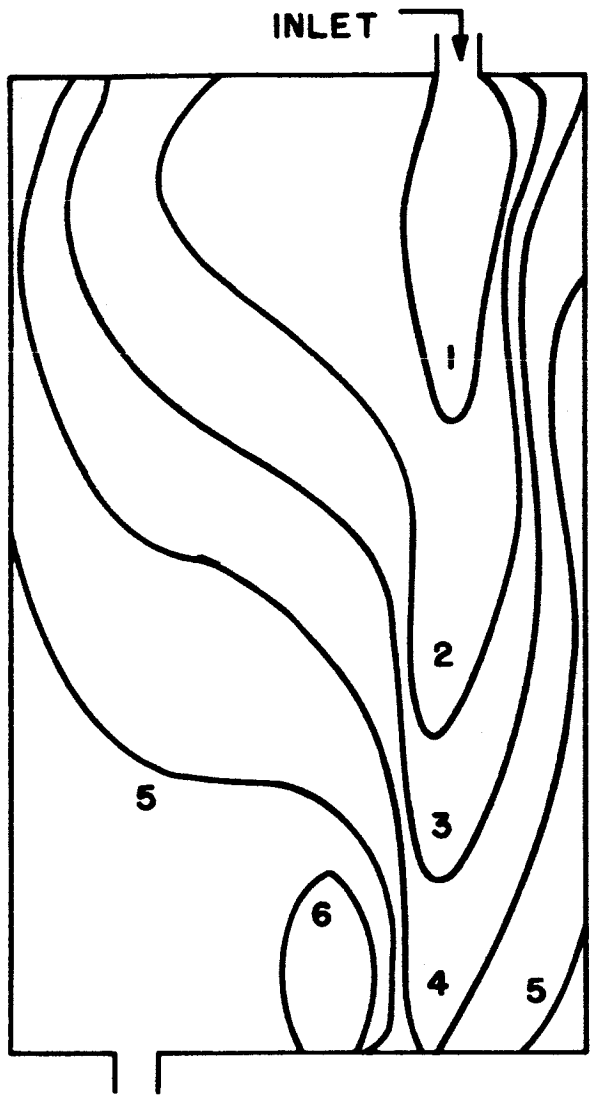

CURRENT = 49 AMPERES

PURGE = ZERO

CURVE	TIME
1	1.0 SEC.
2	3.0 SEC.
3	5.0 SEC.
4	7.5 SEC.
5	10.0 SEC.
6	22.0 SEC.

FIGURE 14

STANDARD HYDROGEN PLATE, PURGE

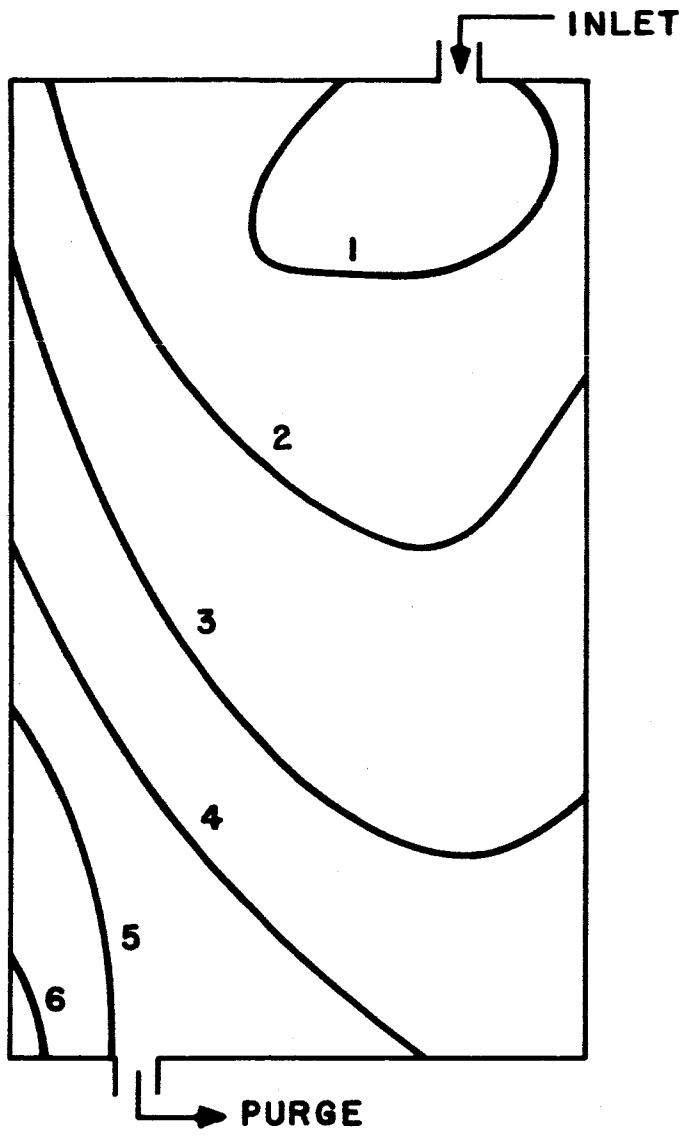

CURRENT = 31 AMPERES

PURGE = 1.5

CURVE	TIME
1	1.0 SEC.
2	2.0 SEC.
3	3.0 SEC.
4	4.0 SEC.
5	5.0 SEC.
6	6.0 SEC.

FIGURE 15

MODIFIED HYDROGEN PLATE, PURGE

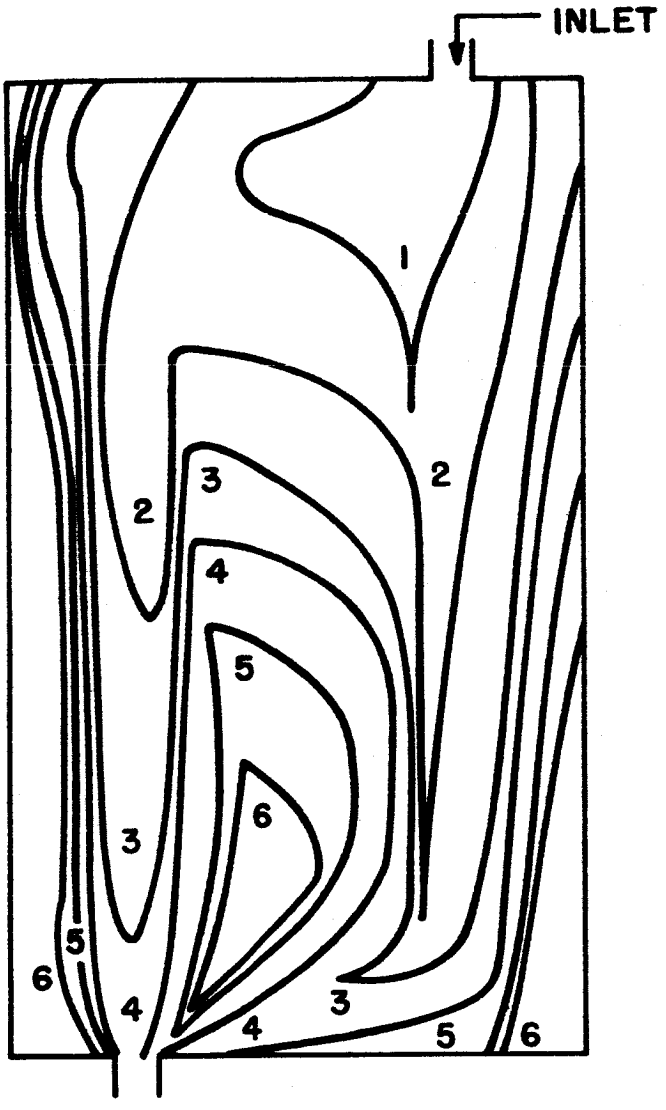

CURRENT = 30 AMPERES

PURGE = 1.5

CURVE	TIME
1	1.0 SEC.
2	2.0 SEC.
3	3.0 SEC.
4	4.0 SEC.
5	5.0 SEC.
6	6.0 SEC.

FIGURE 16

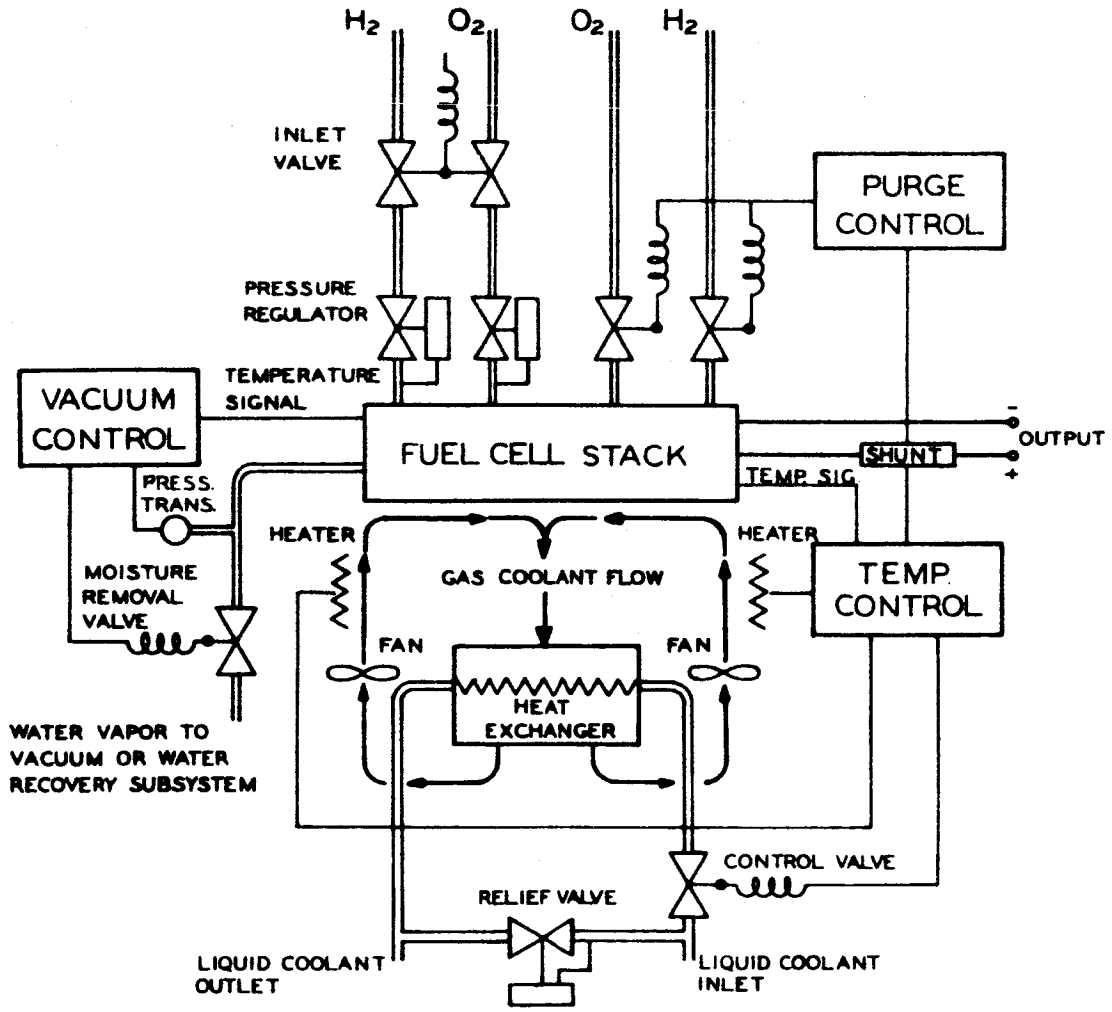

FIGURE 17- FUEL CELL POWER SYSTEM SCHEMATIC DIAGRAM

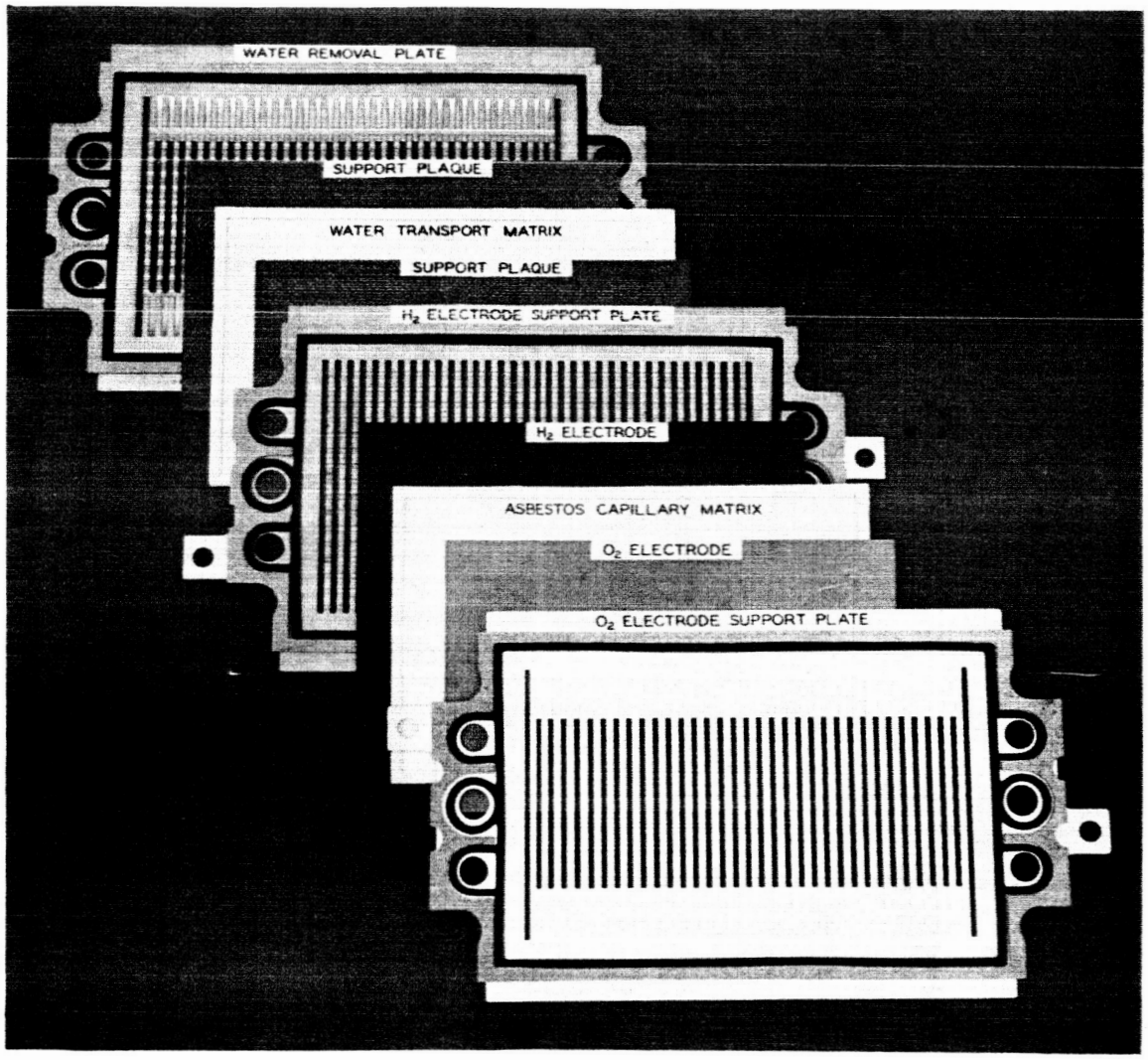

CELL CONSTRUCTION. The cell consists of two porous electrodes separated by an asbestos capillary matrix, which holds the aqueous potassium hydroxide (KOH) electrolyte. The electrode support plates provide passageways for distributing the reactants to the cell, and serve as current collectors and terminals for the electrodes. Product water is removed via the water transport matrix and the water removal plate as water vapor. When assembled, the plates extend slightly beyond the cell, thus serving as cooling fins for removing waste heat.

Figure 18

REPRESENTATIVE FUEL CELL PERFORMANCE AT VARIOUS
ELECTROLYTE CONCENTRATIONS
(20 MIL - SINGLE CELL)

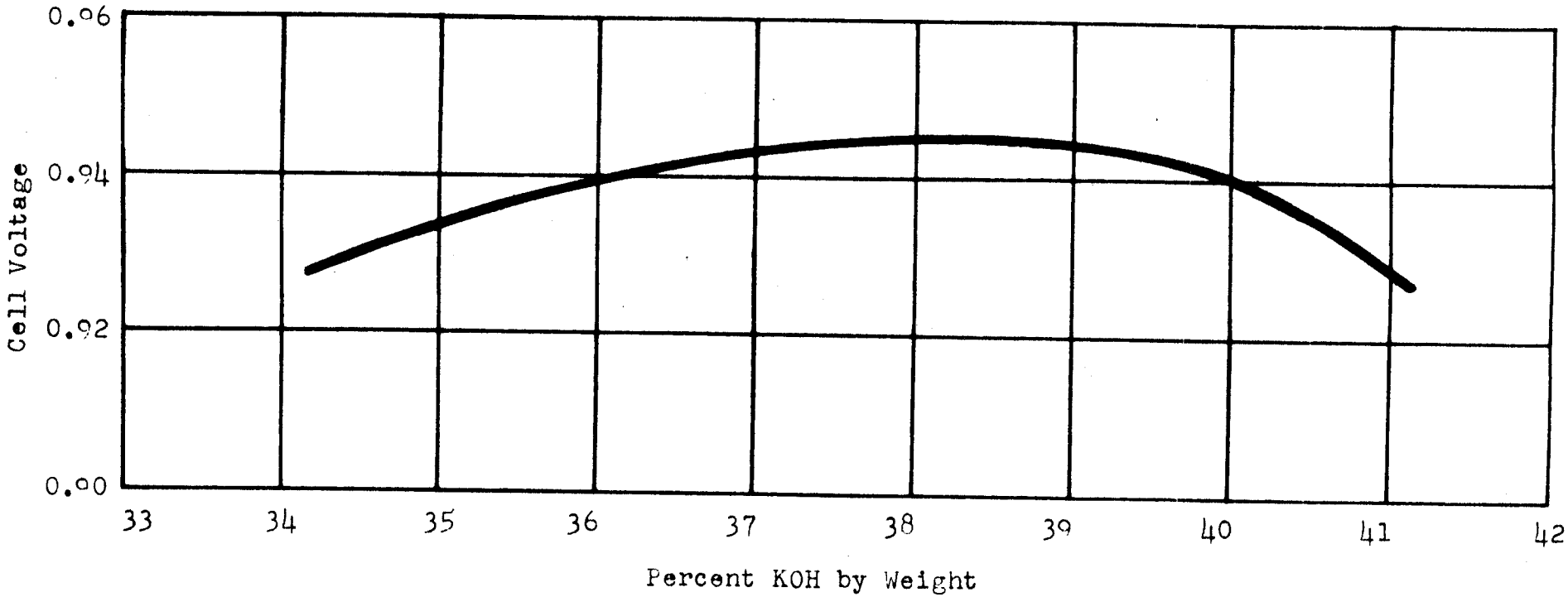

Cell Temperature - 190°F.
Cell Pressure - 37 psia
Current Density - 100 ASF

Figure 19

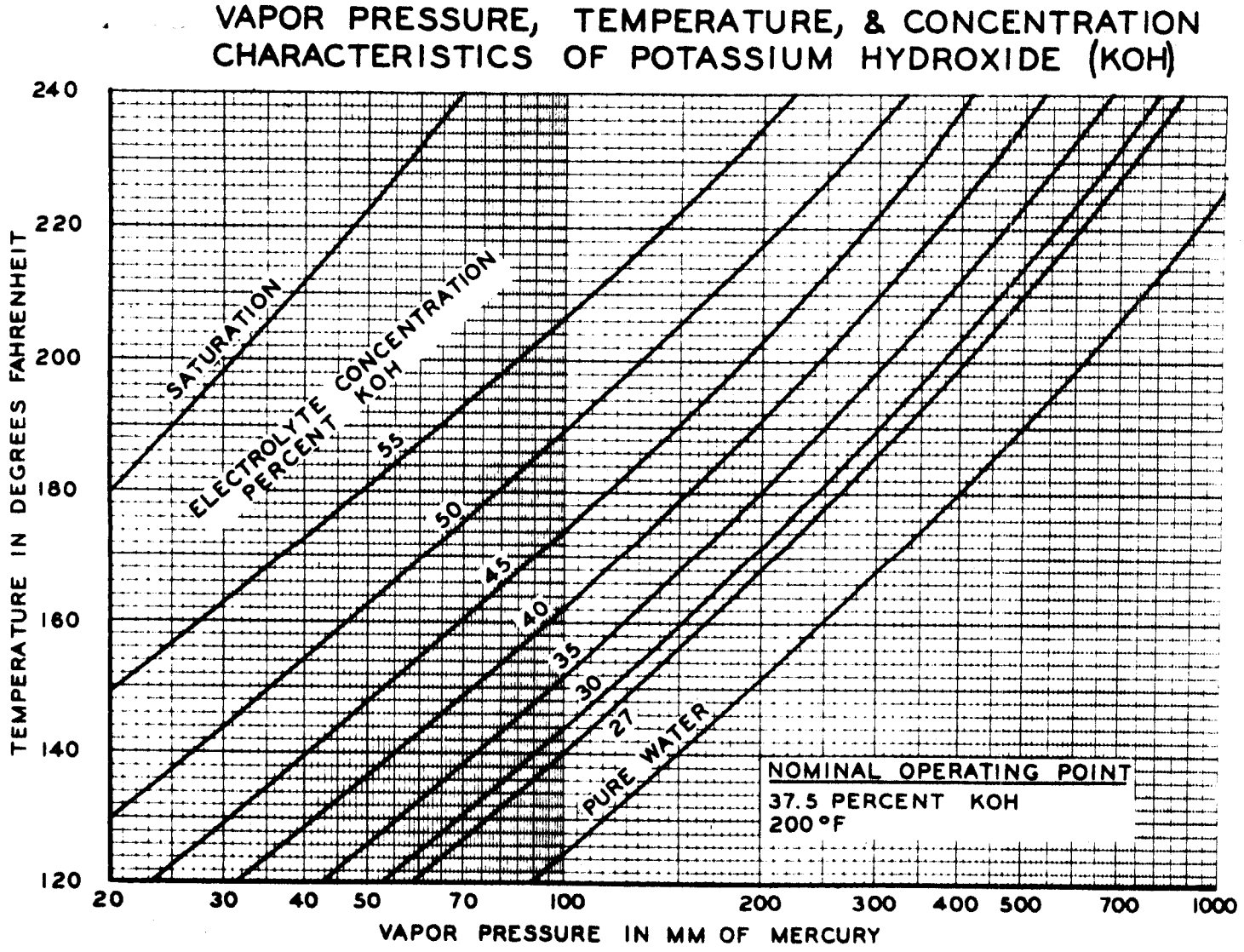
VAPOR PRESSURE, TEMPERATURE, & CONCENTRATION CHARACTERISTICS OF POTASSIUM HYDROXIDE (KOH)
TEMPERATURE IN DEGREES FAHRENHEIT
240
220
200
180
160
140
120
SATURATION
ELECTROLYTE CONCENTRATION PERCENT KOH
55
50
45
40
35
30
27
PURE WATER
NOMINAL OPERATING POINT
37.5 PERCENT KOH
200°F
20
30
40
50
70
100
200
300
400
500
700
1000
VAPOR PRESSURE IN MM OF MERCURY

Figure 20

CELL CONSTRUCTION SHOWING TYPICAL KOH GRADIENTS

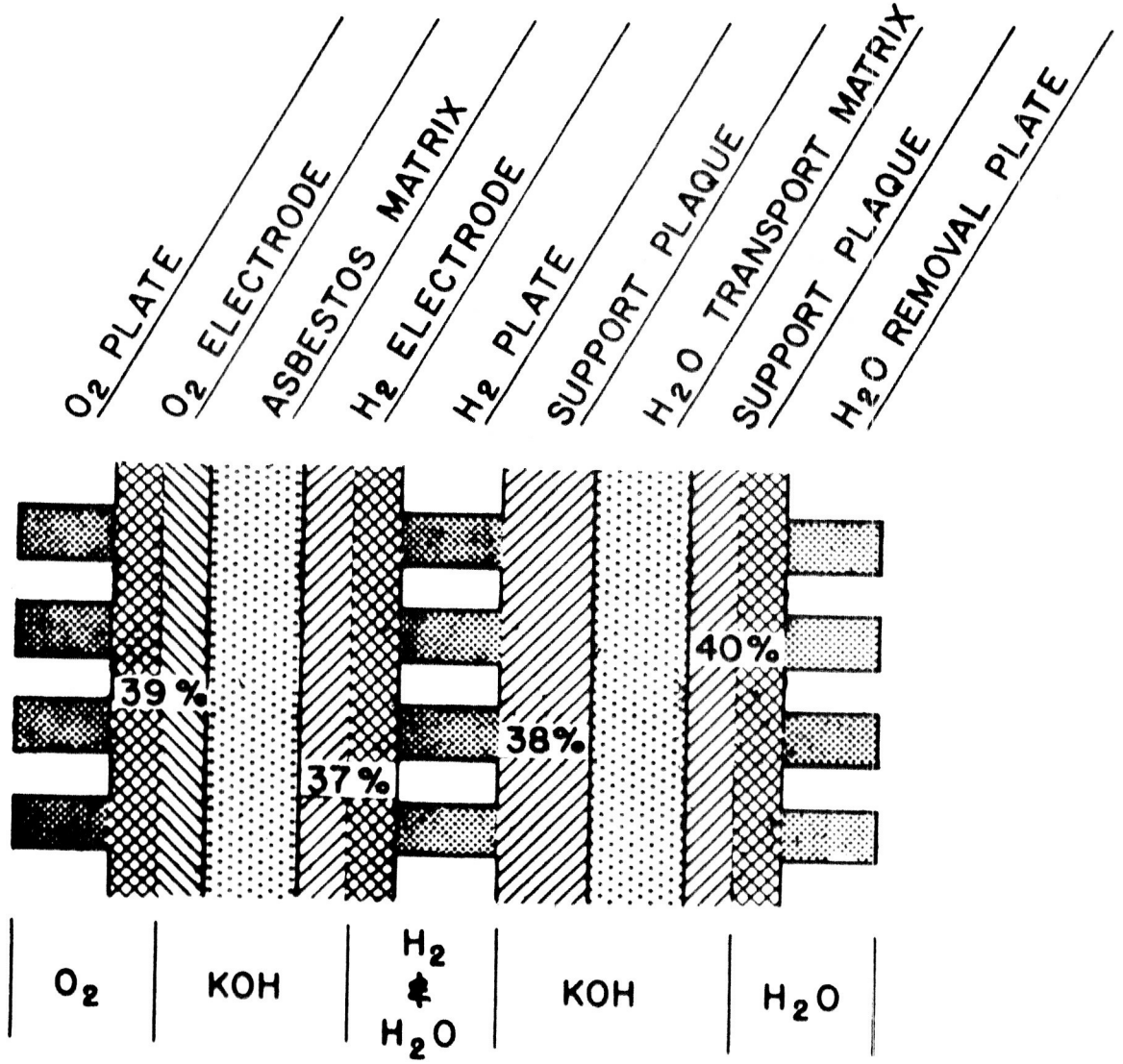

Figure 21

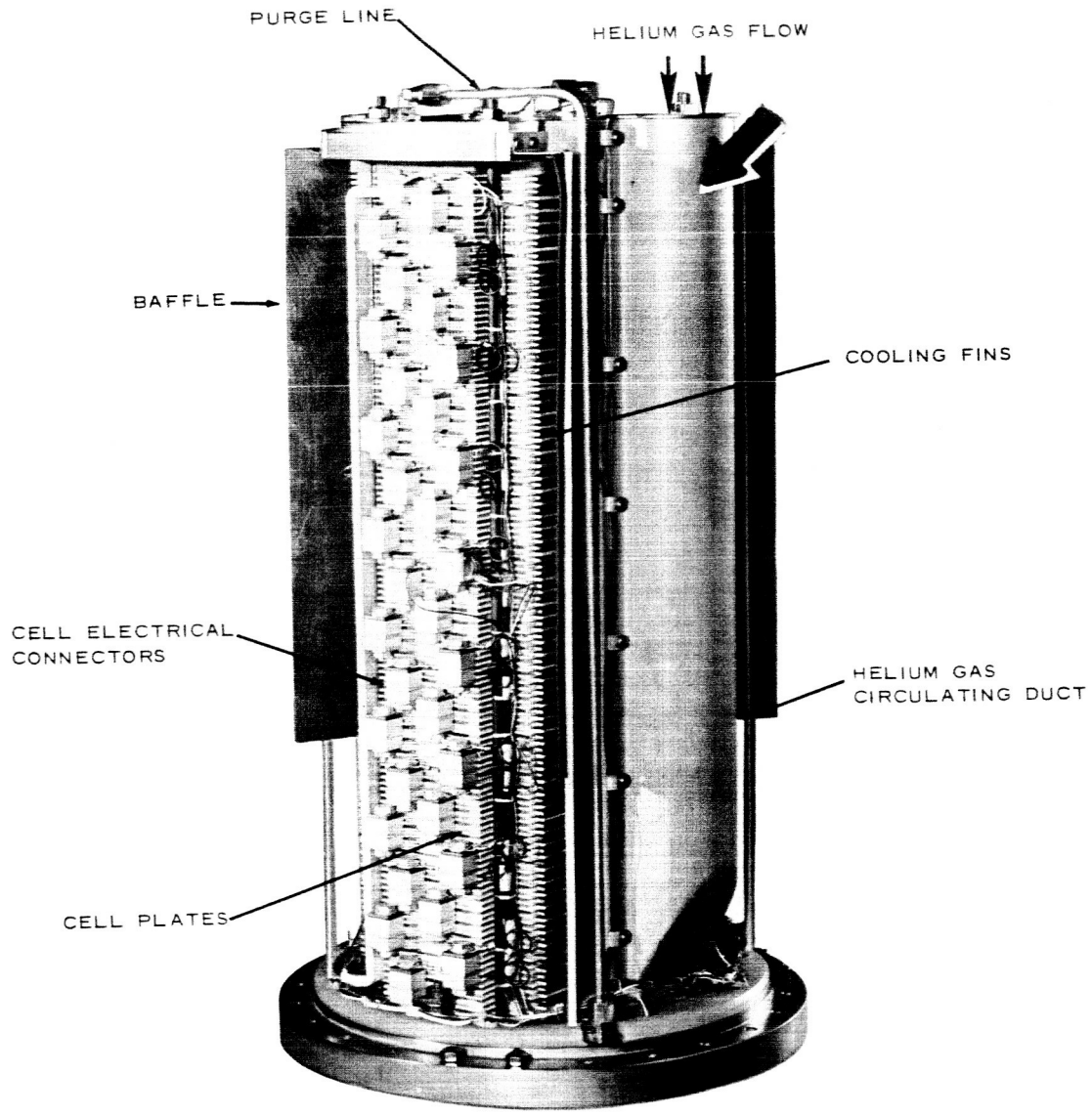

FUEL CELL STACK. The stack, the power producing element of the system, consists of 33 two-cell sections. Each cell has an effective electro-chemical reaction area of 0.2 square foot. By-product water is removed from the stack in the vapor state using a simple and characteristically stable static moisture removal technique. Plastic ducts (arrow) direct coolant gas over the cell edges for thermal conditioning.

Figure 22

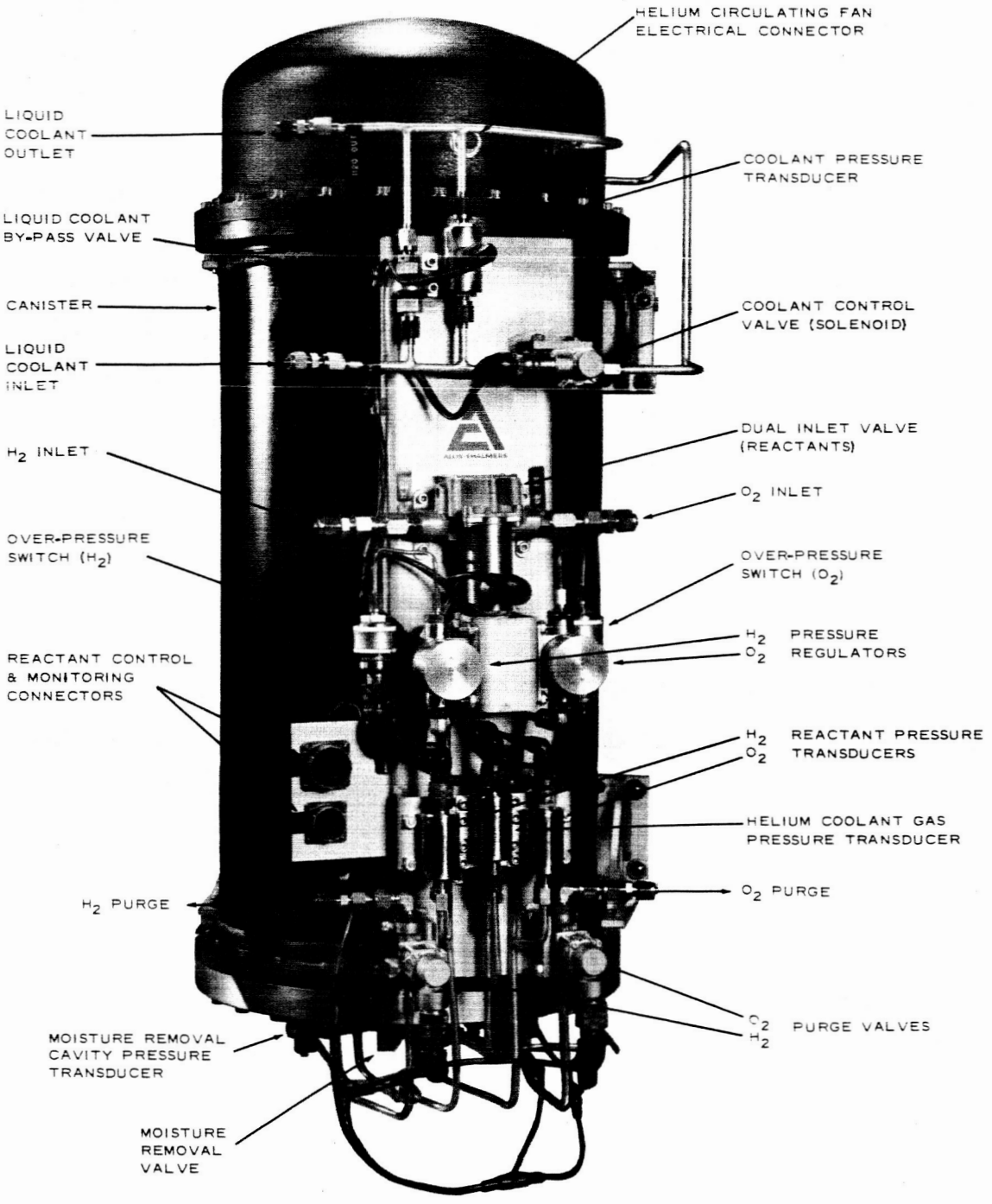

Figure 23 - Fuel Cell Assembly

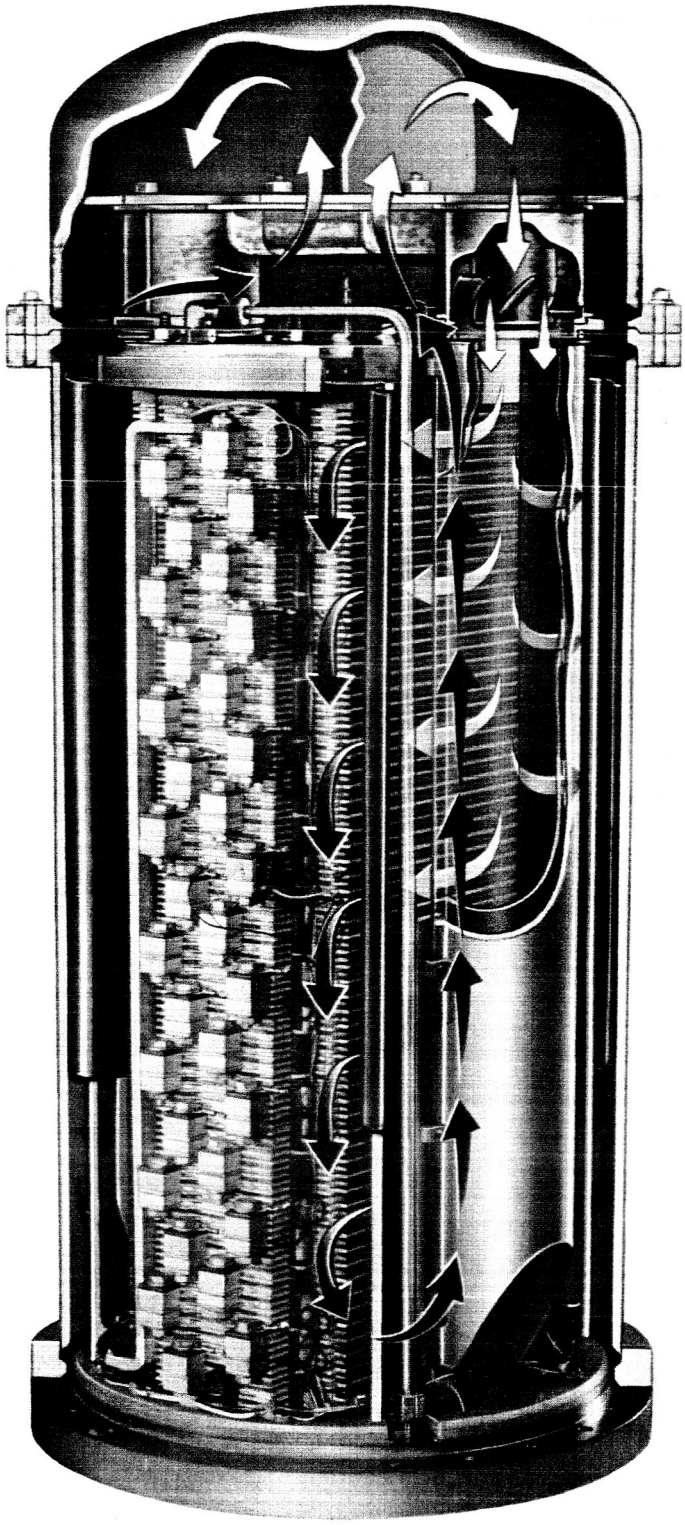

Figure 24 - Gas Coolant Flow Diagram

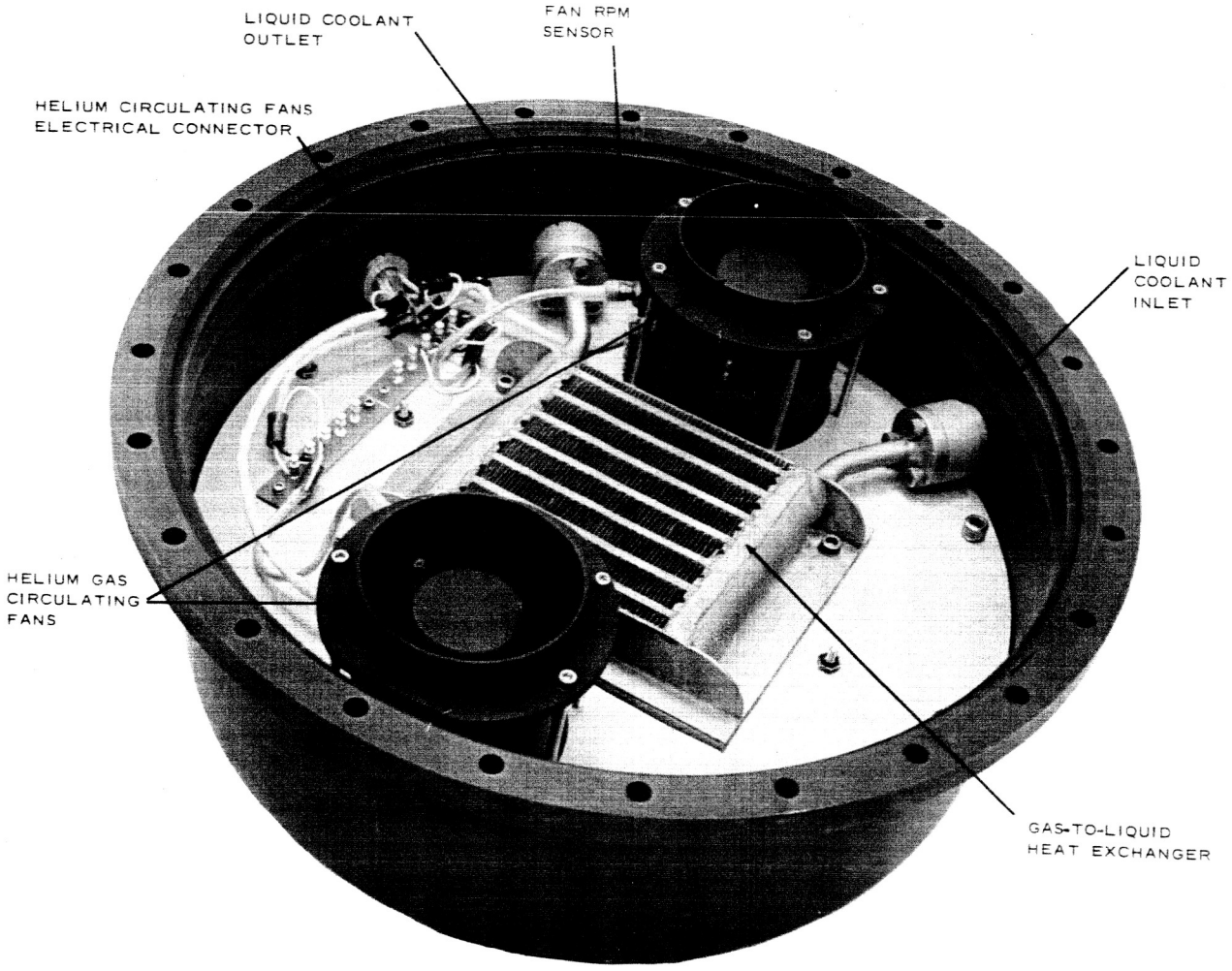

THERMAL CONTROL AND CONDITIONING. Circulating fans and a gas-to-liquid heat exchanger, mounted in the canister dome, provide thermal conditioning for the stack. The fans circulate helium gas through distribution ducts, over protruding cell fins, and then through the heat exchanger. Stack temperature is maintained by controlling the flow of liquid coolant through the heat exchanger.

Figure 25

THERMAL CONDITIONING AND CONTROL SUBSYSTEM (TCCS)

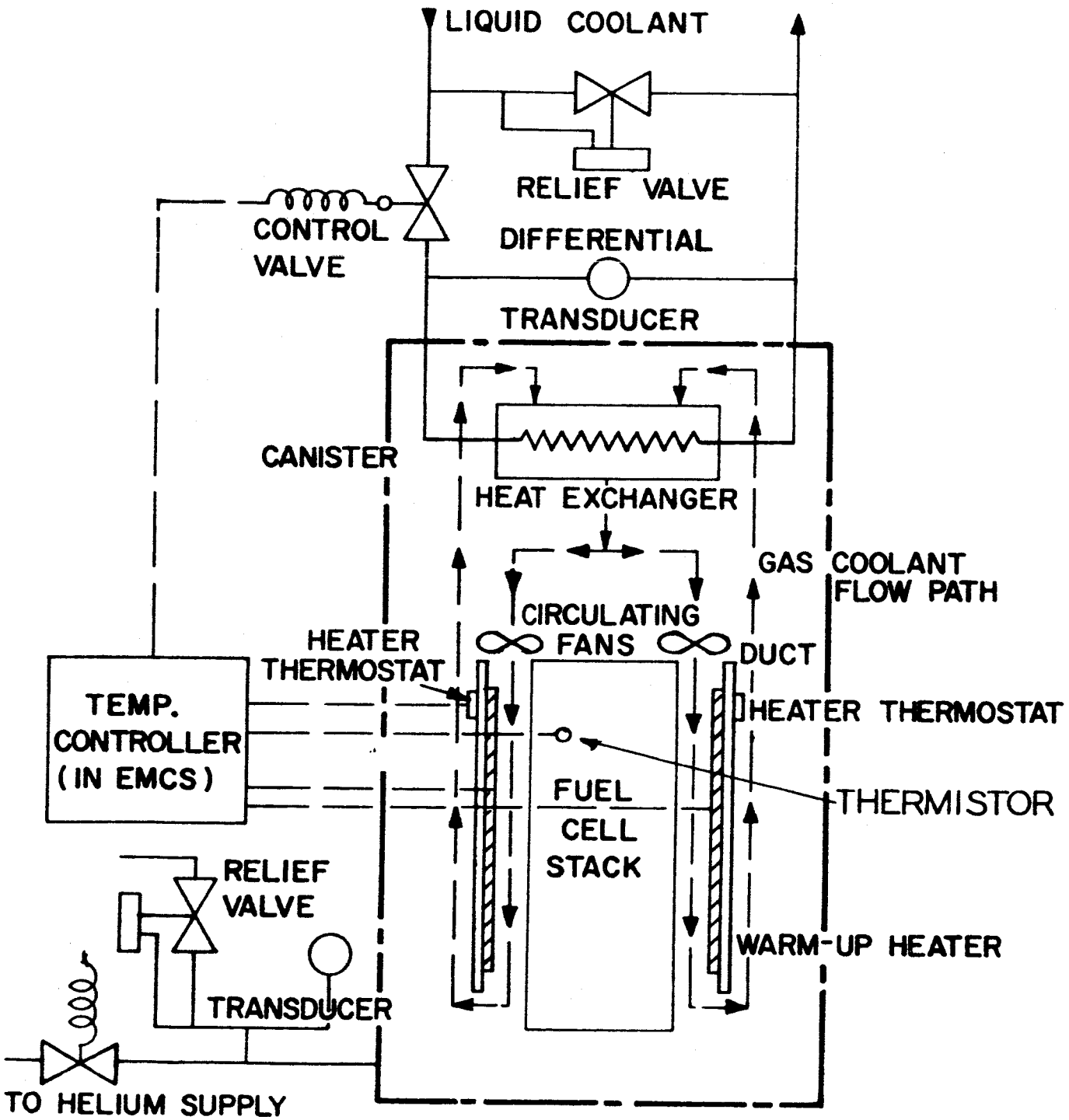

Figure 26

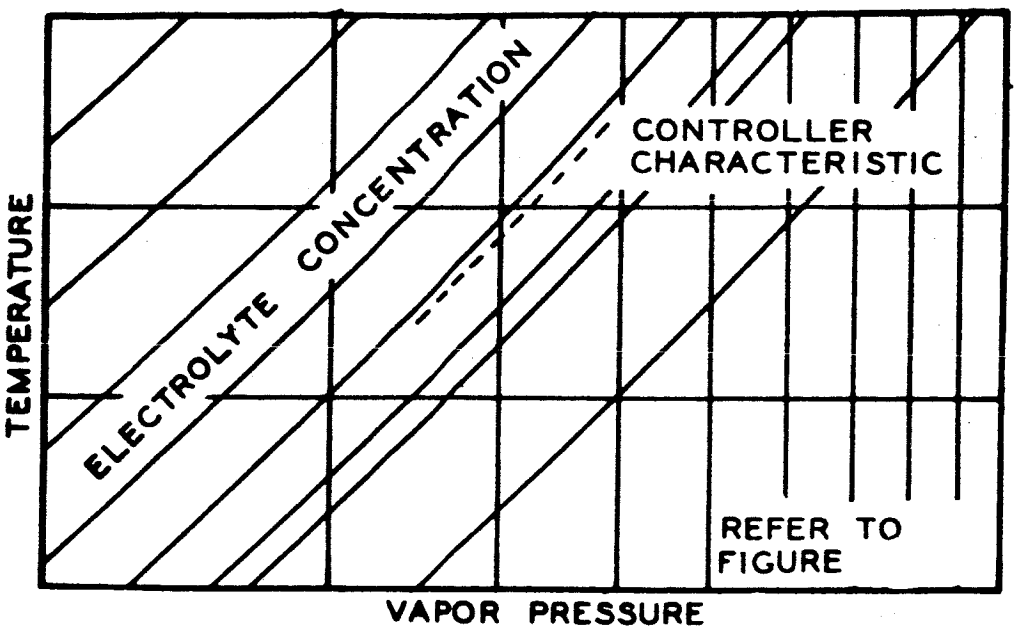

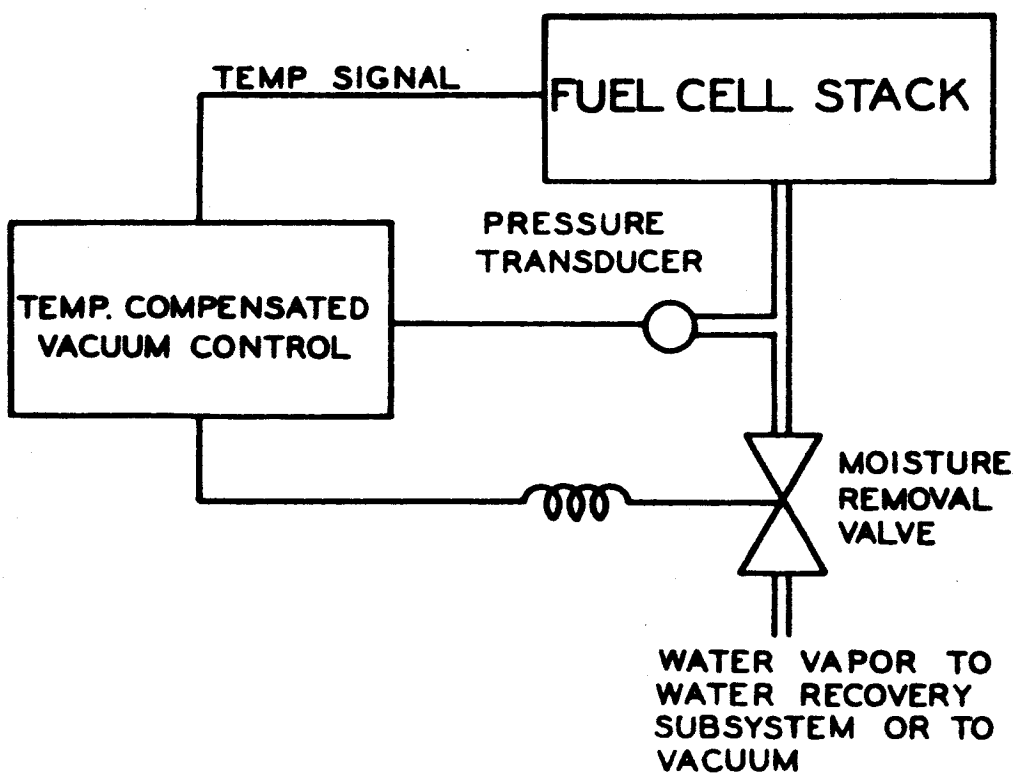

MOISTURE REMOVAL CONTROL

Figure 27

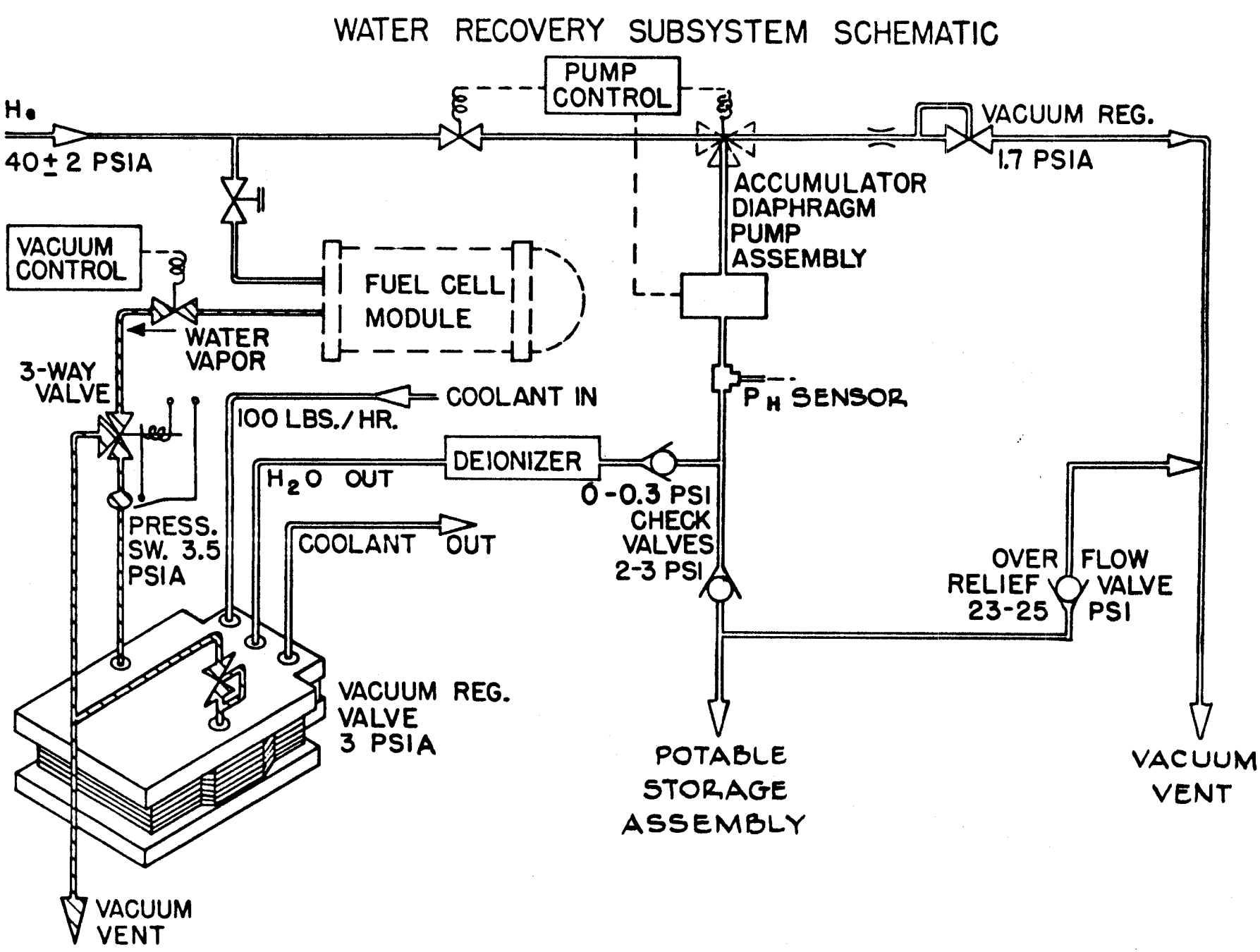
WATER RECOVERY SUBSYSTEM SCHEMATIC
PUMP CONTROL
H2
40 ± 2 PSIA
VACUUM REG.
1.7 PSIA
ACCUMULATOR DIAPHRAGM PUMP ASSEMBLY
VACUUM CONTROL
FUEL CELL MODULE
WATER VAPOR
3-WAY VALVE
COOLANT IN
100 LBS./HR.
PH SENSOR
DEIONIZER
H2O OUT
0-0.3 PSI CHECK VALVES 2-3 PSI
PRESS. SW. 3.5 PSIA
COOLANT OUT
OVER RELIEF 23-25 PSI
FLOW VALVE
VACUUM REG. VALVE 3 PSIA
POTABLE STORAGE ASSEMBLY
VACUUM VENT
VACUUM VENT

Figure 28

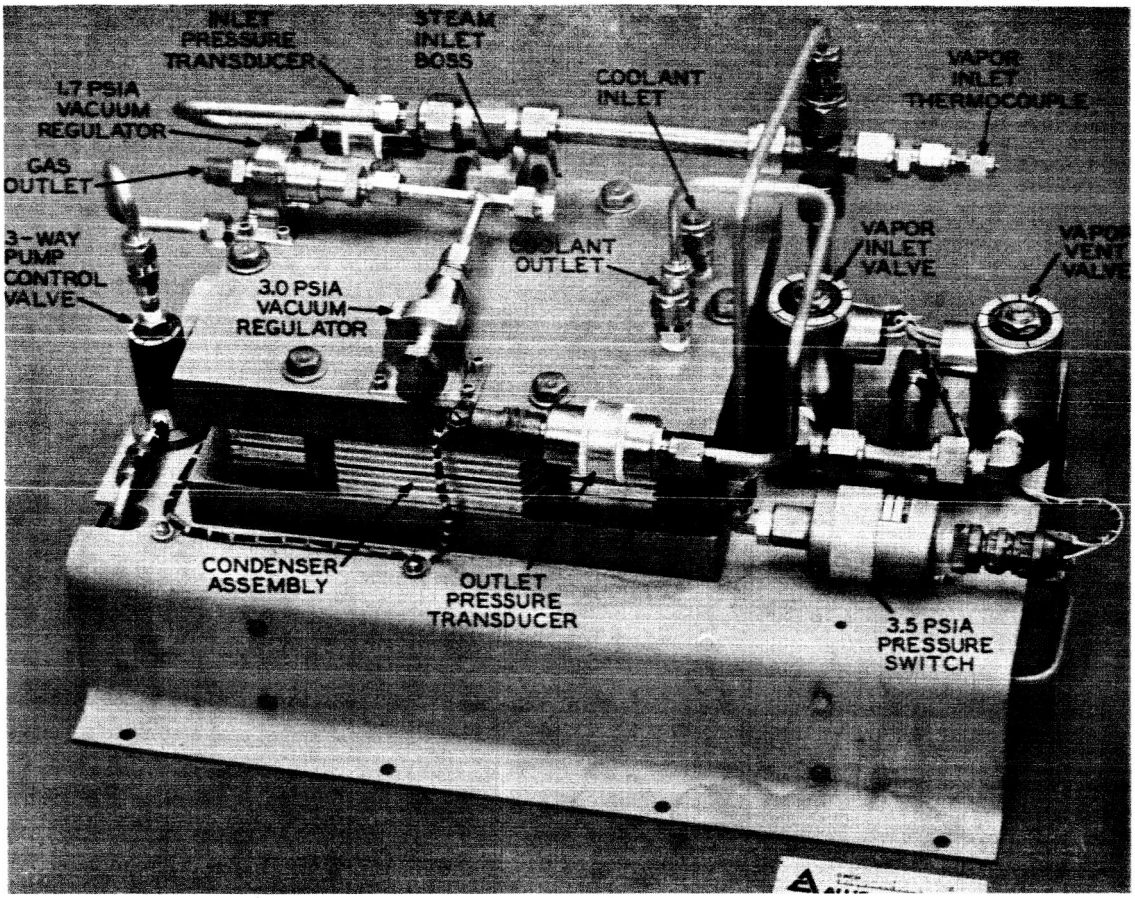

TOP VIEW

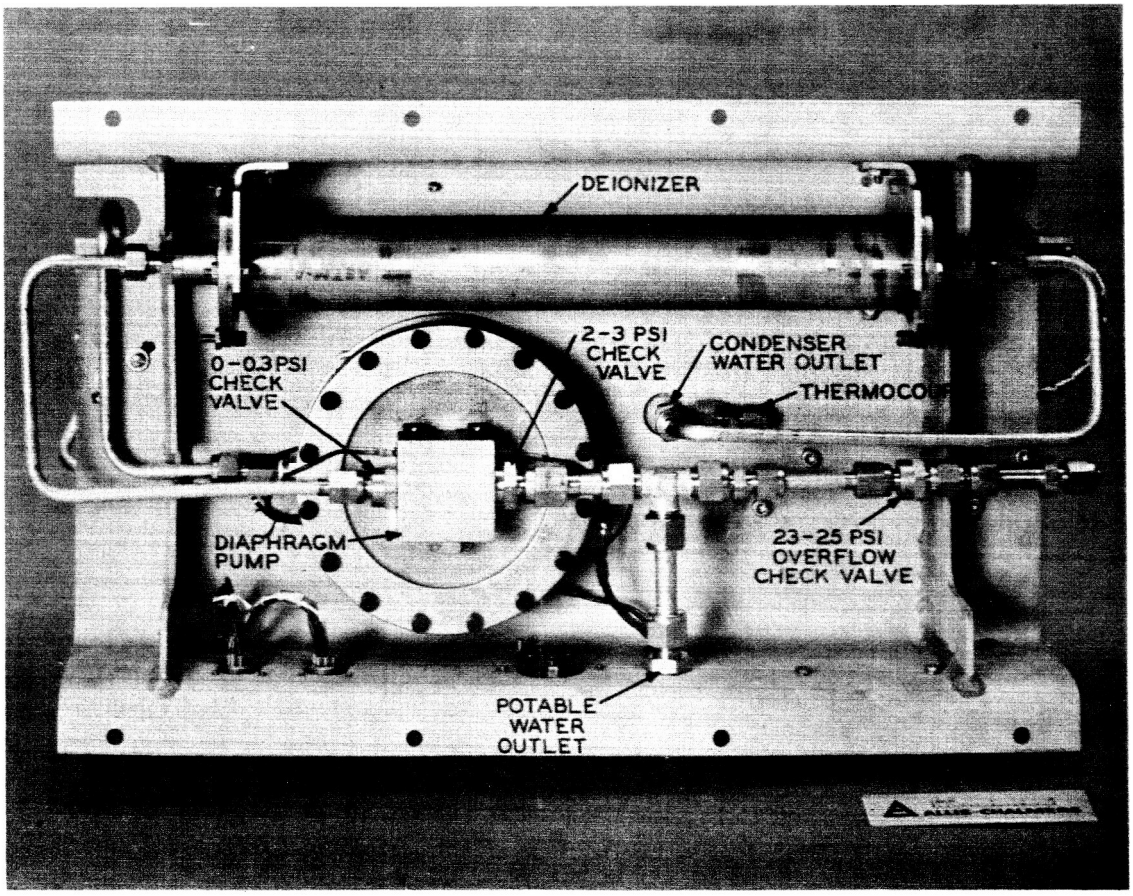

BOTTOM VIEW

Figure 29 - Breadboard Model Water Recovery Subsystem

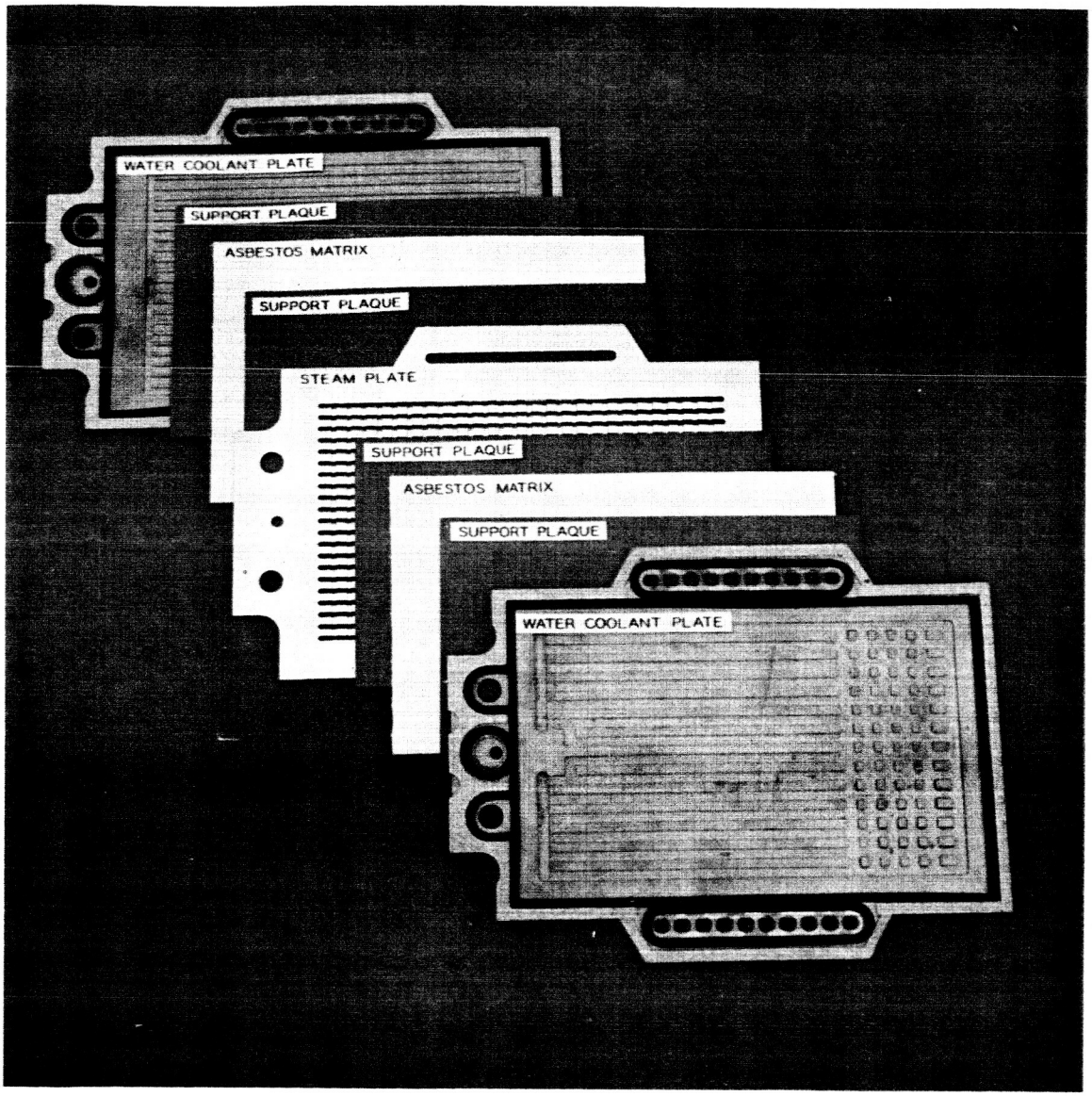

Figure 30- Condenser Cell Construction

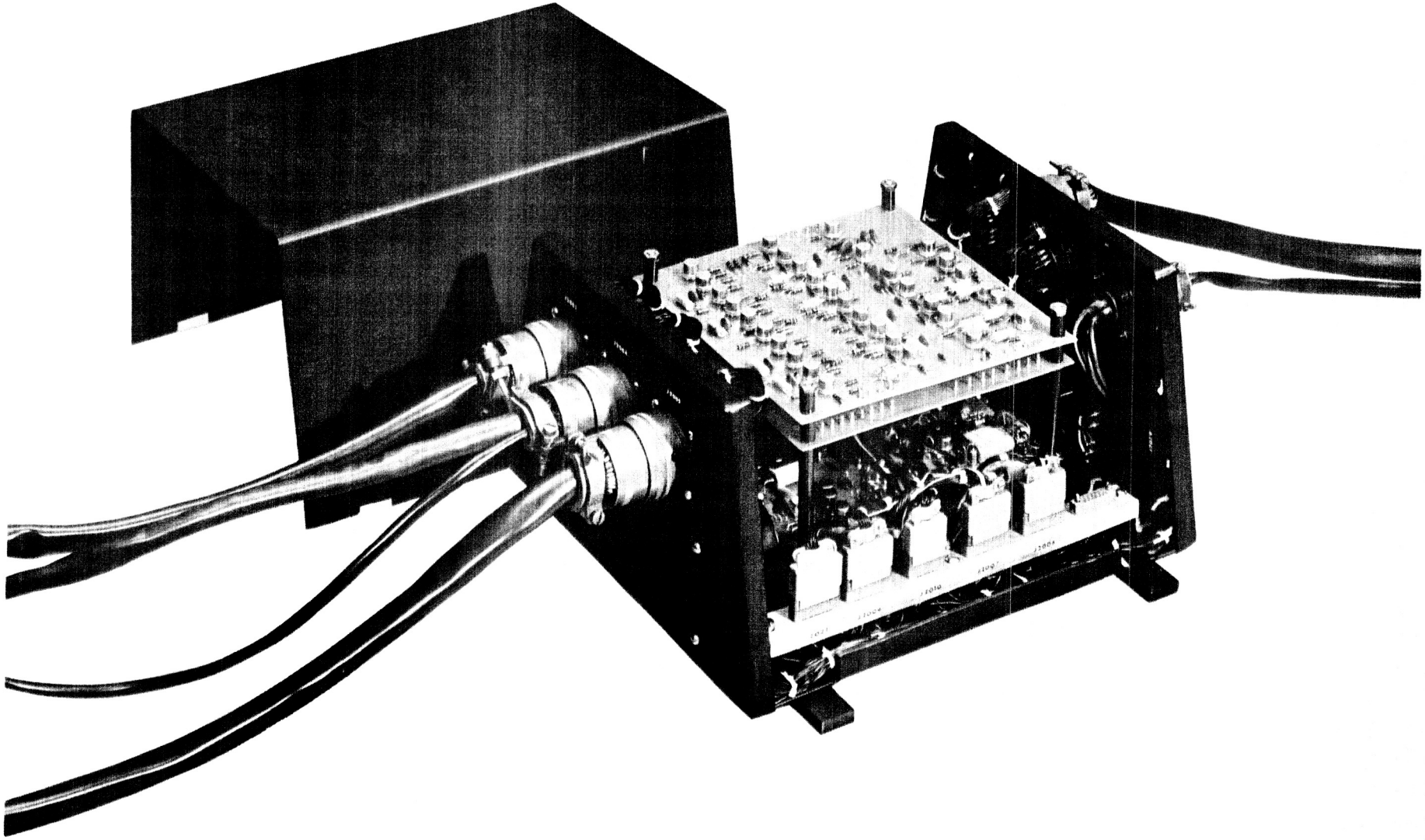

Figure 31 - Breadboard Model EMCS

System No. 5 Performance

Stack Temperature 185-200°F.

Reactant Pressure 36.3-38.7psia

KOH Concentration 37-42%

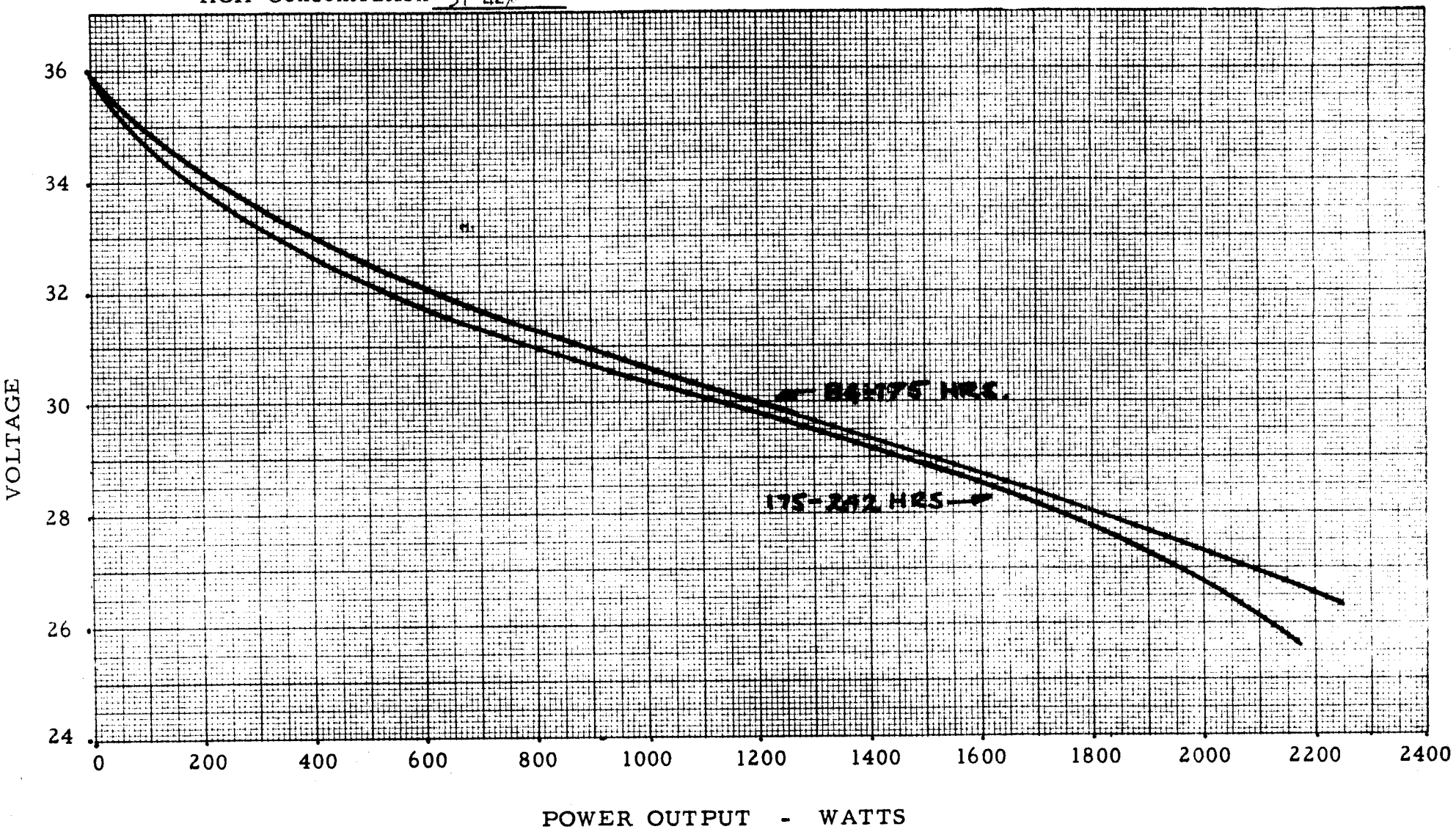

Figure 32

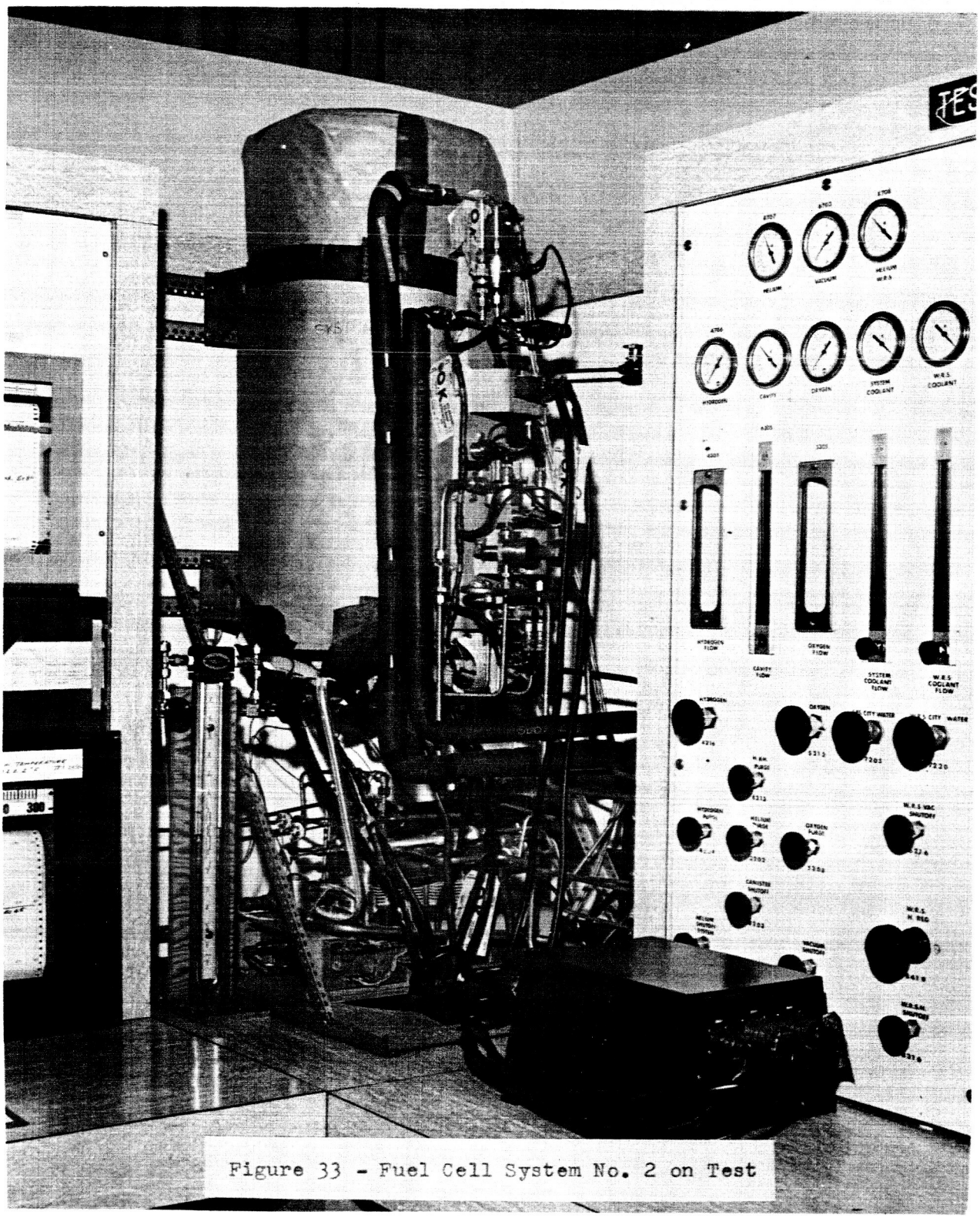

Figure 33 - Fuel Cell System No. 2 on Test

Sample	K^+ (ppm)	$CO_3^=$ or OH^-	HCO_3^- (ppm)	Cl^- (ppm)	Fe (ppm)	Mg (ppm)	Pt	Pd	Ni (ppm)	Ag
1	0.1	None	19	0.74	0.04	0.3	None	None	0.01	None
2	None	None	17	0.29	0.02	None	None	None	0.01	None
3	None	None	17	0.11	0.12	None	None	None	0.01	None
4	None	None	15	0.45	0.04	None	None	None	0.01	None
5	None	None	17	0.58	0.04	None	None	None	0.01	None

Water Removed

Sample	Elapsed Time	Qty of Water (ml)
1	11.0	4345
2	19.0	3620
3	27.0	3670
4	36.0	3610
5	42.5	3980

Figure 34 - Chemical Analysis of Product Water-System No. 2

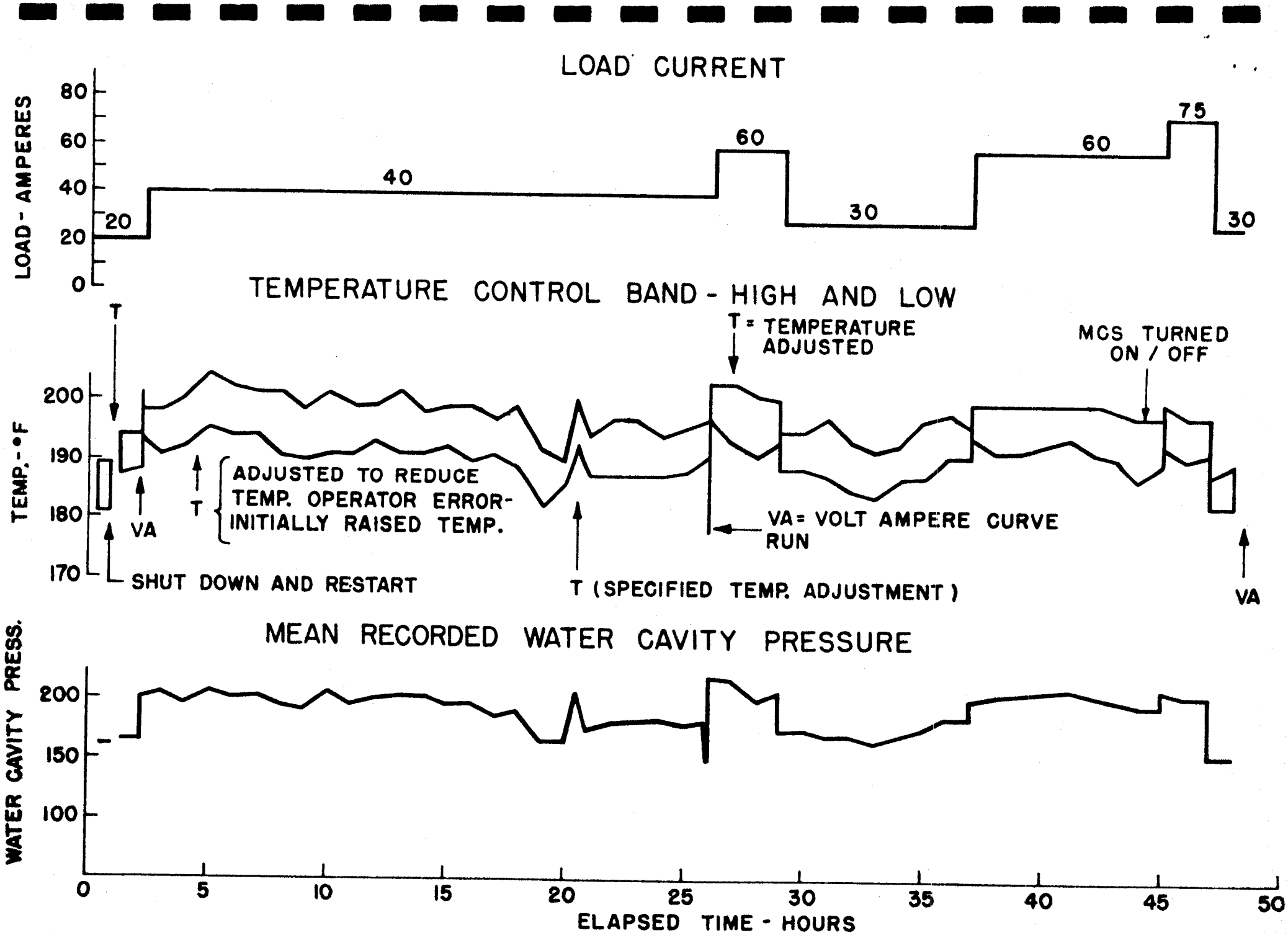
LOAD CURRENT
LOAD - AMPERES
80
60
40
20
0
20
40
60
30
60
75
30
TEMPERATURE CONTROL BAND - HIGH AND LOW
T
T = TEMPERATURE ADJUSTED
MCS TURNED ON / OFF
TEMP. - °F
200
190
180
170
T
ADJUSTED TO REDUCE TEMP. OPERATOR ERROR- INITIALLY RAISED TEMP.
VA
VA = VOLT AMPERE CURVE RUN
SHUT DOWN AND RESTART
T (SPECIFIED TEMP. ADJUSTMENT)
VA
MEAN RECORDED WATER CAVITY PRESSURE
WATER CAVITY PRESS.
200
150
100
0
5
10
15
20
25
30
35
40
45
50
ELAPSED TIME - HOURS

FIGURE 35

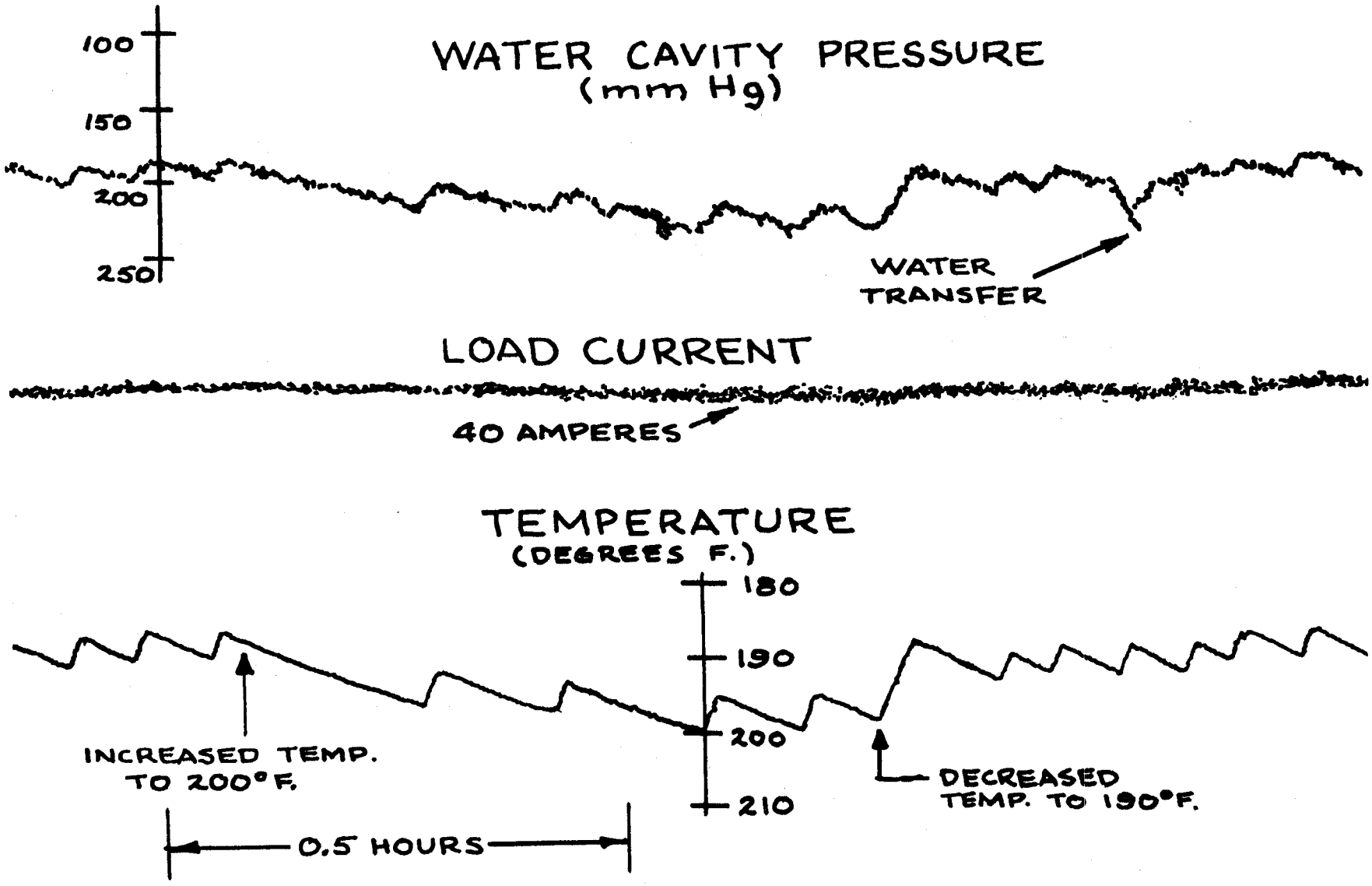

Figure 36 – Thermal Response to Temperature Adjustment — System No. 2

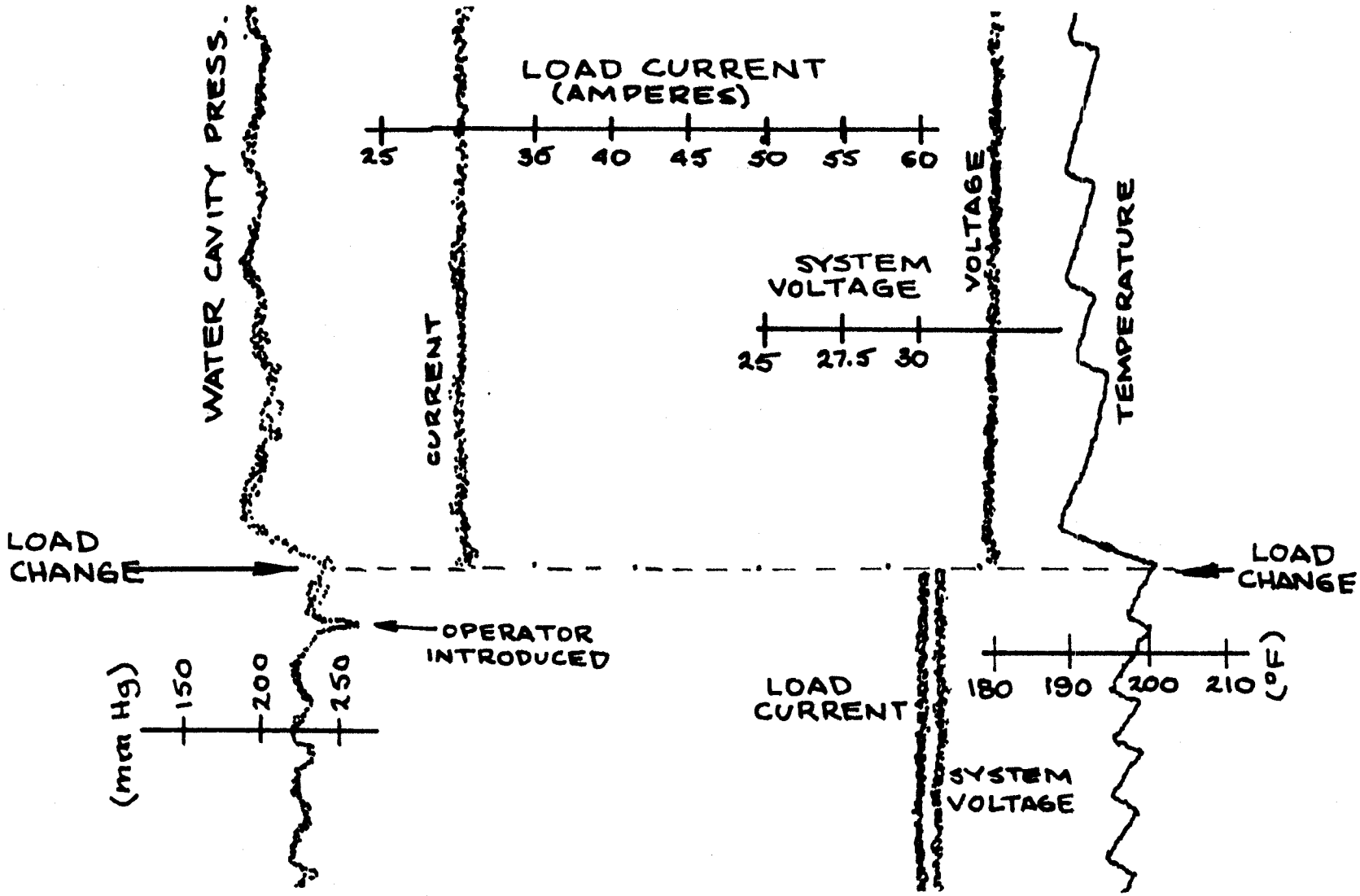

Figure 37 - Thermal Response to Load Change
System No. 2

CELL TEMPERATURE CYCLIC PERIOD
VS LOAD

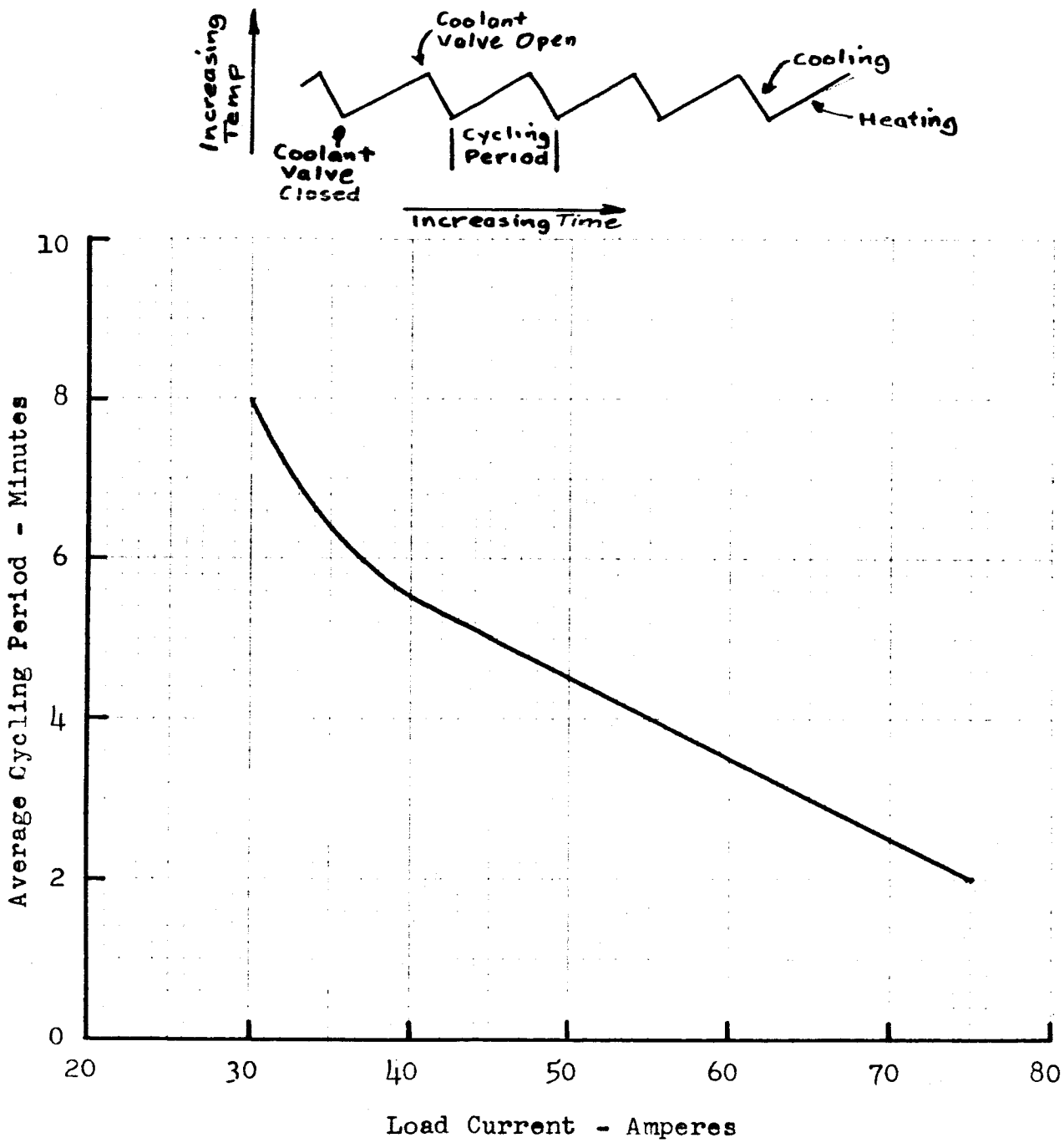

Figure 38

HEATING AND COOLING RATES DURING
TEMPERATURE CONTROL CYCLING

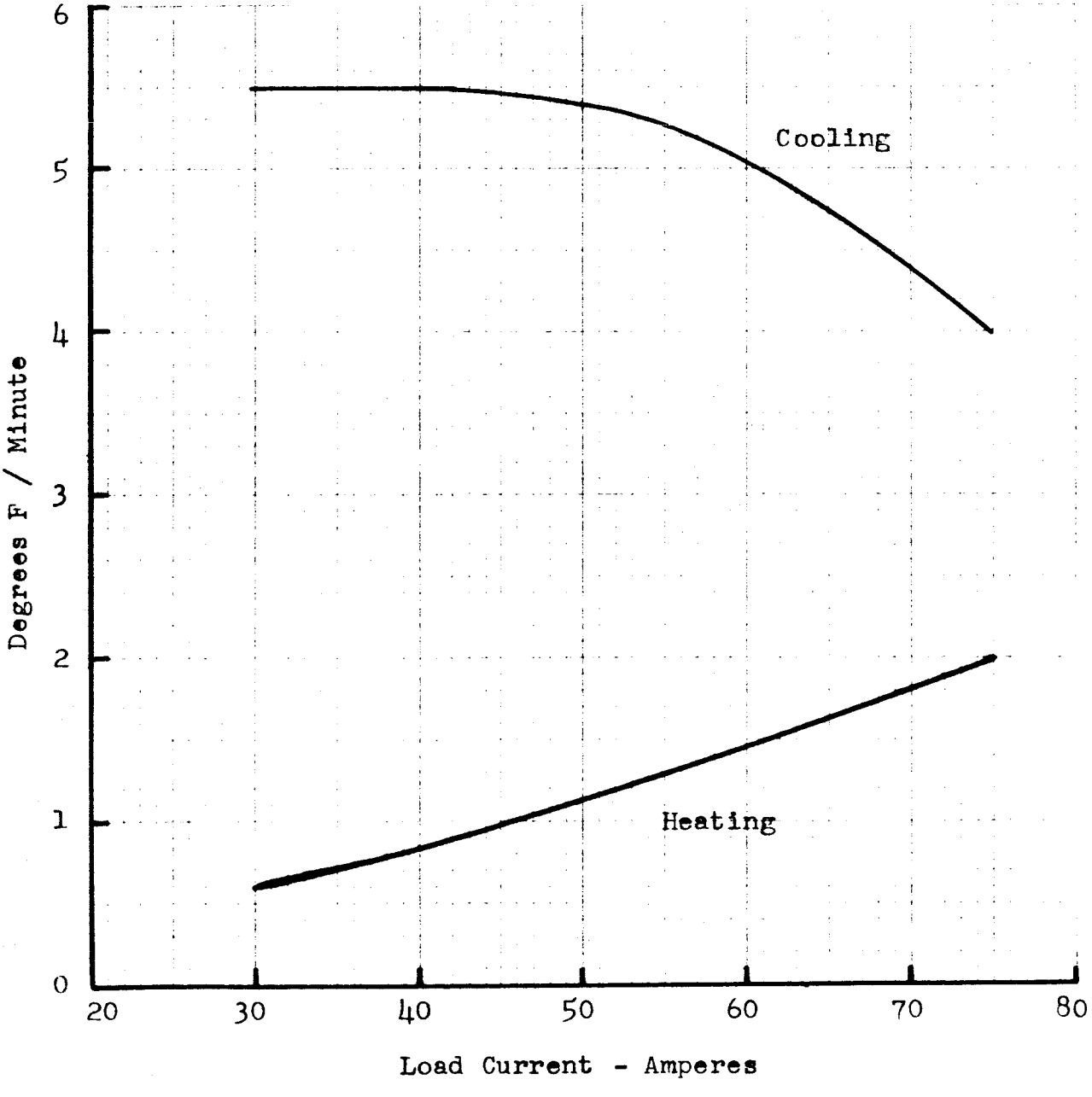

Figure 39

PRIMARY COOLANT VALVE
PERCENT OPEN TIME VS LOAD

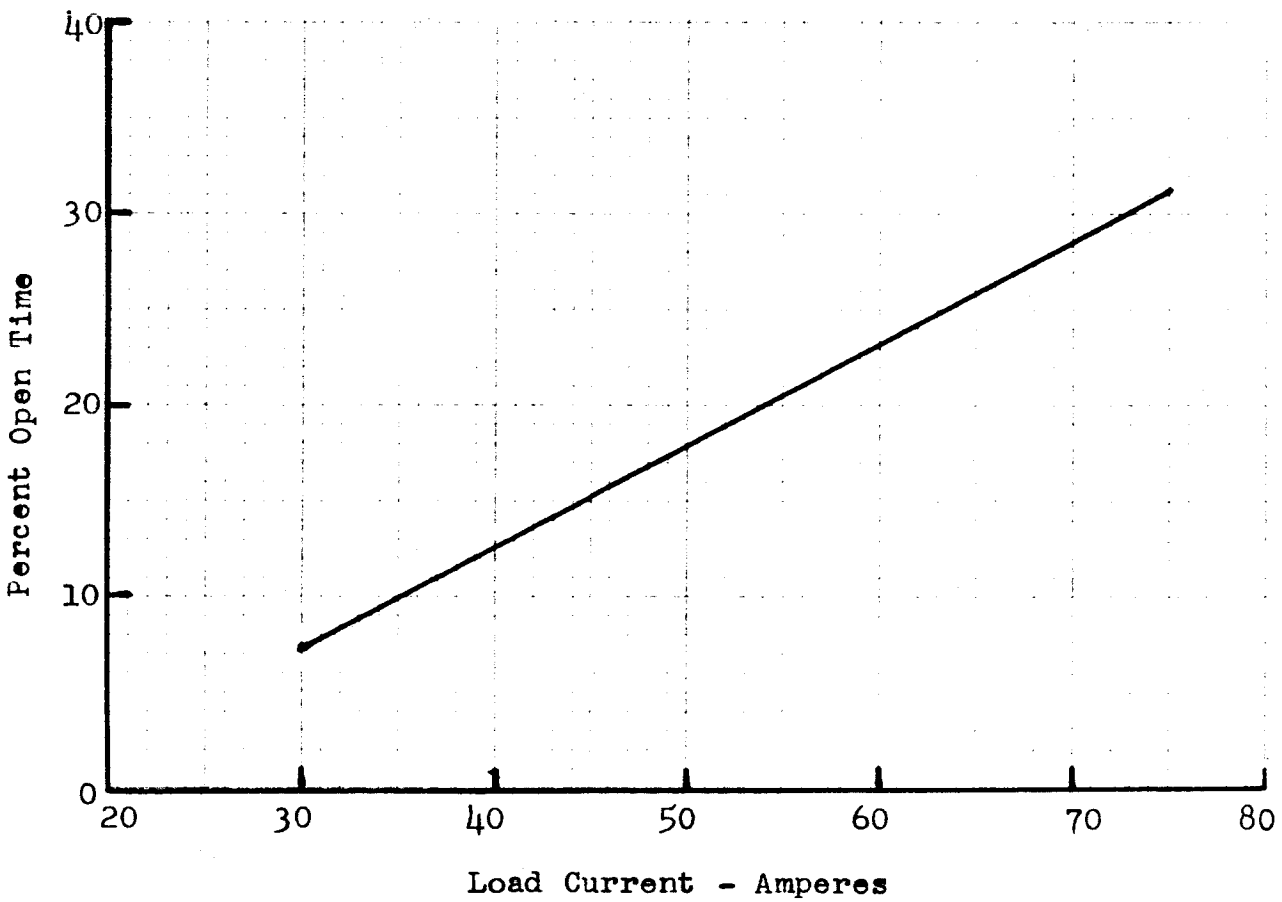

Figure 40

FUEL CELL SYSTEM NO. 2 - MODULE IMPEDANCE
(41 amps dc, nominal load - 5 amps ac, nominal load except below 40 cps)

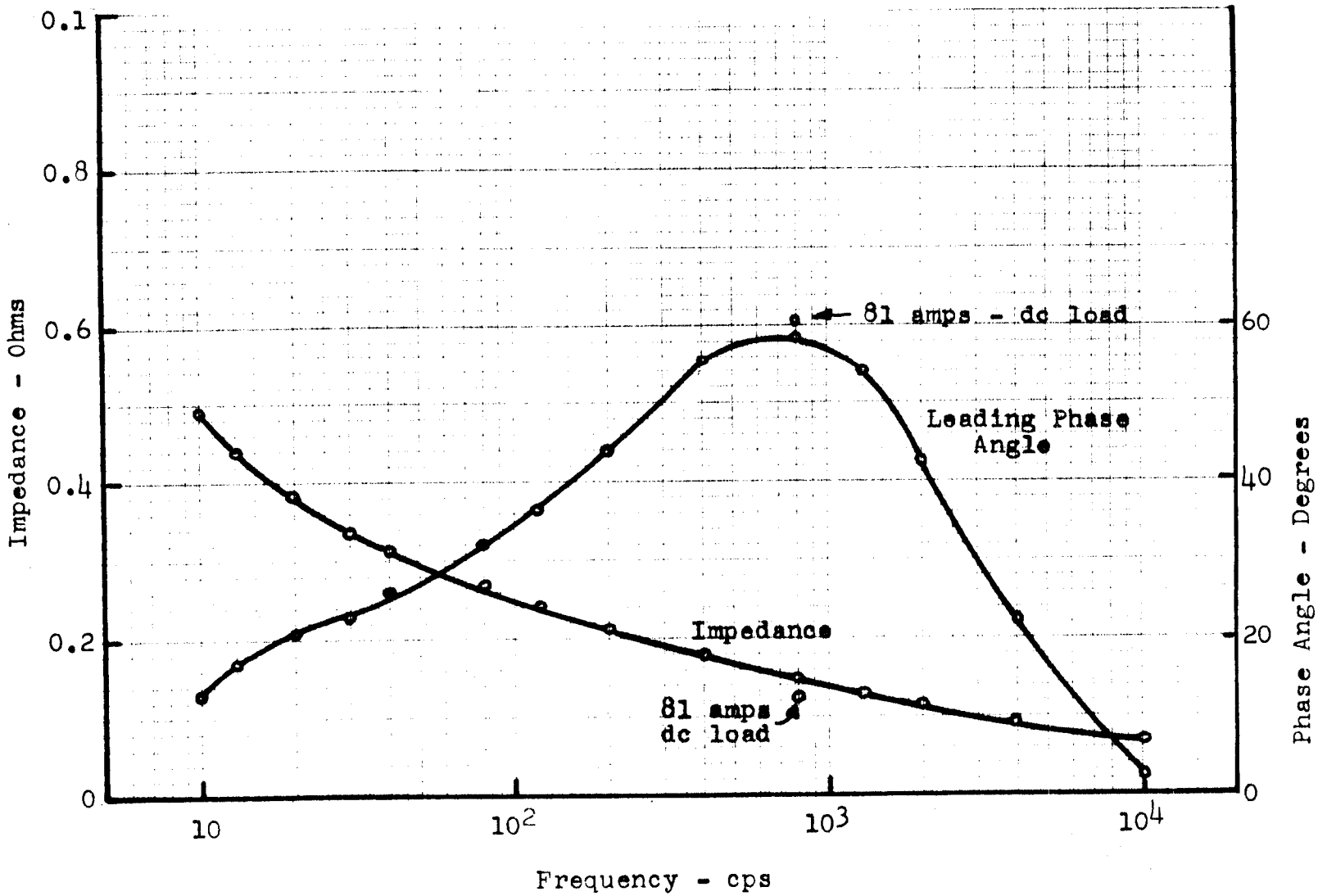

Figure 41

SYSTEM NO. 2 PERFORMANCE

Stack Temperature 195°F

Reactant Pressure 37 psia

KOH Concentration 37%

Date November 18, 1965

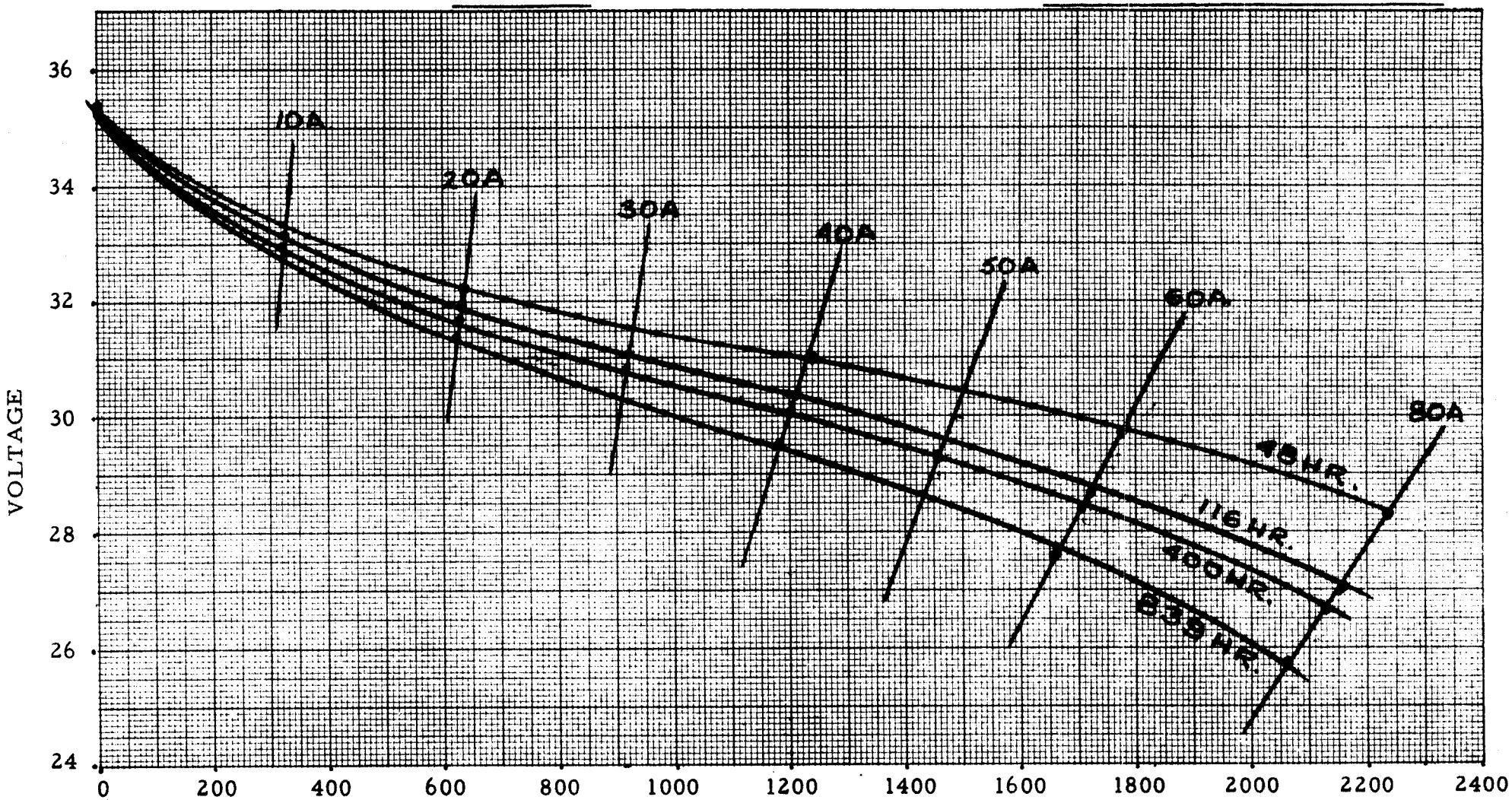

Figure 42

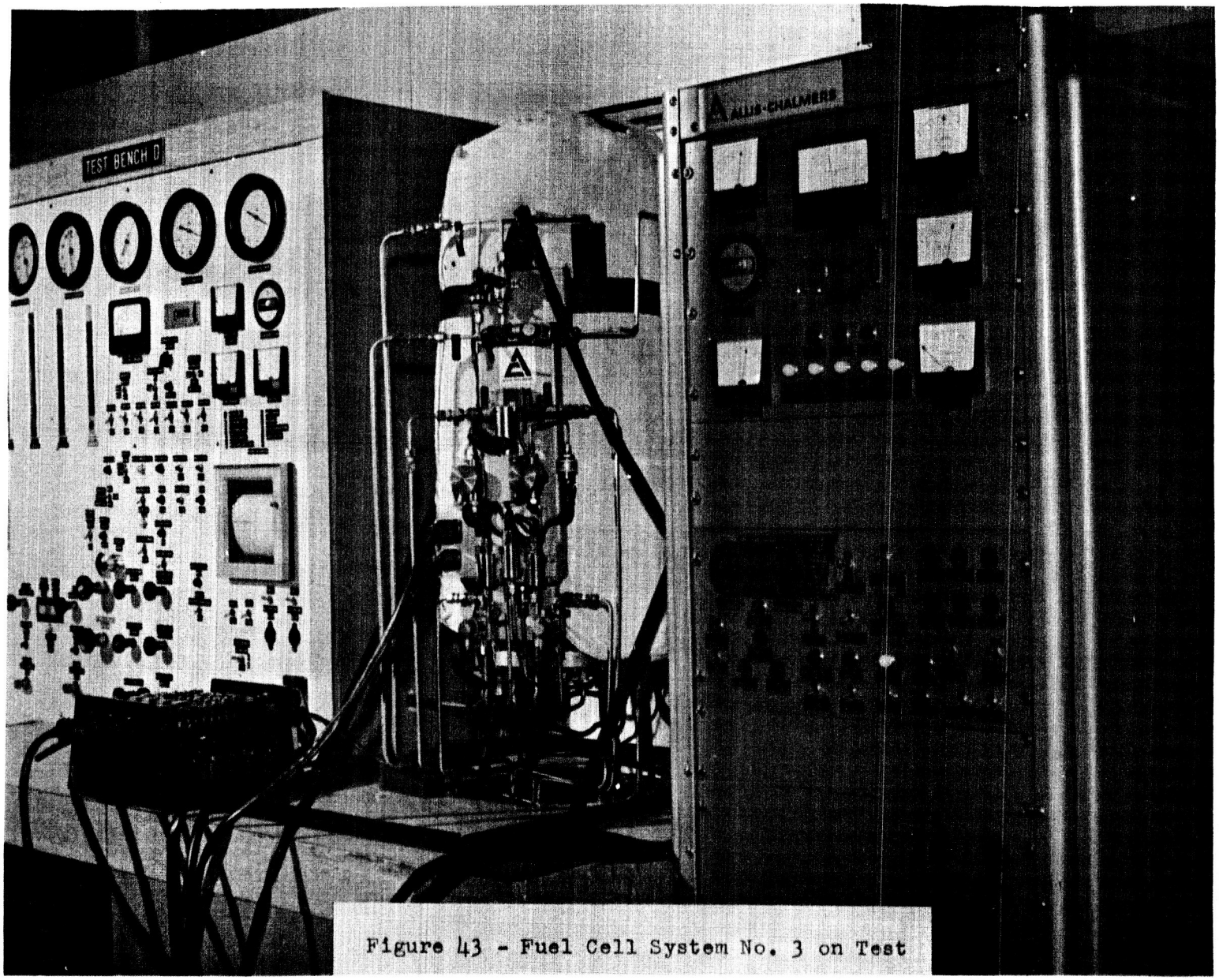

Figure 43 - Fuel Cell System No. 3 on Test

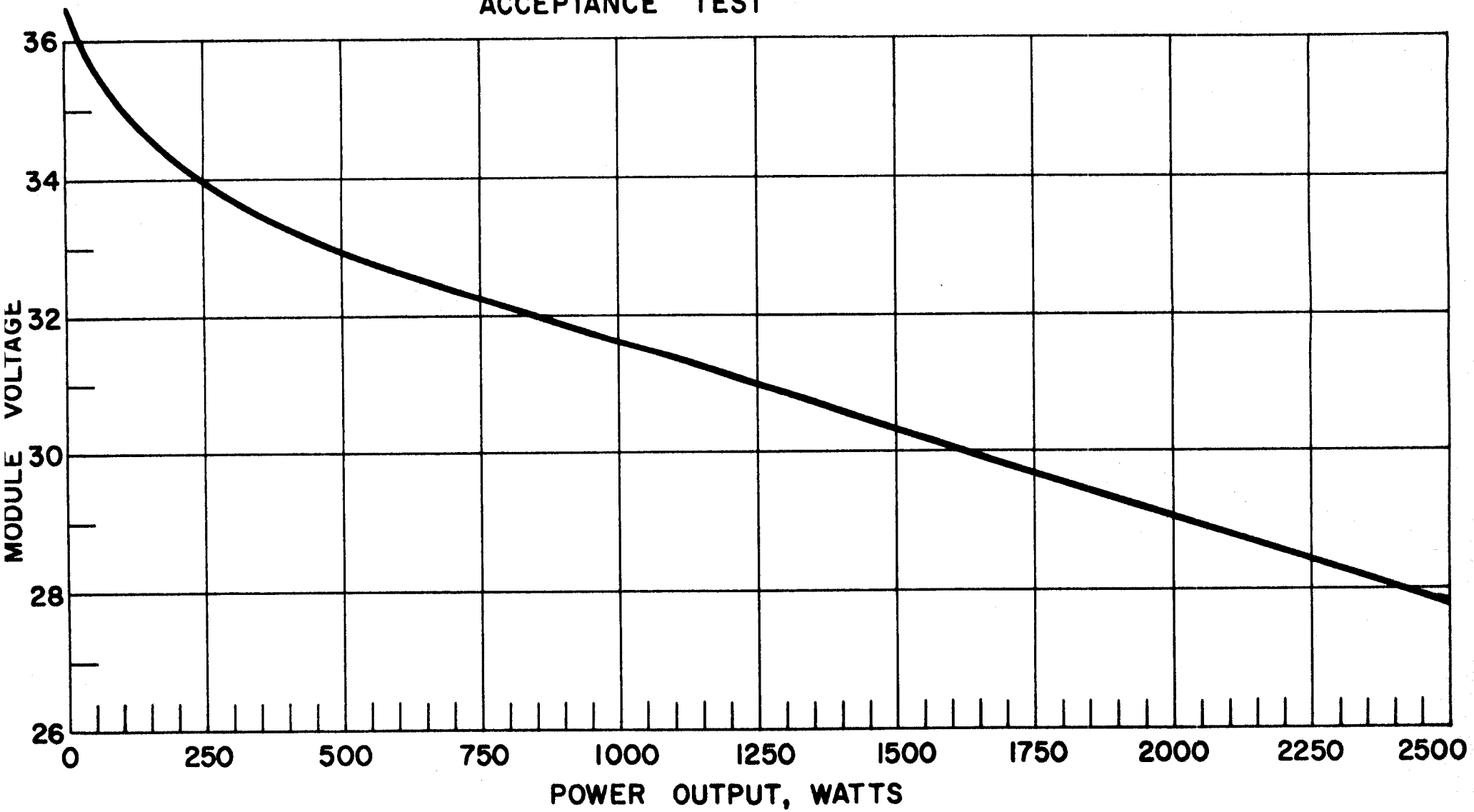
FUEL CELL ASSEMBLY
SYSTEM # 3
ACCEPTANCE TEST
MODULE VOLTAGE
36
34
32
30
28
26
0
250
500
750
1000
1250
1500
1750
2000
2250
2500
POWER OUTPUT, WATTS

FIGURE 44

Sample	K^+ (ppm)	$CO_3^=$ or OH^-	HCO_3^- (ppm)	Cl^- (ppm)	Fe (ppm)	Mg (ppm)	Pt	Pd	Ni (ppm)	Ag
1	0.1	None	21	15	0.03	5	None	None	0.02	None
2	0.1	None	39	10	0.02	3	None	None	0.01	None
3	0.1	None	21	6.5	0.05	None	None	None	0.01	None
4	0.1	None	26	5	0.05	None	None	None	0.01	None
5	0.1	None	25	11	0.03	None	None	None	0.02	None
6	0.1	None	21	3.5	0.02	None	None	None	None	None

Water Removed

Sample	Elapsed Time	Qty of Water (ml)	pH	Resistance (ohms)
1	13.0	4200	9.7	120K
2	15.0	826	9.3	258K
3	17.0	960	9.8	215K
4	21.0	2490	9.5	320K
5	27.5	4120	9.6	257K
6	32.0	2670	9.1	360K

Figure 45 - Chemical Analysis of Product Water–System No. 3

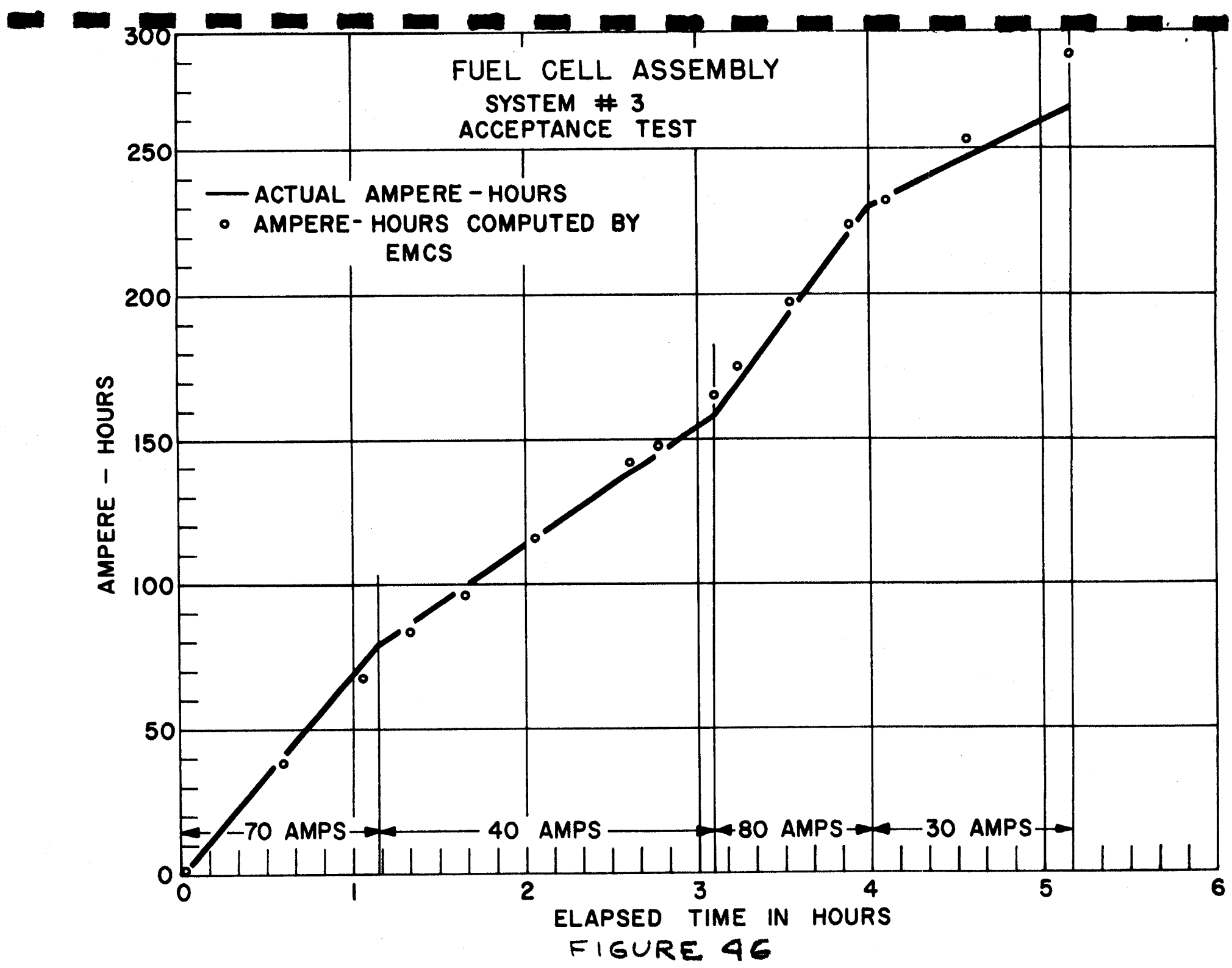
FUEL CELL ASSEMBLY
SYSTEM # 3
ACCEPTANCE TEST
ACTUAL AMPERE - HOURS
AMPERE - HOURS COMPUTED BY EMCS
AMPERE - HOURS
300
250
200
150
100
50
0
0
1
2
3
4
5
6
70 AMPS
40 AMPS
80 AMPS
30 AMPS
ELAPSED TIME IN HOURS

FIGURE 46

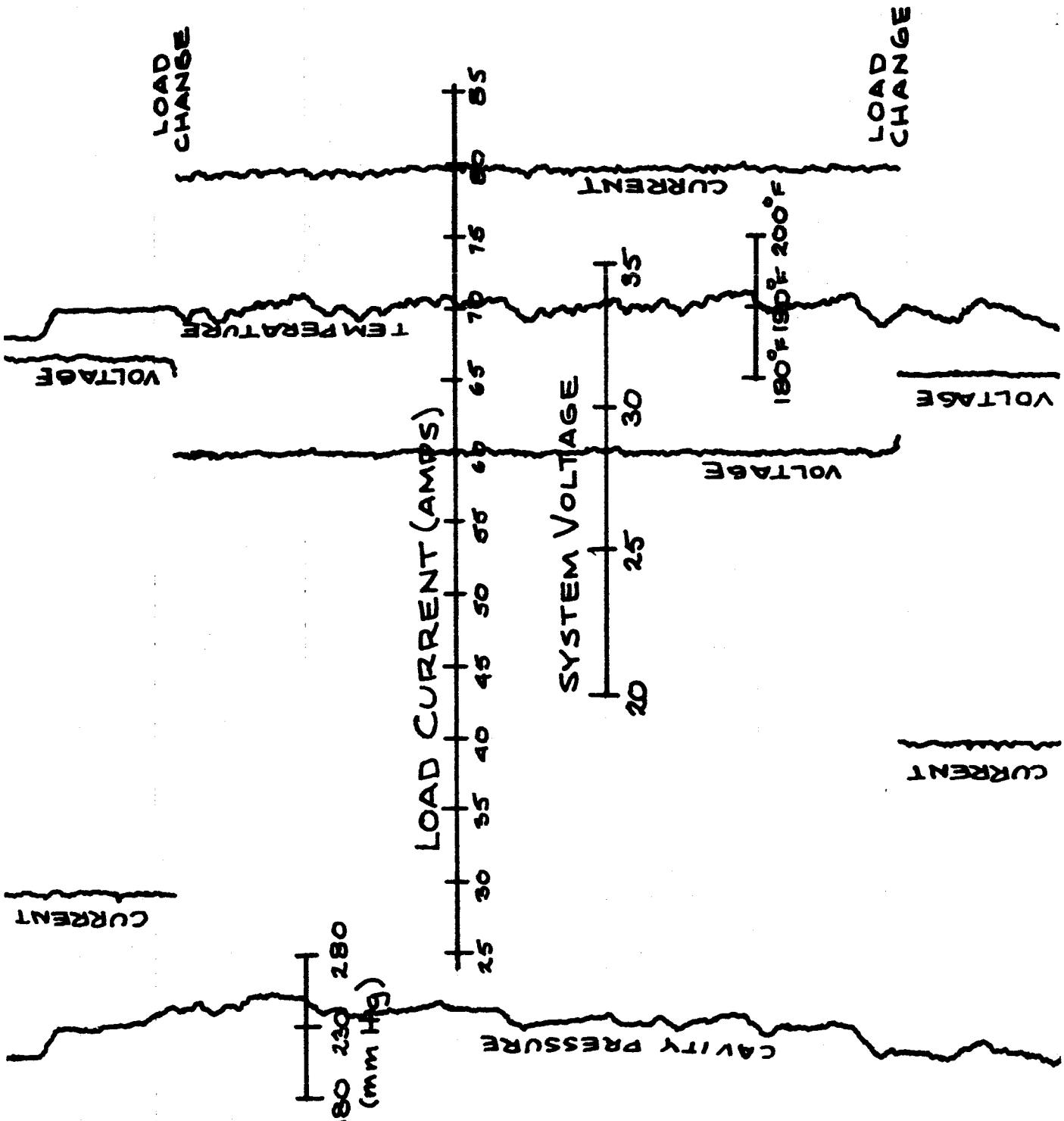

Figure 47 – Performance of System No. 2
During Acceptance Test

SYSTEM NO. 4 PERFORMANCE

Stack Temperature 195°F

Reactant Pressure 37 psia

KOH Concentration 37-43%

Date December 29, 1965

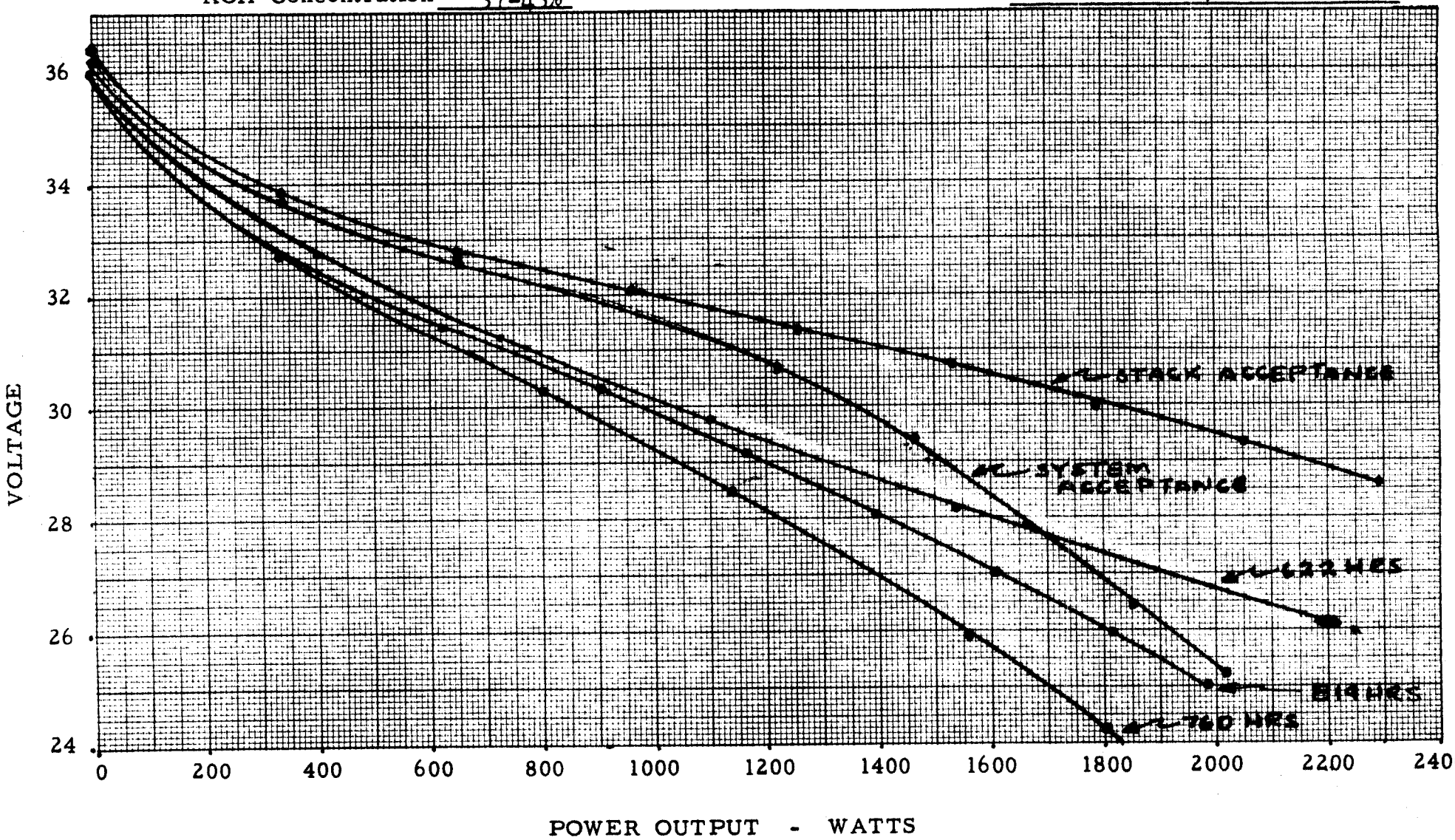

Figure 48

SYSTEM NO. 8 PERFORMANCE

Stack Temperature 195°F

Reactant Pressure 37 psia

KOH Concentration Optimum at about 45% Date December 15, 1965

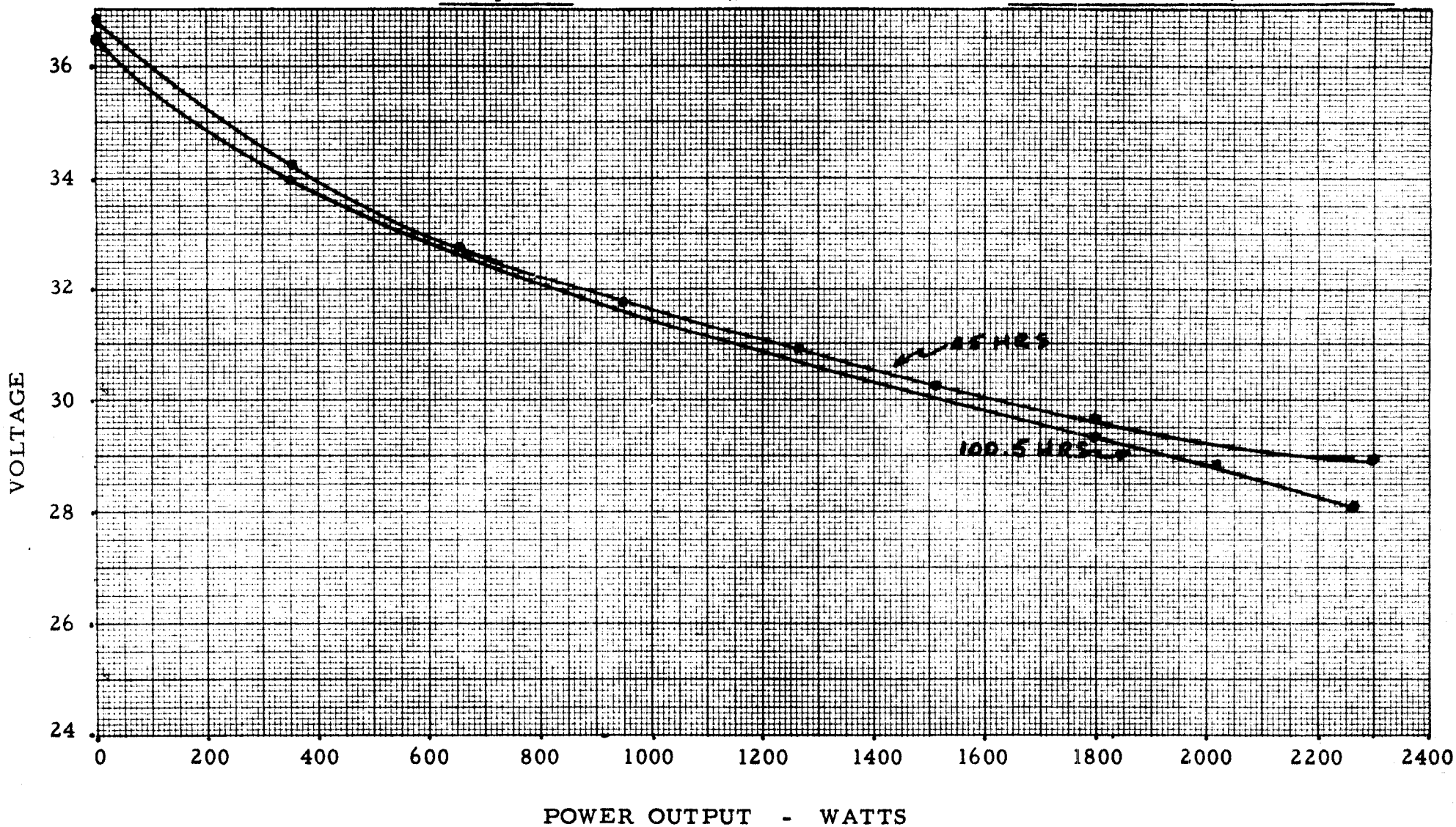

Figure 49

SYSTEM NO. 1 PERFORMANCE
(STACK ACCEPTANCE)

Stack Temperature 195°F

Reactant Pressure 37 psia

KOH Concentration 45%

Date December 1, 1965

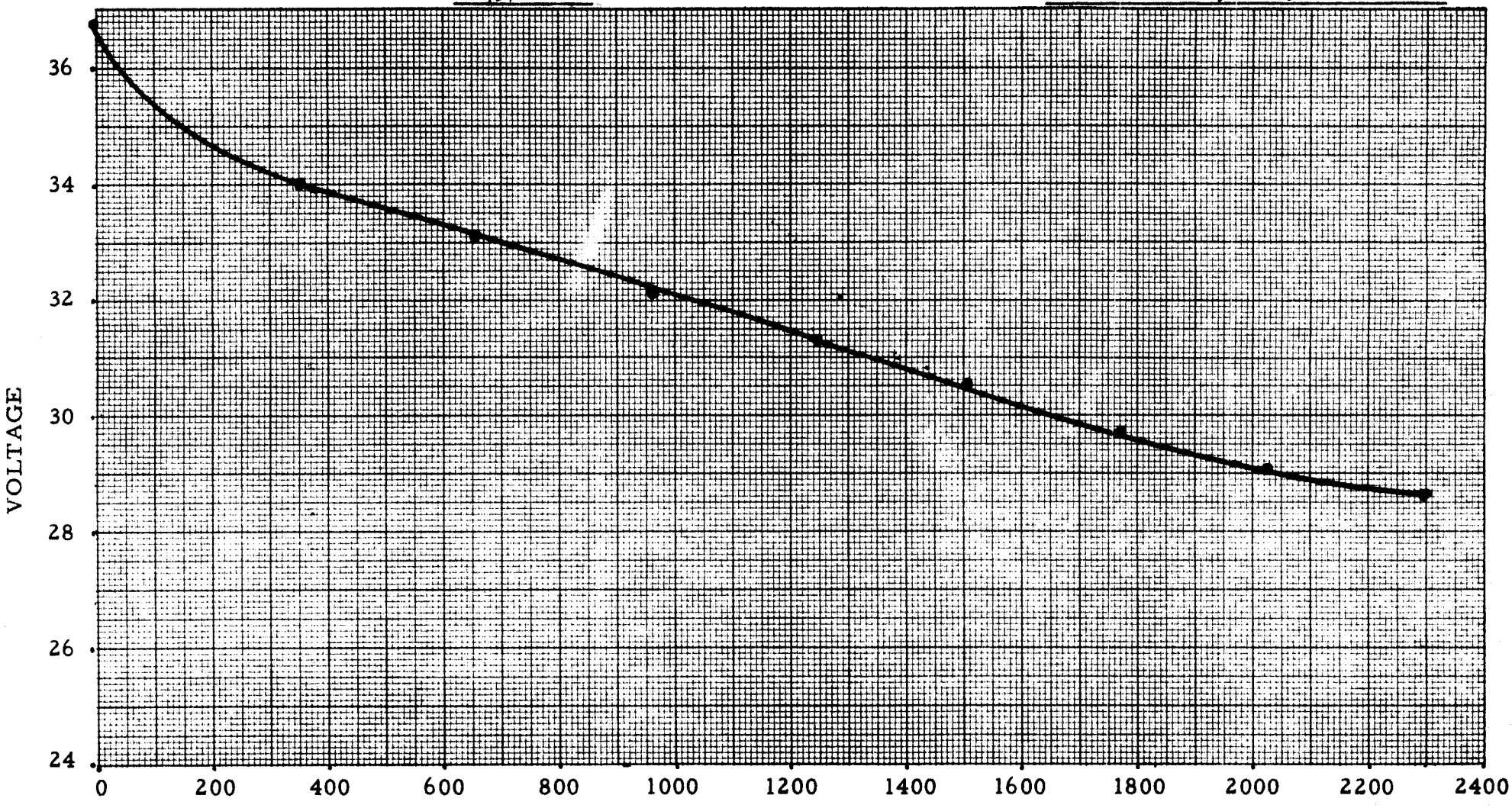

Figure 50

DISTRIBUTION LIST FOR

QUARTERLY & FINAL FUEL CELL REPORTS NAS8-2696

July, 1965

National Aeronautics & Space Administration
George C. Marshall Space Flight Center
Huntsville, Alabama 35812
Attn: Code PR-RC

National Aeronautics & Space Administration
George C. Marshall Space Flight Center
Hunstville, Alabama 35812
Attn: Code MS-IL

National Aeronautics & Space Administration
George C. Marshall Space Flight Center
Huntsville, Alabama 35812
Attn: Code MS-T

National Aeronautics & Space Administration
George C. Marshall Space Flight Center
Huntsville, Alabama 35812
Attn: Code MS-I (2 Copies)

National Aeronautics & Space Administration
George C. Marshall Space Flight Center
Huntsville, Alabama 35812
Attn: Mr. R. J. Boehme, Code R-ASTR-EC (10 Copies)

National Aeronautics & Space Administration
George C. Marshall Space Flight Center
Huntsville, Alabama 35812
Attn: Code R-ASTR-Z

Distribution List for Fuel Cell Reports (July 1965) Cont'd)

1. National Aeronautics & Space Administration
   Washington, D. C. 20546
   Attn: Mr. Ernst M. Cohn, Code RNW

2. National Aeronautics & Space Administration
   Washington, D. C. 20546
   Attn: Mr. George F. Esenwein, Code MAT

3. National Aeronautics & Space Administration
   Washington, D. C. 20546
   Attn: Mr. A. M. Andrus, Code ST

4. National Aeronautics & Space Administration
   Washington, D. C. 20546
   Attn: Mr. J. R. Miles, Code SL

5. National Aeronautics & Space Administration
   Office of Manned Space Flight
   Washington, D. C. 20546
   Attn: Mr. Tom Albert, OMSF/AES

6. National Aeronautics & Space Administration
   Scientific and Technical Information Facility
   P. O. Box 5700
   Bethesda, Maryland 20014

7. National Aeronautics & Space Administration
   Goddard Space Flight Center
   Greenbelt, Maryland 20771
   Attn: Mr. Thomas Hennigan

8. National Aeronautics & Space Administration
   Langley Research Center
   Langley Station
   Hampton, Virginia 23365

9. National Aeronautics & Space Administration
   Lewis Research Center
   21000 Brookpark Road
   Cleveland, Ohio 44135

10. National Aeronautics & Space Administration
    Lewis Research Center
    2100 Brookpark Road
    Cleveland, Ohio 44135
    Attn: Mr. Robert Miller

11. National Aeronautics & Space Administration
Lewis Research Center
21000 Brookpark Road
Cleveland, Ohio 44135
Attn: Mr. Robert L. Cummings

12. National Aeronautics & Space Administration
Lewis Research Center
21000 Brookpark Road
Cleveland, Ohio 44135
Attn: Mr. Harvey L. Schwartz

13. National Aeronautics & Space Administration
Ames Research Center
Pioneer Project
Moffett Field, California 94035
Attn: Mr. James R. Swain

14. National Aeronautics & Space Administration
Ames Research Center
Mountain View, California 94042
Attn: Mr. Jon Rubenizer,
Biosatellite Project

15. Jet Propulsion Laboratory
4800 Oak Grove Drive
Pasadena, California 91103
Attn: Mr. Aiji Uchiyama

16. National Aeronautics & Space Administration
Manned Spacecraft Center
Houston, Texas 77001
Attn: Mr. Richard Ferguson, EP-5

17. National Aeronautics & Space Administration
Manned Spacecraft Center
Houston, Texas 77001
Attn: Mr. Robert Cohen

18. National Aeronautics & Space Administration
Manned Spacecraft Center
Houston, Texas 77058
Attn: Mr. Hoyt McBryar, EP-5, Building 16 (2 copies)

19. National Aeronautics & Space Administration
Manned Spacecraft Center
Houston, Texas 77058
Attn: Mr. Forrest E. Eastman, EE-4

DEPARTMENT OF THE ARMY

20. U. S. Army Engineer R&D Labs.
Fort Belvoir, Virginia 22060
Attn: Electrical Power Branch

21. U. S. Army Engineer R&D Labs.
Fort Monmouth, New Jersey 07703
Attn: (Code SELRA/SL-PS)

22. U. S. Army Research Office
Physical Sciences Division
3045 Columbia Pike
Arlington, Virginia 22204

23. Army Materiel Command
Research Division
AMCRD-RSCM T-7
Washington, D. C. 20012

24. Army Missile Command
Redstone Arsenal, Alabama 35808
Attn: James B. Wright AMICOM-DR&D

25. Natrick Labs.
Clothing & Organic Materials Div.
Natrick, Massachusetts 01760
Attn: Mr. Leo A. Spano/R.N. Walsh

26. U. S. Army TRECOM
Physical Sciences Group
Fort Eustis, Virginia 23604
Attn: (SMOFE)

27. U. S. Army Research Office
Box CM, Duke Station
Durham, North Carolina 27706
Attn: Dr. Wilhelm Jorgensen/Mr. Paul Greer

28. U. S. Army Mobility Command
Research Division
Center Line, Michigan 48015
Attn: O. Renius (AMSMO-RR)

29. Hq., U. S. Army Materiel Command
Development Division
Washington, D. C. 20310
Attn: Marshall D. Aiken (AMCRD-DE-MO-P)

DEPARTMENT OF THE NAVY

30. Office of Naval Research
Department of the Navy
Washington, D. C. 20350
Attn: Dr. Ralph Roberts/Mr. H. W. Fox

31. Bureau of Naval Weapons
Department of the Navy
Washington, D. C. 20350
Attn: (Code RAAE)

32. U. S. Naval Research Laboratory
Washington, D. C. 20390
Attn: (Code 6160)

33. Bureau of Ships
Department of the Navy
Washington, D. C. 20350
Attn: Mr. Bernard B. Rosenbaum/Mr. C. F. Viglotti

34. Naval Ordnance Laboratory
Department of the Navy
Corona, California 91720
Attn: Mr. William C. Spindler (Code 441)

35. Naval Ordnance Laboratory
Department of the Navy
Silver Spring, Maryland 20907
Attn: Mr. Philip B. Cole (Code WB)

36. U. S. Navy Marine Engineering Laboratory
Special Projects Division
Annapolis, Maryland 21402
Attn: Mr. J. H. Harrison

DEPARTMENT OF THE AIR FORCE

37. Wright-Patterson AFB
Aeronautical Systems Division
Dayton, Ohio 45433
Attn: Mr. George W. Sherman, APIP

38. AF Cambridge Research Lab.
Attn: CRZE
L. G. Hanscom Field
Bedford, Massachusetts 01731
Attn: Francis X. Doherty/Mr. E. Raskind (Wing F)

39. Rome Air Development Center, ESD
Griffiss AFB, New York 13442
Attn: Mr. Frank J. Mollura

40. Wright Air Development Div.
Wright-Patterson AFB, Ohio 45433
Attn: WWRMFP-2

ATOMIC ENERGY COMMISSION

41. Mr. Donald B. Hoatson
Army Reactor, DRD
U. S. Atomic Energy Commission
Washington, D. C. 20545

OTHER GOVERNMENT AGENCIES

42. Office, DDR&E: USW & BSS
The Pentagon
Washington, D.C. 20301
Attn: G. B. Wareham

43. Mr. Kenneth B. Higbie
Staff Metallurgist
Office, Director of Metallurgy Research
Bureau of Mines
Interior Building
Washington, D.C. 20240

44. Institute for Defense Analyses
Research and Engineering Support Division
400 Army-Navy Drive
Arlington, Virginia 22202
Attn: Dr. George C. Szego/Dr. R. Briceland/R. Hamilton

45. Power Information Center
University of Pennsylvania
Moore School Building
200 South 33rd Street
Philadelphia, Pennsylvania 19104

46. Office of Technical Services
Department of Commerce
Washington, D.C. 20009

PRIVATE INDUSTRY

47. Alfred University
Alfred, New York
Attn: Professor T. J. Gray

48. Allison Division of General Motors
Indianapolis, Indiana 46206
Attn: Dr. Robert E. Henderson

49. American Cyanamid Company
1937 W. Main Street
Stamford, Connecticut
Attn: Dr. R. G. Haldeman

50. American Machine & Foundry
689 Hope Street
Springdale, Connecticut 06879
Attn: Dr. L. H. Shaffer
Research & Development Division

51. Astropower Inc.
2968 Randolph Avenue
Costa Mesa, California 92626
Attn: Dr. Carl Berger

52. Aerospace Corp.
P. O. Box 95085
Los Angeles, California 90045
Attn: Tech. Library Documents Group

53. Battelle Memorial Institute
505 King Ave.
Columbus, Ohio 43216
Attn: Dr. C. L. Faust

54. Bell Telephone Laboratories, Inc.
Murray Hill, New Jersey 07971
Attn: Mr. U. B. Thomas

55. Clevite Corporation
Mechanical Research Division
540 East 105th Street
Cleveland, Ohio 44108
Attn: A. D. Schwope

56. Electrochimica Corp.
1140 O'Brien Drive
Menlo Park, California 94025
Attn: Dr. Morris Eisenberg

57. Electro-Optical Systems, Inc.
300 North Halstead Street
Pasadena, California 91107
Attn: E. Findl

58. Engelhard Industries, Inc.
497 Delancy Street
Neward 5, New Jersey 07105
Attn: Dr. J. G. Cohn

59. Esso Research and Engineering Company
Products Research Division
P.O. Box 215
Linden, New Jersey 07036
Attn: Dr. Robert Epperly

60. The Franklin Institute
Philadelphia, Pennsylvania 19105
Attn: Mr. Robert Goodman

61. Garrett Corp.
1625 Eye St. N.W.
Washington, D.C. 20013
Attn: George R. Shepherd

62. General Dynamics/Convair
P.O. Box 1128
San Diego, California 92112
Attn: Mr. R. W. Antell
Electrical Systems Dept. 549-6

63. General Electric Company
Direct Energy Conversion Operations
Lynn, Massachusetts 01901

64. General Electric Company
Research Laboratory
Schenectady, New York 12301
Attn: Dr. H. Liebhafsky

65. General Electric Company
Missile and Space Vehicle Department
P.O. Box 8555
Philadelphia, Pennsylvania 19101
Attn: A. D. Taylor

66. General Motors Corp.
Box T
Santa Barbara, California 93102
Attn: Dr. C. R. Russell/ Dr. Joseph Smatko

67. Globe-Union, Inc.
900 E. Keefe Avenue
Milwaukee, Wisconsin 53401
Attn: Dr. C. K. Morehouse

68. Institute of Gas Technology
State and 34th Streets
Chicago 16, Illinois
Attn: Mr. B. S. Baker

69. Johns Hopkins University
Applied Physics Laboratory
8621 Georgia Avenue
Silver Spring, Maryland 20910
Attn: W. A. Tynan

70. Lessona Moos Laboratories
Lake Success Park
Community Drive
Great Neck, New York 11020
Attn: Dr. A. Moos

71. McDonnell Aircraft Corporation
Attn: Project Gemini Office
P.O. Box 516
St. Louis 66, Missouri 63166

72. Monsanto Research Corporation
Boston Laboratories
Everett, Massachusetts 02149
Attn: Dr. J. O. Smith

73. Monsanto Research Corporation
Dayton Laboratory
Dayton, Ohio 44221
Attn: Librarian

74. North American Aviation Co.
S&ID Division
Downey, California 90241
Attn: Dr. James Nash

75. Oklahoma State University
Stillwater, Oklahoma 74075
Attn: Prof. William L. Hughes
School of Electrical Engineering

76. Pratt and Whitney Aircraft Division
United Aircraft Corporation
East Hartford, Connecticut 06108
Attn: Librarian

77. Radio Corporation of America
Astro Division
Heightstown, New Jersey 08520
Attn: Dr. Seymour Winkler

78. Radio Corporation of America
Somerville, New Jersey 08876
Attn: Dr. G. Lozier

79. Speer Carbon Company
Research and Development Laboratories
Packard Road at 47th Street
Niagara Falls, New York 14304

80. Stanford Research Institute
820 Mission Street
So. Pasadena, California 91108
Attn: Dr. Fritz Kalhammer

81. Thiokol Chemical Corporation
Reaction Motors Division
Denville, New Jersey 07834
Attn: Dr. D. J. Mann

82. Thompson Ramo Wooldridge, Inc.
23555 Euclid Avenue
Cleveland, Ohio 44115
Attn: Mr. Victor Kovacik

83. Unified Science Associates, Inc.
826 S. Arroyo Parkway
Pasadena, California 91105
Attn: Dr. Sam Naiditch

84. Union Carbide Corporation
12900 Snow Road
Parma, Ohio 44129
Attn: Dr. George E. Evans

85. University of California
Space Science Laboratory
Berkeley, California 94701
Attn: Prof. Charles W. Tobias

86. University of Pennsylvania
Electrochemistry Laboratory
Philadelphia, Pennsylvania 19104
Attn: Prof. John O'M. Bockris

87. University of Pennsylvania
Philadelphia, Pennsylvania 19104
Attn: Dr. Manfred Altman

88. Western Reserve University
Cleveland, Ohio 44101
Attn: Prof. Ernest Yeager

89. Yardney Electric Corp.
New York, New York 10001
Attn: Dr. Paul Howard

Note:

Any requests for changes or additions to this distribution list must be addressed to :

National Aeronautics & Space Administration
George C. Marshall Space Flight Center
Huntsville, Alabama 35812

Attention : Code PR - RC